NTNU

Norwegian University of
Science and Technology

Calculation of the coverage area of mobile broadband communications. Focus on land

Antonio Martínez Gálvez

Master of Science in Communication Technology
Submission date: March Terje Røste, IET
Supervisor:

Norwegian University of Science and Technology
Department of Electronics and Telecommunications

Problem Description

The task is to study the principles and models for calculating transmission loss in radiopropagation in mobile systems for land. Recent models are Okumura et. al [1], COST 231 [2], Bullingtons model [3], Epstein and Peterson's model [4], Picquenards model [5] and a modification of Walter Hill [6]. Another option is to look at Radar Ray Trace models. One must choose to proceed with one or two of these principles in a deeper studium. Furthermore can study Teleplan ASTERIX program (which is made available to the department) for prediction of transmission loss and describe how this program may be further developed with improved models. If time permits can simple modification of ASTERIX performed and tested. It focused on the frequency ranges 800 MHz and 2.6 GHz.

Assignment given: 31. August 2009
Supervisor: Terje Røste, IET

Abstract

This thesis aims to provide information about what different propagation prediction models must be the adequate ones for the radio planning of an LTE network.

In the initial phase, a study of different propagation models was done mainly over COST231 and ITU-R P. Recommendations, emphasizing over the ones for diffraction over rounded obstacles and paths over sea as a recommendation from Teleplan AS. Matlab code is also presented since it was tried to test the convenience of the use of ITU-R P.1546 over sea paths and to compare Lee Model with ITU-R P.526 for rounded obstacles.

This thesis will hopefully serve as a guide for future radio planners, where an example of an Astrix user case of coverage prediction and a comparison with live measurements are presented. The task has been performed on the initiative of LTE Networking Oslo using Astrix 5.2, the radio planning tool of Teleplan AS.

Preface

This thesis has been written as the final project of a master program in Telecommunication Engineering with the specialization in Communication Systems. The program has been carried out partly at the Telecommunications Faculty at UPV in Valencia (Spain) and at the Department of Electronics and Telecommunications at the NTNU.

During May 2009, I met with Lars Lundheim to discuss about possible project assignments. Wireless communications was always what I wanted to work on and I found over the list he provided to me two proposals from Terje Røste that seemed pretty interesting. I was then introduced to Terje Røste who showed me the plan of the thesis and the possibility of working on a summer job at Teleplan AS to get introduced to LTE and Astrix. Unhopefully the summer job could not finally be done but anyway being able to get that thesis was a fantastic option to me.

As of today, after writing that thesis, I feel I have acquired a better understanding in propagation prediction models and radio planning process over advanced wireless technology. I truly hope that my newly gained knowledge will be of help for future Mobile LTE and/or 4G radio planners, and for being able to find a desired position to continue working and researching over that lovely field.

Antonio Martínez Gálvez

28.03.2010

Acknowledgements

During the time I have been writing the master thesis, I have had the pleasure of enjoying that particular and lovely country and the privilege of meeting many nice and interesting people. I am truly grateful to have had the opportunity to research over a technology such as LTE.

I would like to give special thanks to the following persons:

Terje Røste , from the department of electronics and telecommunications at NTNU, has been the tutor of the master thesis. Mr. Røste have been always available and open for questions, discussions and support.

Kun Yang , from the department of electronics and telecommunications at NTNU, has been the co-supervisor of the master thesis. He has provided me with some knowledge about over sea radio communications for ITU-R P.1546 and Matlab code for testing purposes.

Inge AH Schøyen and Teleplan AS have been the reason why the NTNU and hopefully I could have had afterwards the possibility of researching over new mobile broadband communications as LTE using a radio planning tool used by many telephone companies like Telenor or Netcom.

Erik Aarnes , from Teleplan AS, for providing me with the radio planning tool. He installed the older 5.1 version and gave me a deep explanation of the tool on a presentation together with Mr. Schøyen.

Ola Aanstad , Senior Software Engineer at Teleplan AS, has been of great help by updating the new 5.2 version. He has also contributed with his experience and knowledge for solving some problems found on the tool.

Finally I did not want to end up that point without giving my best thanks to my family and friends for all the unconditional support I have got all this time especially these days I got stuck and frustrated.

Contents

4 Propagation Prediction Models

List of Tables

List of Figures

Abbreviations

2G 2nd Generation technology

3G 3rd Generation technology

3GPP 3rd Generation Partnership Project

4G 4th Generation technology

BS Base Station

cdmaOne also known as IS-95

CDMA2000 also known as IMT-MC

DL Down link

DVB-H Digital Video Broadcasting - Handheld

EDGE Enhanced Data Rates for GSM Evolution

EPC Evolved Packet Core

ERP Effective Radiated Power

E-UTRAN Evolved UMTS Terrestrial Radio Access Network

FSPL Free Space Path Loss

FTP File Transfer Protocol

GIS Geographical Information System

GPS Global Positioning System

GSM Global System for Mobile communications

HDTV High Definition Television

HSPA High Speed Packet Access

HSDPA High Speed Downlink Packet Access

HSUPA High Speed Uplink Packet Access

IMT International Mobile Telecommunications

IMT-MC International Mobile Telecommunications Multi Carrier

IP Internet Protocol

ITU International Telecommunications Union

IS-95 Interim Standard 95

LMA Local Mean Attenuation

LOS Line Of Sight

LTE 3GPP Long Term Evolution

MBSFN Multicast Broadcast Single Frequency Network

MIMO Multiple-Input and Multiple-Output

MMOG Multimedia Online Gaming

MS Mobile Station

MU-MIMO Multi-User MIMO

NLOS Non Line Of Sight

NTNU Norwegian University of Science and Technology

OFDM Orthogonal Frequency Division Multiplexing

RAT Radio Access Technologies

PLOS Partial Line Of Sight

PU2RC Per-User Unitary Rate Control

QAM Quadrature Amplitude Modulation

QoS Quality of Service

QPSK Quadrature Phase Shift Keying

SINR Signal-to-interference plus noise ratio

TETRA Terrestrial Trunked Radio

UE User Equipment

UL Up link

UMTS Universal Mobile Telecommunications System

VoIP Voice over IP

W-CDMA Wideband Code Division Multiple Access

1

Introduction

Wireless technology has lately become the fastest evolving one of the communications industry. From the entry of GSM, customers have continuously increased the demand for mobility, services and capacity. Third generation mobile technology and UMTS appeared as a solution by supporting higher data rates than GSM and providing more advanced services as video conference.

The recent increase of mobile data usage and emergence of new applications such as MMOG, HDTV streaming, Web 2.0, music applications have motivated the 3GPP to work on the LTE. LTE is the latest standard in the mobile network technology tree that previously realized the GSM/EDGE and UMTS/HSPA network technologies that will ensure 3GPP's competitive edge over other cellular technologies.

LTE, whose radio access is called E-UTRAN, is expected to substantially improve end-user throughputs, sector capacity and reduce user plane latency, bringing significantly improved user experience with full mobility. With the emergence of IP as the protocol of choice for carrying all types of traffic, LTE is scheduled to provide support for IP-based traffic with end-to-end QoS. Voice traffic will be supported mainly as VoIP enabling better integration with other multimedia services. Initial deployments of LTE are expected by 2010 and commercial availability on a larger scale 1-2 years later with expected data rates of 100 Mbps DL and 50 Mbps UL over a 20 MHz channel at 2.6 GHz band.

1.1 Scope

Radio planning is normally a vast and demanding process ranging from the initial process of setting up a business model, deploying the network, and releasing the services for commercial purposes. In order to limit the scope of this thesis, one focus has been on the actual radio planning with Astrix 5.2.

On an initiative from Teleplan AS the main focus was to cover the study of some propagation predictions models in order to get to know if it would be interesting implementing them on the new versions of Astrix or the possibility of introducing improvements for the existing models.

It is also presented an Astrix user case of the LTE Networking Oslo live measurements campaign performed together by Teleplan AS and one of the main Norwegian telephone companies over the Nydalen area in January 2010.

Finally as a conclusion of the propagation model study is given a recommendation to introduce Causebrook method instead of Deygout model for diffraction. They are also provided suggestions for study the convenience of adding ITU-R P.526 recommendation for rounded obstacles and ITU.R P.1546 recommendation for over-sea paths and as a latest point a discussion about future work is commented.

1.2 Readers Guide

Chapter 2 gives a brief introduction to LTE.

Chapter 3 introduces the concepts of path loss and shadowing used in Chapter 4 on the different propagation models.

Chapter 4 discusses the most common propagation models for urban areas and a study of the diffraction over rounded obstacles and the over-sea path loss.

Chapter 5 presents the radio planning methodology and illustrates the predicted radio planning coverage with an example of the LTE Oslo Networking live measurements campaign done by Teleplan AS in January 2010 using Astrix 5.2.

Chapter 6 summarizes and concludes upon the work performed, as well as recommends future work.

Appendices contains additional information on topology and demographics of Oslo, antenna specifications, an Astrix User Case and suggested Matlab codes for testing the convenience of a possible introduction of some models on the Astrix radio planning tool.

Part I

Theory

2

About LTE

2.1 Introduction

LTE is the project name of a new interface for cellular mobile communication systems. It is the last step towards the 4G of radio technologies designed to increase the capacity and speed of mobile telephone networks. Where the current generation of mobile telecommunication networks are collectively known as 3G, LTE is marketed as 4G. However, it does not fully comply with the IMT Advanced 4G requirements. The world's first publicly available LTE service was opened by TeliaSonera in the two Scandinavian capitals Stockholm and Oslo on the 14th of December 2009. LTE is a set of enhancements to the UMTS which will be introduced in 3GPP Release 8.

3GPP is specifying a new Packet Core, the EPC network architecture to support the E-UTRAN through a reduction in the number of network elements, simpler functionality, improved redundancy but most importantly allowing for connections and hand-over to other fixed line and wireless access technologies, giving the service providers the ability to deliver a seamless mobility experience

LTE has been set aggressive performance requirements that rely on physical layer technologies, such as, OFDM and MIMO systems, Smart Antennas to achieve these targets. The main objectives of LTE are to minimize the system and User Equipment (UE) complexities, allow flexible spectrum deployment in existing or new frequency spectrum and to enable co-existence with other 3GPP RATs.

2.2 Performance goals for LTE

E-UTRA is expected to support different types of services including web browsing, FTP, video streaming, VoIP, online gaming, real time video, push-to-talk and push-to-view. Therefore, LTE is being designed to be a high data rate and low latency system as indicated by the key performance criteria shown in Table 1. The bandwidth capability of a UE is expected to be 20MHz for both transmission and reception. The service provider can however deploy cells with any of the bandwidths listed in the table. This gives flexibility to the service providers' to tailor their offering dependent on the amount of available spectrum or the ability to start with limited spectrum for lower upfront cost and grow the spectrum for extra capacity.

Beyond the metrics LTE is also aimed at minimizing cost and power consumption while ensuring backward-compatibility and a cost effective migration from UMTS systems. Enhanced multicast services, enhanced support for end-to-end QoS and minimization of the number of options and redundant features in the architecture are also being targeted.

The spectral efficiency in the LTE DL is 3 to 4 times of that of Release 6 HSDPA while in the UL, it is 2 to 3 times that of Release 6 HSUPA. The handover procedure within LTE is intended to minimize interruption time to less than that of circuit-switched handovers in 2G networks. Moreover the handovers to 2G/3G systems from LTE are designed to be seamless.

Table 2.1: LTE performance requirements [L1]

Metric	Requirement
Peak data rate	DL: 100Mbps UL: 50Mbps (for 20MHz spectrum)
Mobility support	Up to 500kmph but optimized for low speeds from 0 to 15kmph
Control plane latency (Transition time to active state)	< 100ms (for idle to active)
User plane latency	< 5ms
Control plane capacity	> 200 users per cell (for 5MHz spectrum)
Coverage (Cell sizes)	5 – 100km with slight degradation after 30km
Spectrum flexibility	1.25, 2.5, 5, 10, 15, and 20MHz

2.3 Current state

While 3GPP Release 8 is a formative standard, much of the Release addresses upgrading 3G UMTS to 4G mobile communications technology, which is essentially a mobile broadband system with enhanced multimedia services built on top.

The standard includes:

* For every 20 MHz of spectrum, peak download rates of 326.4 Mbit/s for 4x4 antennas, and 172.8 Mbit/s for 2x2 antennas. [L2]

* Peak upload rates of 86.4 Mbit/s for every 20 MHz of spectrum using a single antenna. [L2]

* Five different terminal classes have been defined from a voice centric class up to a high end terminal that supports the peak data rates. All terminals will be able to process 20 MHz bandwidth.

* At least 200 active users in every 5 MHz cell. (Specifically, 200 active data clients)

* Sub-5 ms latency for small IP packets

* Increased spectrum flexibility, with supported spectrum slices as small as 1.5 MHz and as large as 20 MHz W-CDMA requires 5 MHz slices, leading to some problems with roll-outs of the technology in countries where 5 MHz is a commonly allocated amount of spectrum, and is frequently already in use with legacy standards such as 2G GSM and cdmaOne. Limiting sizes to 5 MHz also limited the amount of bandwidth per handset).

* Optimal cell size of 5 km, 30 km sizes with reasonable performance, and up to 100 km cell sizes supported with acceptable performance. This statement should be treated with caution. Comment: Without considering the radio propagation environment and the frequency used, that it is 2.6 GHz, it is meaningless to talk about cell size. For a given power budget, the higher the frequency, the more challenging range becomes in a mobile cellular system.

* Co-existence with legacy standards (users can transparently start a call or transfer of data in an area using an LTE standard, and, should coverage be unavailable, continue the operation without any action on their part using GSM/GPRS or W-CDMA-based UMTS or even 3GPP2 networks such as cdmaOne or CDMA2000).

* Support for MBSFN. This feature can deliver services such as Mobile TV using the LTE infrastructure, and is a competitor for DVB-H-based TV broadcast.

* PU2RC as a practical solution for MU-MIMO. The detailed procedure for the general MU-MIMO operation is handed to the next release, e.g., LTE-Advanced, where further discussions will be held.

A large amount of the work is focused on simplifying the architecture of the system, as it transits from the existing UMTS circuit + packet switching combined network to an all-IP flat architecture system.

3

Path Loss and Shadowing

Path loss is caused by dissipation of the power radiated by the transmitter as an effect of the propagation channel. Shadowing is caused by obstacles between the transmitter and receiver that attenuate signal power due to absorption, reflection, scattering, and diffraction. Variation due to path loss occurs over very large distances (100-1000 meters), whereas variation due to shadowing occurs over distances proportional to the length of the obstructing object (10-100 meters normally in outdoor environments). Since variations due to path loss and shadowing occur over relatively large distances, this variation is sometimes referred to as large-scale propagation effects. Variation due to multipath occurs over very short distances, on the order of the signal wavelength, so these variations are sometimes referred to as small-scale propagation effects.

After a brief introduction of radio wave propagation, it is presented the simplest model for signal propagation: free space path loss. Ray tracing model is then described. This model is used to approximate wave propagation according to Maxwell's equations, and is an accurate model when the number of multipath components is small and the physical environment is known.

While this chapter presents some channel models for path loss and explains why statistical models are used instead of ray tracing models, an in depth explanation of propagation models at different frequencies is covered in chapter 4.

3.1 Radio Wave Propagation

Electromagnetic waves propagate through environments where they are reflected, scattered, and diffracted by walls, terrain, buildings, and other objects. The ultimate details of this propagation can be obtained by solving Maxwell's equations with boundary conditions. This requires the calculation of large and complex structures. Since these calculations are difficult, and many times the needed parameters are not available, approximations have been developed without using that Maxwell's equations.

The most common approximations use ray-tracing techniques. These techniques approximate the propagation representing the wavefronts as simple particles determining the reflection and refraction effects on the wavefront but ignoring the more complex scattering phenomenon predicted by Maxwell's equations. Many propagation environments are not accurately reflected with ray tracing models. In these cases it is common to develop analytical models based on empirical measurements, and it will be discussed below several of these most common empirical models.

Often the complexity and variability of the radio channel makes it difficult to obtain an accurate deterministic channel model. For these cases statistical models are often used. The attenuation caused by signal path obstructions such as buildings or other objects is typically characterized statistically, as described in chapter 4.

The models are developed mainly for signals in the UHF and SHF bands, from .3-3 GHz and 3-30 GHz, respectively. This range of frequencies is quite favorable for wireless system operation due to its propagation characteristics and relatively small required antenna size. It is assumed for LTE networks that the path distances are small enough so as not to be affected by the earth's curvature since do not normally exceed a 5km length.

The path loss (P_L) of the channel is defined as the difference in dB between the transmitted (P_t) and received (P_r) signal power:

$$P_L \text{ dB} = 10 \log_{10} \frac{P_t}{P_r} \text{ dB}. \tag{3.1}$$

3.2 Free-Space Path Loss

When a signal is transmitted through free space to a receiver located at distance d from the transmitter, assuming there are no obstructions between the transmitter and receiver, the channel model associated with this transmission is called a line-of-sight (LOS) channel.

The received signal power falls off inversely proportional to the square of the distance d between the transmitting and receiving antennas and to the square of the signal wavelength. This dependence of received power on the signal wavelength λ is due to the effective area of the receive antenna [P1]. Thus, the received power can be expressed in dBm as:

$$P_r \text{ dBm} = P_t \text{ dBm} + 10\log_{10}(G_l) + 20\log_{10}(\lambda) - 20\log_{10}(4\pi) - 20\log_{10}(d) \quad (3.2)$$

FSPL is defined as the path loss of the free-space model:

$$P_L \text{ dB} = 10\log_{10}\frac{P_t}{P_r} = -10\log_{10}\frac{G_l\lambda^2}{(4\pi d)^2} \quad (3.3)$$

where: - P_L is the path loss in dB.

- P_t is the transmitted power in dBm.

- P_r is the received power in dBm.

- G_l is the product of the transmitting and receiving antennas gain in the LOS direction.

- λ is the signal wavelength.

- d is the path length.

3.3 Ray Tracing

Typically in an urban environment, a radio signal transmitted encounters multiple objects that produce reflected, diffracted, or scattered copies of the transmitted signal. These additional copies of the transmitted signal, called multipath signal components, can be attenuated in power, delayed in time, and shifted in phase and/or frequency from the LOS signal path at the receiver. The multipath and transmitted signals are summed together at the receiver, which often produces distortion in the received signal relative to the transmitted signal.

In ray tracing a finite number of reflectors with known location and dielectric properties are assumed. The details of the multipath propagation can then be solved using Maxwell's equations with appropriate boundary conditions [P2, P3]. The error of the ray tracing approximation is pretty small when the receiver is many wavelengths from the nearest scatterer, and all the scatterers are large relative to a wavelength and fairly smooth. However, the computational complexity of this solution makes it impractical as a general modeling tool.

If the transmitter, receiver and reflectors are all immobile, then the impact of the multiple received signal paths and their delays relative to the LOS path are fixed. However, if the source or receiver is moving, then the characteristics of the multiple paths vary with time. These time variations are deterministic when the number, location, and characteristics of the reflectors are known over time. Otherwise, statistical models must be used. Similarly, if the number of reflectors is very large or the reflector surfaces are not smooth then we must use statistical approximations to characterize the received signal. Hybrid models, which combine ray tracing and statistical fading, can also be found in the literature [P4, P5], however they will not be described here since they are out of the scope of a master thesis task.

3.4 Empirical Path Loss Models

Mobile communication systems normally operate in complex propagation environments that cannot be accurately modeled by free-space path loss or ray tracing. A number of path loss models have been developed to predict path loss in typical wireless environments such as large urban macrocells or microcells and more recently inside buildings. These models are mainly based on empirical measurements over a given distance in a given frequency range and over a particular geographical area. However, the application of these models is not always restricted to environments in which the empirical measurements were made, what makes the accuracy of such empirically-based models applied to more general environments questionable somehow. Nevertheless, many wireless systems use these models as a basis for performance analysis.

Analytical models characterize Pr/Pt as a function of distance, so path loss is well defined. In contrast, empirical measurements of Pr/Pt as a function of distance include the effects of path loss, shadowing, and multipath. In order to remove multipath effects, empirical measurements for path loss typically average their received power measurements and the corresponding path loss at a given distance over several wavelengths. This average path loss is called the local mean attenuation (LMA) at distance d, and generally decreases with d due to free space path loss and signal obstructions. The LMA in a given environment, like a city, depends on the specific location of the transmitter and receiver corresponding to the LMA measurement. To characterize LMA more generally, measurements are typically taken throughout the environment, and possibly in multiple environments with similar characteristics. Thus, the empirical path loss PL(d) for a given environment is defined as the average of the LMA measurements at distance d, averaged over all available measurements in the given environment. The empirical path loss models given in chapter 4 are all obtained from average LMA measurements.

Statistical methods (also called stochastic or empirical) are based on measured and averaged losses along typical classes of radio links. For wireless communications in the VHF and UHF frequency band, one of the most commonly used methods is that of Okumura-Hata [P6] as refined by the COST 231 project [P7]. Other well-known models are those of Walfisch-Ikegami [P8] and W.C.Y. Lee [P9].

The path loss in other frequency bands (microwave) is predicted with similar methods, though the concrete algorithms and formulas may be very different from those for VHF/UHF. Reliable prediction of the path loss in the SHF band is particularly difficult, and its accuracy is comparable to weather predictions.

Finally, easy approximations for calculating the path loss over distances significantly shorter than the distance to the radio horizon are presented as a prior approach:

* In free space the path loss increases with 20 dB per decade (one decade is when the distance between the transmitter and the receiver increases ten times) or 6 dB per octave (one octave is when the distance between the transmitter and the receiver doubles). This can be used as a very rough first-order approximation for SHF (microwave) communication links.

* For signals in the UHF/VHF band propagating over the surface of the Earth the path loss increases with roughly 35-40 dB per decade (10-12 dB per octave). This can be used in cellular networks as a first guess. [P9]

4

Propagation Prediction Models

A propagation prediction model is an empirical formulation to calculate and predict radio propagation. There exist many such models, each based on experienced and observed measurements. A model takes in account four effects as attenuation, reflection, diffraction, scattering and it is impossible to calculate deterministically.

Propagation models are tailored for specific propagation scenarios, making the propagation statistics as realistic as possible. Propagation in open areas is calculated by using terrain models, whereas metropolitan areas are calculated by using a model which has been developed in a similar scenario (urban and sub-urban areas).

As will be described in Appendix A, a city comprises of different environmental classifications, hence different propagation models and parameters can be used for a more accurate prediction of the coverage area. This chapter will describe some of the existing models relevant for this thesis.

4.1 General Considerations

Wave propagation models are necessary to determine propagation characteristics for any mobile radio systems. The phenomena which influence radio wave propagation can generally be described by four basic mechanisms: attenuation, reflection, diffraction and scattering. For the practical prediction of propagation in a real environment these mechanisms must be described by approximations.

This requires a three-stage modeling process: In the first step the real terrain has to be digitized. The information includes terrain height information, land usage data, building shape and building surface characteristics. Further investigations have been stressed on proper processing techniques to extract the relevant information in a time-efficient manner. The second modeling step includes the definition of mathematical approximations for the physical propagation mechanisms. Based on the solutions for the basic problems both deterministic and empirical approaches have been developed for the various environments, which is the third modeling step.

As the definition of cell types is not unique in the literature, the cell type definition used in this chapter is explained more detailed.

Cell type	**Typical cell radius**	**Typical position of BS**
Macro-cell	1 to 30 km	Outdoor; mounted above medium roof-top level, heights of all surrounding buildings are below base station antenna height
Small macro-cell	0.5 to 3 km	Outdoor; mounted above medium roof-top level, heights of some surrounding buildings are above base station antenna height
Micro-cell	Up to 1km	Outdoor; mounted below medium roof top level
Pico-cell / in-house	Up to 500m	Indoor or outdoor mounted below roof-top level

Table 4.1: Definition of cell types.

In "large cells" and small cells" the base station antenna is installed above roof-tops. In this case the path loss is determined mainly by diffraction and scattering at roof-tops in the vicinity of the mobile, i.e. the main rays propagate above the roof tops. In "micro-cells" the base station antennas are mounted generally below roof tops. Wave propagation is determined by diffraction and scattering around buildings, i.e., the main rays propagate in street canyons somehow like in grooved waveguides. "Pico-cells" are applied to cover mainly indoor or very small outdoor areas. In any case the base station antenna of a pico-cell is mounted inside a building or fairly below roof-top level in outdoors. The summary of the different cell types is shown in Table 4.1.

LTE solutions are mainly within large-cell and small macro-cell types from 0.5 to 5km.

4.2 Propagation Mechanisms

4.2.1 Introduction

The propagation mechanisms are examined to help the development of propagation prediction models and to enhance the understanding of electromagnetic wave propagation phenomena.

Propagation models are more efficient when only the most dominant phenomena are taken into account. Which radio propagation phenomena need to be taken into account and in how much detail does it need to be considered will also differ depending if it is liked modeling the average signal strength, the fading statistic, the delay spread or any other characteristics.

The mobile radio environment causes some special difficulties to the investigation of propagation phenomena:

1) The distances between a BS and a MS range from some meters to several kilometers.

2) Man-made structures and natural features have size ranging from smaller to much larger than a wavelength and affect the propagation of radio waves.

3) The description of the environment is usually not at our disposal in very much detail.

Two complementary approaches can be identified to deal with these difficulties:

4) Experimental investigations (i.e. live measurements) which are closer to the reality but at the expense of weaker control on the adaption to the environment.

5) Theoretical investigations which consider only simplified model of the reality but give an excellent control of the adaptation to the environment.

A brief description of the possibilities, advantages and disadvantages offered by experimental or theoretical investigations are given below to give some insights on how the propagation phenomena can be determined.

Experimental investigations.

Based on measurements, the propagation mechanisms can be identified if the experiments are designed carefully over a chosen area or/and if numerous measurements are analyzed. The major disadvantage of experimental investigations is the difficulty in the design of the experiments and in the interpretation of the results which usually exhibit a mix of several propagation phenomena.

Theoretical investigations.

Software simulation or analytical studies of propagation phenomena have one main advantage over experimental investigations: The environment and the geometry are more easily described and modified. The major disadvantage of theoretical investigations is that the validity of the results may hold only for the particular case being simulated or investigated. That is why should always be validated in practice.

4.2.2 Main mechanisms

The main propagation mechanisms are explained below. As smaller wavelengths, the wave propagation becomes similar to the propagation of light rays. A radio ray is assumed to propagate along a straight line bent mainly by refraction, reflection, diffraction or scattering.

Refraction

Refraction is the change in direction of a wave due to a change in its speed. Refraction is described by Snell's law, which states that the angle of incidence θ1 is related to the angle of refraction θ2 by:

$$\sin \theta 1 / \sin \theta 2 = v1 / v2 = n2 / n1 \quad (4.1)$$

where v1 and v2 are the wave velocities in the respective media, and n1 and n2 the refractive indices. In general, the incident wave is partially refracted and partially reflected; the details of this behavior are described by the Fresnel equations [M1].

Specular reflection

The specular reflection is a phenomena where a ray is reflected at an angle equal to the incidence angle. The reflected wave fields are related to the incident wave fields through a reflection coefficient. The most common expression for the reflection is the Fresnel reflection coefficient which is valid for an infinite boundary between two mediums, for example: air and concrete. The Fresnel reflection coefficient depends upon the polarisation and the wavelength of the incident wave field and on the permittivity and conductivity of each medium.

Specular reflections are mainly used to model reflection from the ground surface and from building walls. Whether scattering or truly specular reflection is the proper propagation phenomena was not mentioned and cannot be readily determined since the two phenomena are usually involved simultaneously, which can be tested using the Rayleigh criterion for surface roughness.

Diffraction

The diffraction process is the propagation phenomena which explain the transition from the lit region to the shadow regions behind the corner of a building or over the roof-tops. Diffraction by a single wedge can be solved in various ways: Empirical formulas [M2]. Perfectly Absorbing Wedge (PAW) [M3], Geometrical Theory of Diffraction Propagation Prediction Models (GTD) [M4], Uniform Theory of Diffraction (UTD) [M5] or even more exact formulations [M6], [M7]. The advantages and disadvantages of using either one formulation is difficult to address since it may not be independent on the environments under investigations.

One major difficulty is to express and use the proper boundaries in the derivation of the diffraction formulas. Another problem is the existence of wedges in real environments: the complexity of a real building corner or of the building roofs clearly illustrates the modelling difficulties.

Multiple diffraction

For the case of multiple diffraction, the complexity increases dramatically. In the case of propagation over roof-top the results of Walfisch and Bertoni [M8] has been used to produce the COST-Walfisch-Ikegami model [P7]. The approximate procedures of Giovannelli [M9] or Deygout [M10] have been revisited by Causebrook [M11]. The limitations of these approximations lead several researchers to more accurate methods. All these methods are numerical schemes to compute the multiple diffraction and apart from the last contribution they do not give a clear physical understanding of the multiple diffraction process, at least not yet.

For the case of diffraction over multiple screens of arbitrary heights and spacings a solution is obtained by Saunders in [M12] from a Vogler method that is very time-consuming to evaluate. The limitation of the solution is, that it is not applicable when one spacing becomes very small relative to other spacings. Thus the method cannot predict the collapse of two screens into one.

In ITU-R P.526 [R1] additional equations are given to compute effects of multiple diffractions around curved cylinders what corresponds with one of the main part of the study of this thesis.

Scattering

Rough surfaces and finite surfaces scatter the incident energy in all directions with a radiation diagram which depends on the roughness and size of the surface or volume (Page 108, W.C.Y Lee [P9]). The dispersion of energy through scattering means a decrease of the energy reflected in the specular direction explained by the Rayleigh criterion.

More realistic scattering processes have been investigated within the COST 231 but the influence of individual urban scatterers such as lamp post, traffic light, windows, and cars has not yet been introduced. That remains as a future research.

Other additional mechanisms are the ones listed below. Despite they are not usually taken into account in the most common propagation models nowadays they might be considered in a near future researchs,

Penetration and absorption

Penetration loss due to building walls have been investigated within COST 231 and found very dependent on the particular situation.

Absorption due to trees, body absorption or atmospherics effects are also propagation mechanisms difficult to quantify with precision.

Guided wave

The wave guiding phenomena can be viewed as a particular propagation mechanism based on multiple reflections or propagation modes in street canyon, in corridors or tunnels.

Atmospheric effects

Atmospheric effects are not usually taken into account for mobile radio applications at UHF frequencies, although empirical correction factors can be incorporated in some coverage prediction tools to handle seasonal variations. However, it is an important factor when higher frequencies (e.g., 60 GHz) are used.

For different propagation mechanisms the range dependence of the field strength is given in the following (See Fig 4.1):

· For specular reflection the field is proportional to $(d1+d2)^{-1}$

· For single diffraction, the field is proportional to $(d1/d2(d1+d2))^{-0.5}$

· For multiple diffraction, the field is proportional to $d^{-1.9}$ [M8]

· For volume scattering and rough surface scattering, the field is proportional to $(d1d2)^{-1}$

· For penetration and absorption, the field is mainly attenuated by a constant.

· For the wave guiding phenomena, the logarithm of the field is proportional to d^{-1}.

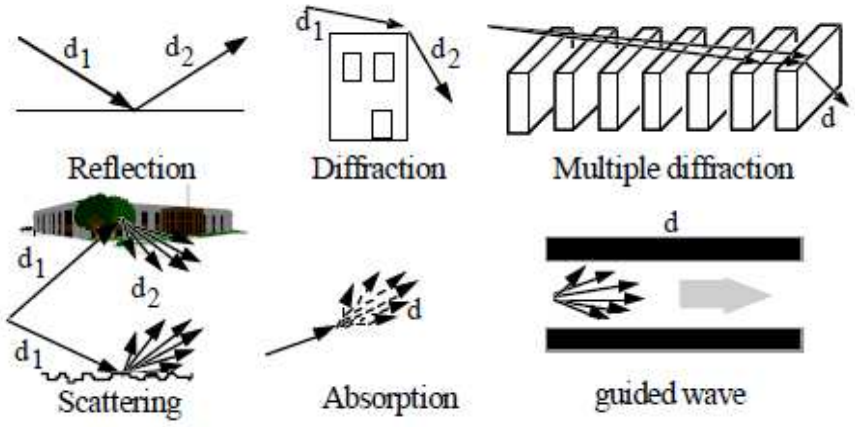

Fig. 4.1: Propagation phenomena [P7]

4.3 Propagation Model List

This section presents the different propagation models studied within the scope of this thesis, explain the different particularities, advantages and innovations respect to the other literature models found that makes them interesting for a possible future implementation on Astrix and ends up recommending some advices for trying to help somehow a possible improvement of the mentioned Teleplan AS radio planning tool.

4.3.1 Okumura-Hata Model

Introduction

Okumura-Hata is the most widely used model in radio frequency propagation for predicting the behavior of cellular transmissions in city outskirts and other rural areas. This model incorporates the graphical information from Okumura model [M13] and develops it further to better suite the need. This model also has two more varieties for transmission in Urban Areas and Open Areas.

Okumura's report presents an empirical formula for propagation loss in order to put his propagation prediction method to computational use. The propagation loss is presented in a simple form: A + B log10 R, where A and B are frequency and antenna height functions and R is the distance. The introduced formula is applicable to system designs for UHF and VHF land mobile radio services, with a small formulation error, under the following condition: frequency range 100-1500 MHz, distance 1-20 km, base station antenna height 30-200 m, and vehicular antenna height 1-10 m [M14].

Since the propagation loss can be treated as a formula, it becomes possible to put the formula into various calculations about system planning. However, since the formula can only be applied in restricted ranges, it is necessary to take notice of its applicable ranges and units as explained in the Table 4.2 below.

Propagation loss and empirical formula

EXPERIMENTAL FORMULA FOR PROPAGATION LOSS

Urban Area	$Lp = 69.55 + 26.16 \cdot \log_{10} f_c - 13.82 \cdot \log_{10} h_b - a(h_m)^*$ $+ (44.9 - 6.55 \cdot \log_{10} h_b) \cdot \log_{10} R$ (dB)
	*• correction factor for vehicular station antenna height medium-small city $a(h_m) = (1.1 \cdot \log_{10} f_c - 0.7) \cdot h_m - (1.56 \cdot \log_{10} f_c - 0.8)$ large city $a(h_m) = 8.29 \cdot (\log_{10} 1.54 h_m)^2 - 1.1$; $f_c \leq 200$ MHz $= 3.2 \cdot (\log_{10} 11.75 h_m)^2 - 4.97$; $f_c \geq 400$ MHz
Suburban Area	$L_{ps} = Lp\{\text{Urban area}\} - 2\{\log_{10}(f_c/28)\}^2 - 5.4$ (dB)
Open Area	$L_{po} = Lp\{\text{Urban area}\} - 4.78 \cdot (\log_{10} f_c)^2 + 18.33 \cdot \log_{10} f_c - 40.94$ (dB)

where

f_c : frequency (MHz) ---------- 150 ~ 1500 (MHz)

h_b : base station effective antenna height (m) ------ 30 ~ 200 (m)

h_m : vehicular station antenna height (m) --------- 1 ~ 10 (m)

R : distance (km) ---------- 1 ~ 20 (km)

Table 4.2: Okumura-Hata formulas for path loss calculation [M14]

Where Lp, Lps and Lpo are the path losses for each type of area.

Some examples of different prediction curves using Okumura-Hata formulas over urban areas are shown in the figures below.

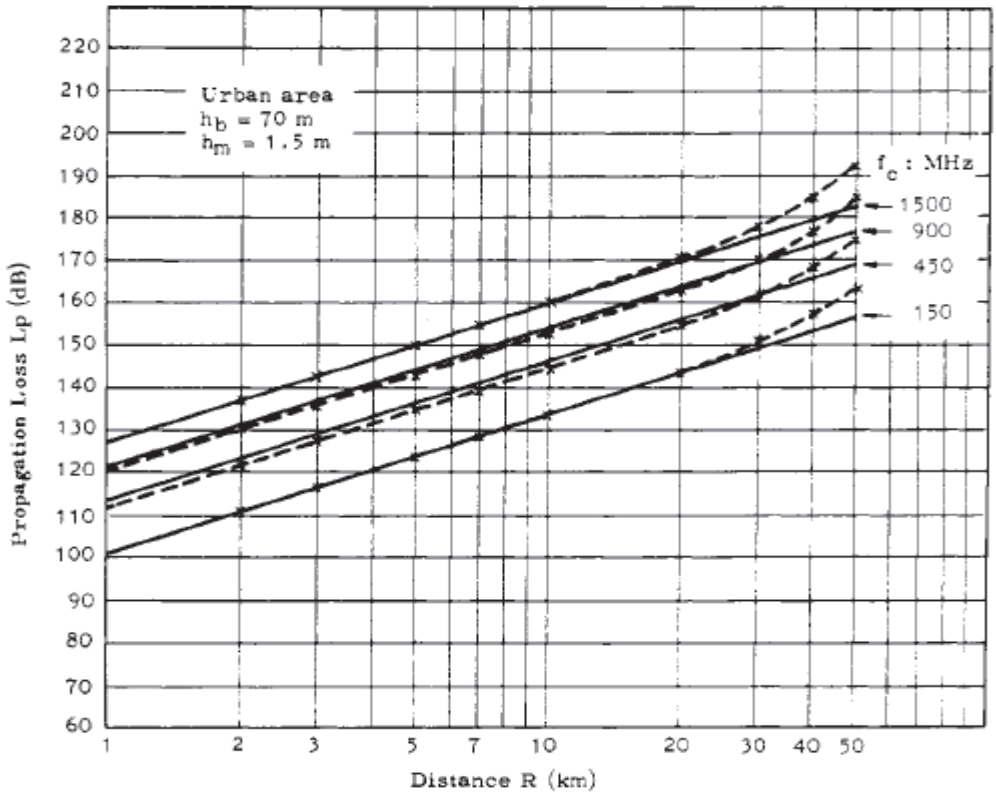

Figure 4.2.:Path loss varying f_c (carrier frequency) [M14]

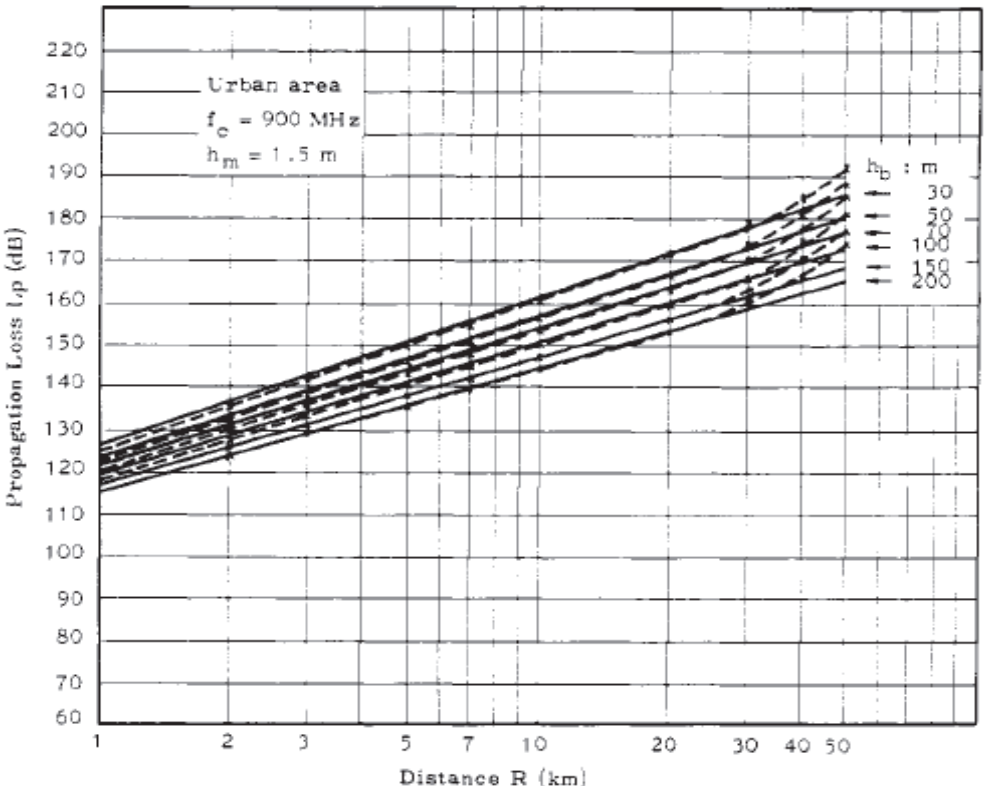

Figure 4.3: Path loss changing h_b (mobile antenna height) [M14]

4.3.2 ITU-R P.526 Propagation by diffraction

Introduction

The methods described in this recommendation are used for the calculation of field strengths over diffraction paths, which may include a spherical earth surface, or irregular terrain with different kinds of obstacles.

Although diffraction is produced only by the surface of the ground or other obstacles, account must be taken of the mean atmospheric refraction on the transmission path to evaluate the geometrical parameters situated in the vertical plane of the path (angle of diffraction, radius of curvature, height of obstacle). For this purpose, the path profile has to be traced with the appropriate equivalent Earth radius (Recommendation ITU-R P.834)[R4]. If no other information is available, an equivalent Earth radius of 8 500 km may be taken as a basis.

Fresnel ellipsoids and Fresnel zones

In studying radio wave propagation between two points M and S, the intervening space can be subdivided by a family of ellipsoids, known as Fresnel ellipsoids, all having their focal points at M and S such that any point P on one ellipsoid satisfies the relation:

$$SPM - SM = n\frac{\lambda}{2} \tag{4.2}$$

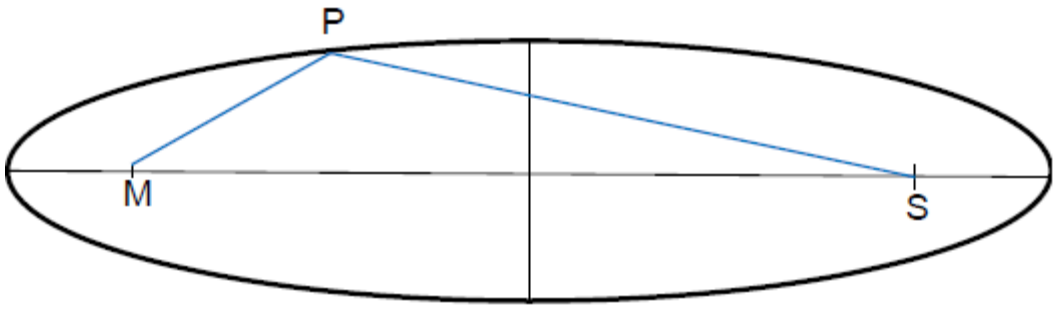

Figure 4.4: Fresnel ellipsoid [M15]

where n is a whole number characterizing the ellipsoid and n = 1 corresponds to the first Fresnel ellipsoid, etc., and λ is the wavelength.

As a practical rule, propagation is assumed to occur in line-of-sight, i.e. with negligible diffraction phenomena if there is no obstacle within the first Fresnel ellipsoid.

The radius of an ellipsoid at a point between the transmitter and the receiver is given by the following formula:

$$R_n = \left[\frac{n \lambda d_1 d_2}{d_1 + d_2} \right]^{1/2} \tag{4.3}$$

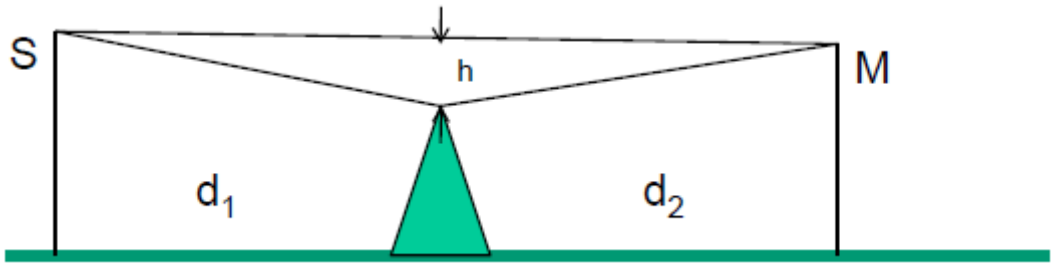

Figure 4.5: Fresnel geometry [M15]

or in practical units:

$$R_n = 550 \left[\frac{n d_1 d_2}{(d_1 + d_2) f} \right]^{1/2} \tag{4.4}$$

where f is the frequency (MHz) and d_1 and d_2 are the distances (km) between transmitter and receiver at the point where the ellipsoid radius (m) is calculated.

Some problems require consideration of Fresnel zones which are the zones obtained by taking the intersection of a family of ellipsoids by a plane. The zone of order n is the part between the curves obtained from ellipsoids n and n – 1, respectively.

Diffraction over obstacles and irregular terrain

Many propagation paths encounter one obstacle or several separate obstacles and it is useful to estimate the losses caused by such obstacles. To make such calculations it is necessary to idealize the form of the obstacles, either assuming a knife-edge of negligible thickness or a thick smooth obstacle with a well-defined radius of curvature at the top. Real obstacles have, of course, more complex forms, so that the indications provided in this Recommendation should be regarded only as an approximation.

In those cases where the direct path between the terminals is much shorter than the diffraction path, it is necessary to calculate the additional transmission loss due to the longer path.

The data given below apply when the wavelength is fairly small in relation to the size of the obstacles, i.e., mainly to VHF and shorter waves (f > 30 MHz).

4.3.2.1 Single knife-edge obstacle

In this extremely idealized case (Figures 4.6.a and 4.6.b), all the geometrical parameters are combined together in a single dimensionless parameter normally denoted by v which may assume a variety of equivalent forms according to the geometrical parameters selected:

$$\nu = h\sqrt{\frac{2}{\lambda}\left(\frac{1}{d_1} + \frac{1}{d_2}\right)} \tag{4.5}$$

$$\nu = \theta\sqrt{\frac{2}{\lambda\left(\frac{1}{d_1} + \frac{1}{d_2}\right)}} \tag{4.6}$$

$$\nu = \sqrt{\frac{2\,d}{\lambda} \cdot \alpha_1 \alpha_2} \tag{4.7}$$

where:

h : height of the top of the obstacle above the straight line joining the two ends of the path. If the height is below this line, h is negative

d1 and d2 : distances of the two ends of the path from the top of the obstacle

d : length of the path

θ : angle of diffraction (rad); its sign is the same as that of h. The angle θ is assumed to be less than about 0.2 rad, or roughly 12°

α1 and α2 : angles between the top of the obstacle and one end as seen from the other end.

α1 and α2 are of the sign of h in the above equations.

Note – In equations (4.5) to (4.7) inclusive h, d, d1, d2 and λ should be in self-consistent units.

Figure 4.6: Geometrical elements [R1]

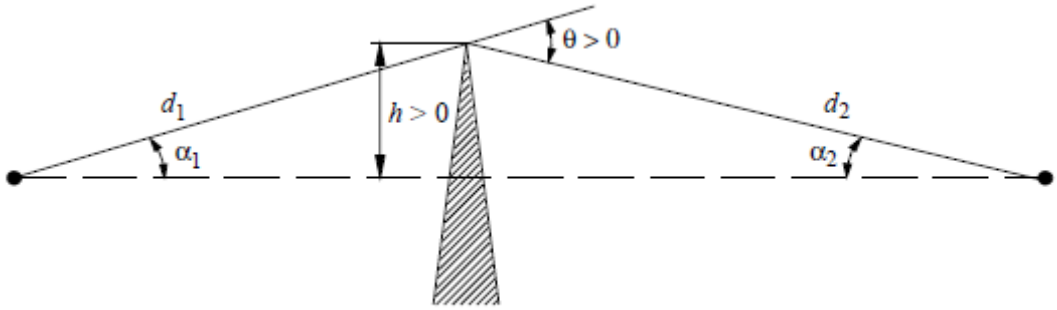

a)

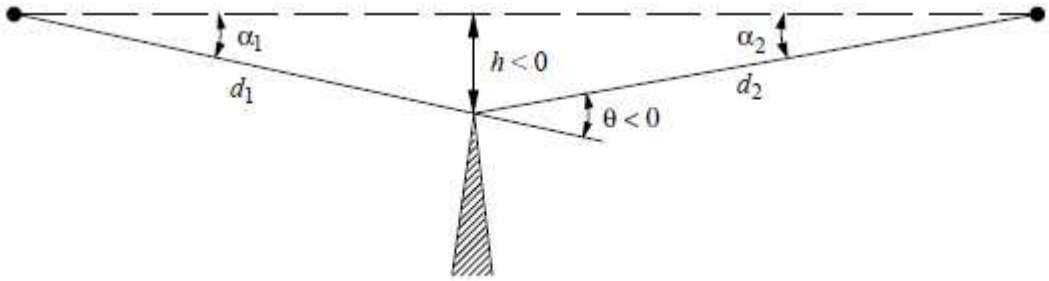

b)

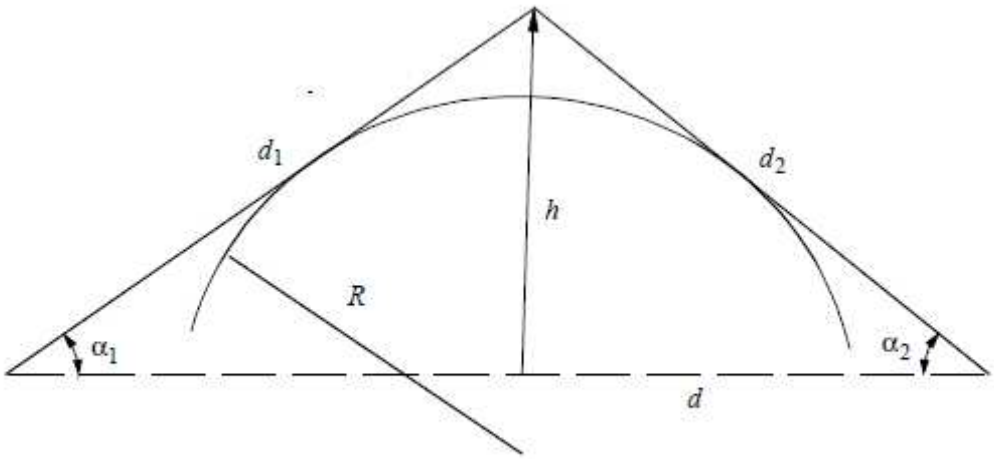

c)

Figure 4.7 gives, as a function of v, the loss (dB) caused by the presence of the obstacle. For v greater than – 0.7 an approximate value can be obtained from the expression:

$$J(\nu) = 6.9 + 20 \log\left(\sqrt{(\nu - 0.1)^2 + 1} + \nu - 0.1\right) \quad \text{dB} \tag{4.8}$$

Figure 4.7: Knife-edge diffraction loss

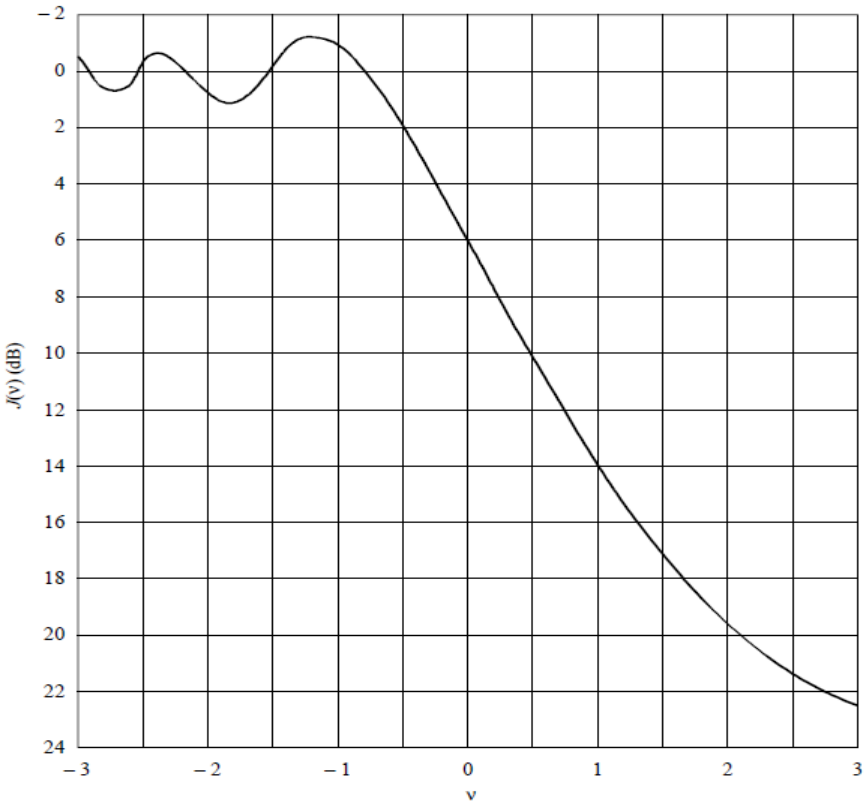

4.3.2.2 Single rounded obstacle

The geometry of a rounded obstacle of radius R is illustrated in Figure 4.6.c. Note that the distances d_1 and d_2, and the height h above the baseline, are all measured to the vertex where the projected rays intersect above the obstacle. The diffraction loss for this geometry may be calculated as:

$$A = J(v) + T(m,n) \text{ dB} \tag{4.9}$$

where:

a) J(v) is the Fresnel-Kirchoff loss due to an equivalent knife-edge placed with its peak at the vertex point. The dimensionless parameter v may be evaluated from any of equations (4.5) to (4.7) inclusive. For example, in practical units equation (4.5) may be written:

$$v = 0.0316\, h \left[\frac{2(d_1 + d_2)}{\lambda\, d_1\, d_2} \right]^{1/2} \tag{4.10}$$

where h and λ are in metres, and d1 and d2 are in kilometres.

J(v) may be obtained from Figure 4.7 or from equation (4.8). Note that for an obstruction to lineof- sight propagation, v is positive and equation (4.8) is valid.

b) T(m,n) is the additional attenuation due to the curvature of the obstacle:

$$T(m,n) = k\ m^b \tag{4.11}$$

where:

$$k = 8.2 + 12.0\, n \tag{4.12}$$

$$b = 0.73 + 0.27 \left[1 - \exp(-1.43\, n) \right] \tag{4.13}$$

and:

$$m = R \left[\frac{d_1 + d_2}{d_1\, d_2} \right] \Big/ \left[\frac{\pi R}{\lambda} \right]^{1/3} \tag{4.14}$$

$$n = h \left[\frac{\pi R}{\lambda} \right]^{2/3} \Big/ R \tag{4.15}$$

and R, d1, d2, h and λ are in self-consistent units.

T(m,n) can also be derived from Figure 4.8.

Note that as R tends to zero, m, and hence T(m,n), also tend to zero. Thus equation (4.9) reduces to knife-edge diffraction for a cylinder of zero radius.

It should be noted that the cylinder model is intended for typical terrain obstructions. It is not suitable for trans-horizon paths over water, or over very flat terrain, when the method of diffraction over a spherical earth [R1, §3] should be used.

Figure 4.8: The value of T(m,n) (dB) as a function of m and n

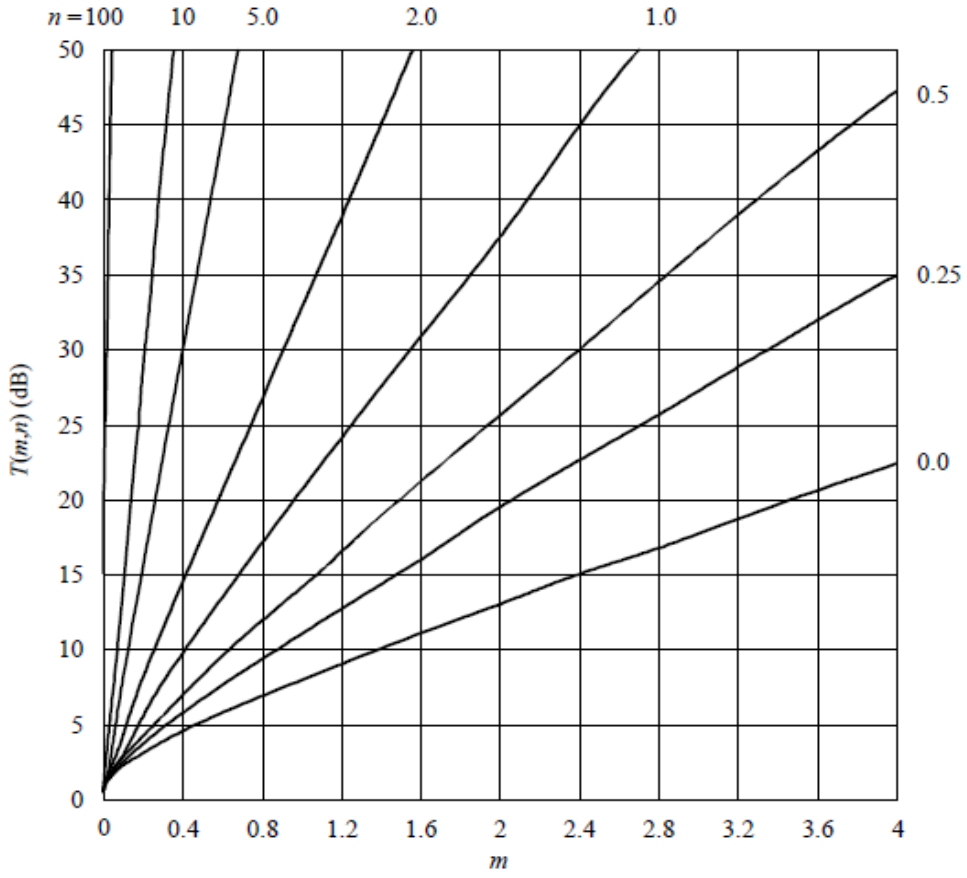

4.3.2.3 Double isolated edges

This method consists of applying single knife-edge diffraction theory successively to the two obstacles, with the top of the first obstacle acting as a source for diffraction over the second obstacle (see Figure 4.9). The first diffraction path, defined by the distances a and b and the height h'1, gives a loss L_1 (dB). The second diffraction path, defined by the distances b and c and the height h'2, gives a loss L_2 (dB). L_1 and L_2 are calculated using formulae of section 4.3.2.1 for single knife edges.

A correction term Lc (dB) must be added to take into account the separation b between the edges. Lc may be estimated by the following formula:

$$L_c = 10 \log \left[\frac{(a + b)(b + c)}{b(a + b + c)} \right] \quad (4.16)$$

which is valid when each of L_1 and L_2 exceeds about 15 dB. The total diffraction loss is then given by:

$$L = L_1 + L_2 + L_c \tag{4.17}$$

The above method is particularly useful when the two edges give similar losses.

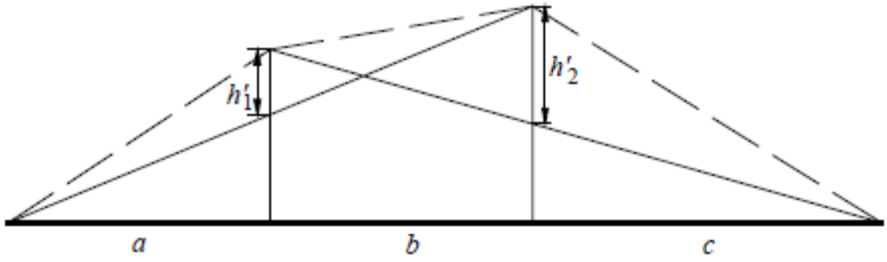

Figure 4.9: Method for double isolated edges

If one edge is predominant (see Figure 4.10), the first diffraction path is defined by the distances a and b + c and the height h1. The second diffraction path is defined by the distances b and c and the height h'2. The losses corresponding to these two paths are added, without addition of a third term.

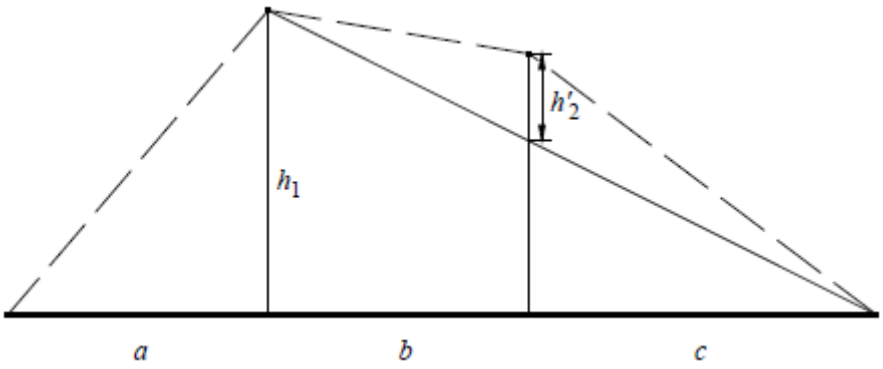

Figure 4.10: Method with one edge predominant

The same method may be applied to the case of rounded obstacles using formulae of section 4.3.2.2.

In cases where the diffracting obstacle may be clearly identified as a flat-roofed building a single knife-edge approximation is not sufficient. It is necessary to calculate the phasor sum of two components: one undergoing a double knife-edge diffraction and the other subject to an additional reflection from the roof surface. It has been shown that, where the reflectivity of the roof surface and any difference in height between the roof surface and the side walls are not accurately known, then a double knife-edge model produces a good prediction of the diffracted field strength, ignoring the reflected component.

4.3.2.4 General method for one or more obstacles

The following method, which is more general than that of section 4.3.2.3, is recommended for the diffraction loss over irregular terrain which forms one or more obstacles to line-of-sight propagation. The calculation takes Earth curvature into account via the concept of an effective Earth radius. This method is suitable in cases where a single general procedure is required for terrestrial paths over land or sea and for both line-of-sight and transhorizon (for LTE cases of distances less than 5km is not taken into account but for longer distances should be studied. It should be taken into account for paths longer than 20-30km (Page 102, W.C.Y. Lee [P9]) where it has been proved that Earth curvature has a considerable impact over the path loss calculations).

The procedure consists of finding the point within a given section of the profile with the highest value of the geometrical parameter v. The section of the profile to be considered is defined from point index a to point index b (a < b). If a + 1 = b there is no intermediate point and the diffraction loss for the section of the path being considered is zero. Otherwise the construction is applied by evaluating v_n (a < n < b) and selecting the point with the highest value of v. The value of v for the n-th profile point is given by:

$$v_n = h\sqrt{2d_{ab}/\lambda d_{an} d_{nb}} \tag{4.18}$$

where:

$$h = h_n + [d_{an}\, d_{nb}/2\, r_e] - [(h_a\, d_{nb} + h_b\, d_{an})/d_{ab}] \tag{4.19}$$

ha, hb, hn : vertical heights as shown in Figure 4.11

dan, dnb, dab : horizontal distances as shown in Figure 4.11

re : effective Earth radius

λ : wavelength

and all h, d, re and λ are in self-consistent units.

The diffraction loss is then given as the knife-edge loss J(v) according to equation (4.8) for v > −0.7, and is otherwise zero.

Note that equation (4.18) is derived directly from equation (4.5). The geometry of equation (4.19) is illustrated in Figure 4.11. The second term in equation (4.19) is a good approximation to the additional height at point n due to Earth curvature.

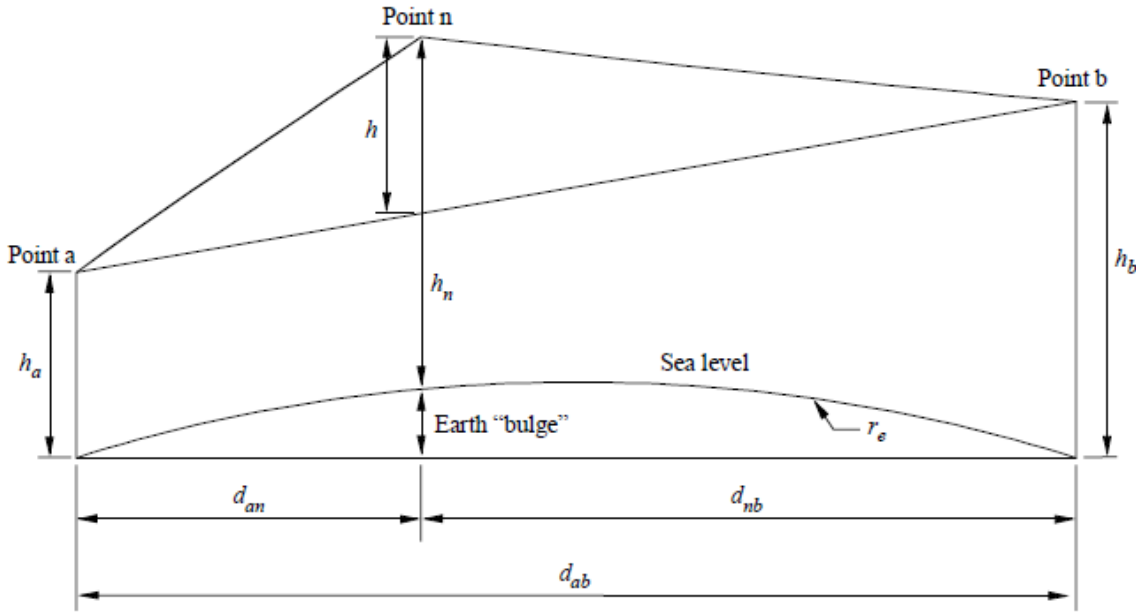

Figure 4.11: Geometry for a single edge

The above procedure is first applied to the entire profile from transmitter to receiver. The point with the highest value of v is termed the principal edge, p (which corresponds with point n in Figure 4.11), and the corresponding loss is J(vp).

If vp > – 0.7 the procedure is applied twice more:

– from the transmitter to point p to obtain vt and hence J(vt);

– from point p to the receiver to obtain vr and hence J(vr).

The excess diffraction loss for the path is then given by:

$$L = J(\nu_p) + T\,[J(\nu_t) + J(\nu_r) + C] \quad \text{for} \quad \nu_p > -0.7 \tag{4.20}$$

$$L = 0 \quad \text{for} \quad \nu_p \leq -0.7 \tag{4.21}$$

where:

C : empirical correction

$$C = 10.0 + 0.04D \tag{4.22}$$

D : total path length (km)

and

$$T = 1.0 - \exp\,[-J(\nu_p)/6.0] \tag{4.23}$$

Note that the above procedure, for transhorizon paths, is based on the Deygout method (which is presented on following Lee model section) limited to a maximum of 3 edges. For line-of-sight paths it differs from the Deygout construction in that two secondary edges are still used in cases where the principal edge results in a non-zero diffraction loss.

Where this method is used to predict diffraction loss for different values of effective Earth radius over the same path profile, it is recommended that the principal edge, and if they exist the auxiliary edges on either side, are first found for median effective Earth radius. These edges should then be used when calculating diffraction losses for other values of effective Earth radius, without repeating the procedure for locating these points. This avoids the possibility, which may occur in a few cases, of a discontinuity in predicted diffraction loss as a function of effective Earth radius due to different edges being selected.

4.3.3 Lee Model

The basis of propagation by diffraction for this thesis was taken from ITU-R P.526 recommendation since it is a model from ITU and was tested over different environments and with a considerable amount of measurements.

But I would also like to mention the approach taken by William C.Y.Lee [P9] which is basically the same one for knife-edge diffraction but it differs a little regarding to propagation over rounded obstacles.

There is presented some figures below to have a visual idea of the different kind of approaches used to calculate the path loss diffraction.

In Bullington's model [M16], two tangential lines are extended, one over each knife-edge obstruction, and the effective height of the knife-edge obstructions is measured as shown in Figure 4.12(a). This model can be difficult to apply, since the same effective height may be associated with various obstruction heights and separations, as shown in Figure 4.12(b). For example, the same effective height could be used to describe pair a or pair b. This model affords reasonable accuracy when two knife-edge obstructions are relatively close to each other.

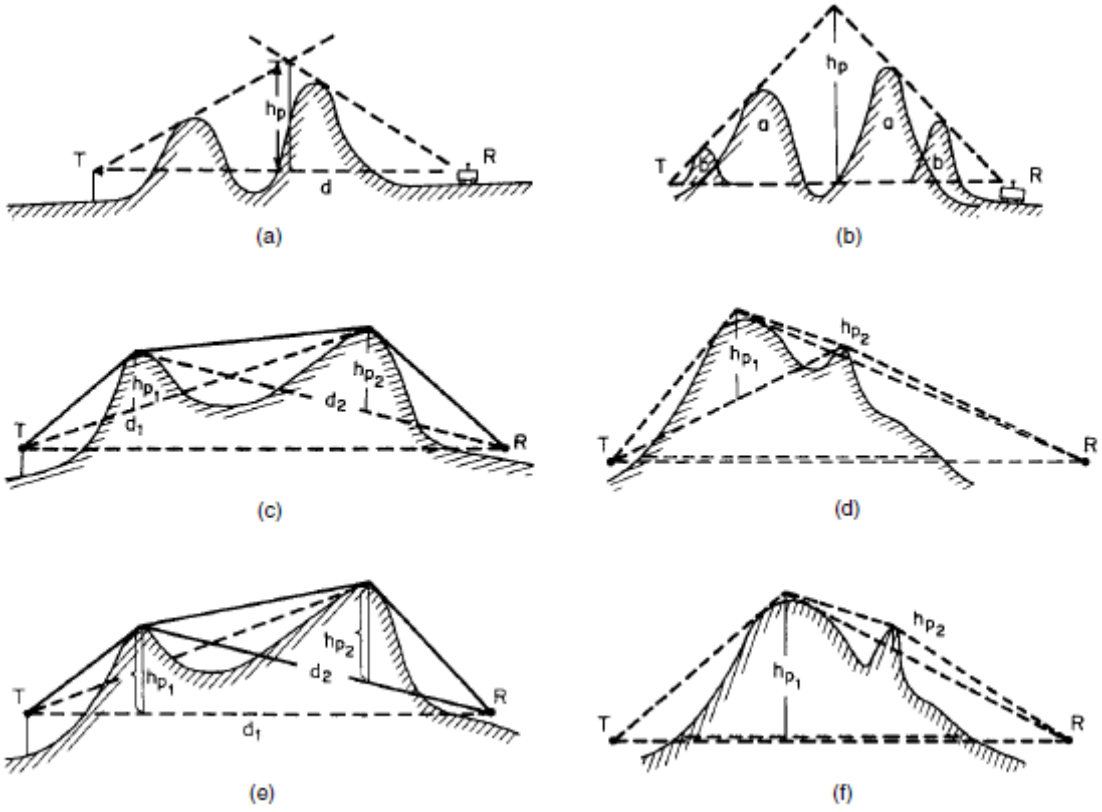

Figure 4.12: Double knife-edge diffraction: (a) and (b) Bullington's models; (c) and (d) Epstein and Peterson's models; (e) and (f) Picquenard's models

In Epstein and Peterson's model [M17], the heights hp_1 and hp_2 of the two effective knife-edge obstructions are obtained as shown in Figure 4.12(c). The excess path loss is the loss due to hp_1 plus the loss due to hp_2. This model is difficult to apply when the two obstructions are relatively close together, as shown in Fig. 4.12(d). This model provides the highest degree of accuracy when the two knife-edge obstructions are a large distance apart.

In Picquenard's model [M18], the limitations that were apparent in Bullington's and Epstein and Peterson's models are not present. Picquenard's technique is illustrated in Fig. 4.12(e). The height of one obstruction, hp_1, is obtained first without regard for the second obstruction, as though it did not exist. The height of the second obstruction, hp_2, is then measured by drawing a line from the top of the first obstruction to the receiver. The total path loss is then calculated from two loss terms. One term is derived from hp_1 and d_1, and the other from hp_2 and d_2. Since this method provides accurate results without the limitations previously noted [see Fig. 4.12(f)], it is recommended for general use.

4.3.3.1 Diffraction Loss over Rounded Hills according to Lee's Model

The main difference compared to ITU-R P.526 is that here the measurements [M19] shows that the knife-edge prediction value is always either above or below the measurement data values depending on the polarization of waves when the signal is diffracted over a rounded hill.

1. The formula for a knife-edge hill comes from the following integration.

$$F(v) = \frac{1-j}{2}\int_{v}^{\infty} \exp\left(\frac{j\pi z^2}{2}\right) dz \tag{4.24}$$

The parameter v is shown in equations (4.5) to (4.7). It can be expressed another way, as

$$v = \left(\frac{2r}{\lambda}\right)^{1/2} \cdot \theta \tag{4.25}$$

$$\frac{1}{r} = \frac{1}{r_1} + \frac{1}{r_2} \tag{4.26}$$

r, r1 and r2 are distances as shown in Figure 4.13.

θ is the scattering angle shown in Fig. 4.13 with hp shown in Figure 4.12

$$\theta \approx -h_p\left(\frac{1}{r_1} + \frac{1}{r_2}\right) \tag{4.27}$$

2. The calculation of the correction factors of using knife-edge formula due to a round hill top Lee applies the antenna shift δ, which is also called the visual displacement in height. Assuming that r1 > r2, then

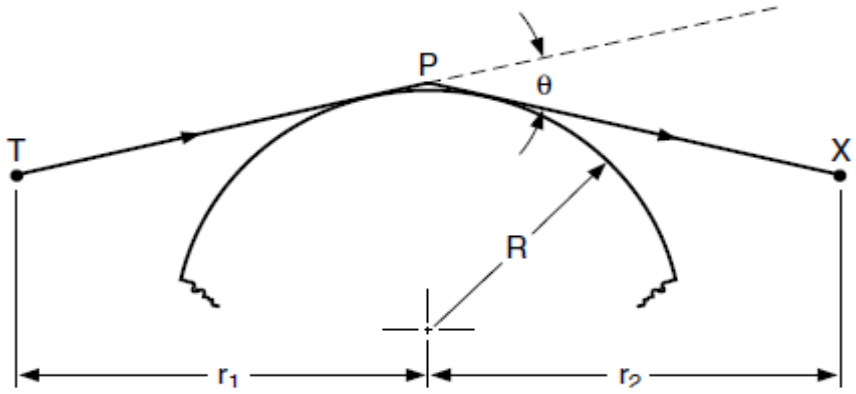

Figure 4.13: Geometry of obstacle arrangement for rounded hills [P9]

$$\delta = +0.316\left(1+\frac{r_2}{r_1}\right)\cdot\lambda\cdot\left(\frac{R}{\lambda}\right)^{1/3} \quad \text{vertical polarization (4.28)}$$

$$= -0.333\left(1+\frac{r_2}{r_1}\right)\cdot\lambda\cdot\left(\frac{R}{\lambda}\right)^{1/3} \quad \text{horizontal polarization (4.29)}$$

The difference σ in power between the knife-edge diffraction loss and the rounded-hill diffraction loss can be found as

$$\sigma = K\cdot\delta \tag{4.30}$$

where

$$K = \frac{1}{2r_2}\cdot\frac{1}{2(r_1+r_2)^2}\sqrt{\frac{2\beta r}{\pi}} \qquad \text{for } r_1 > r_2 \tag{4.31}$$

The power difference σ is shown in Fig. 4.14. The received power for vertical polarization wave over the rounded hills is stronger than that over the knife-edge, but the received power for horizontal polarization wave over the rounded hills is weaker than that over the knife-edge. In other words, for vertical polarization, the region behind the hill is brighter than that behind a knife-edge; for horizontal polarization, the region behind the hill is darker.

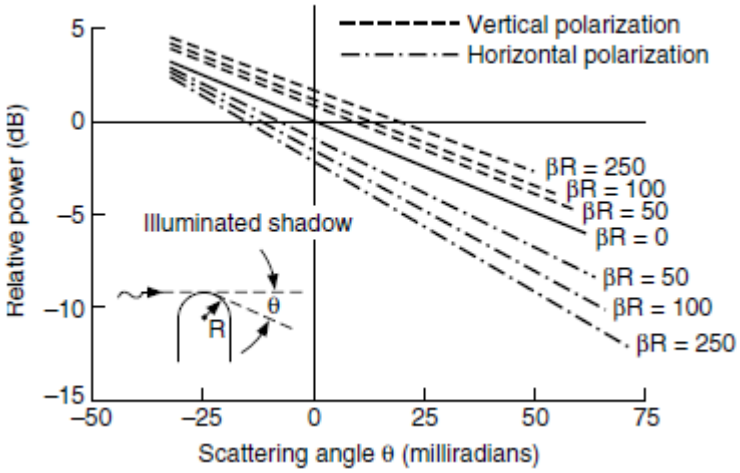

Figure 4.14: Variation of power behind a cylindrical mountain with scattering angle as a function of radius of curvature (far field) [P9]

This polarization concept is the main difference in comparison with ITU-R P.526 and that is what I noticed by comparing them with the Matlab code presented in the Appendix E.

For comparing both methods there are some parameters that change from each other and they are worth mentioning.

h from ITU-R P.526 is called h_p on Lee model.

d, d1 and d2 from ITU-R P.526 are called r, r1 and r2 on Lee model.

For values of R greater than 10m in the extreme case of h greater than 250m, d1 and d2 less than 500m at f=900 MHz, it is got a difference of 20-30 dB or even higher due to that different approach and it seems that ITU-R P.526 could not be an adequate model for that cases because it tends to overestimate the path loss compared with Lee model.

For all the other cases studied both models are kind of similar in performance but the ITU one normally gives a little higher additional values for over rounded obstacles propagation, what supposes that Lee model normally underestimates this additional parameter in comparison with ITU model since it takes that polarization discrimination approach which ITU model does not include so it seems that must be taken into consideration except for extreme cases of short paths and big rounded obstacles as the one mention above.

Anyway it is only a recommendation because it is not available the exact explanation of how the measurement were taken and what suppositions were made to develop each of this models to say exactly which is the most accurate one for each of the different cases that could appear on a radio planning research.

4.3.4 ITU-R P.1546 Method for point-to-area predictions for terrestrial services in the frequency range 30 MHz to 3 GHz

Considering that, for stations working in the same or adjacent frequency channels, the determination of the minimum geographical distance of separation required to avoid unacceptable interference due to long-distance tropospheric propagation is a matter of great importance.

ITU recommends that the procedures given in Annexes 1 to 8 [R2] should be adopted for point-to-area prediction of field strength for the broadcasting, land mobile, maritime mobile and certain fixed services (e.g. those employing point-to-multipoint systems) in the frequency range 30 MHz to 3 000 MHz and for the distances longer than 1 km.

The propagation curves

The propagation curves in Annexes 2, 3 and 4 represent field-strength values for 1 kW Effective Radiated Power (ERP) at nominal frequencies of 100, 600 and 2 000 MHz, respectively, as a function of various parameters; some curves refer to land paths, others refer to sea paths. Interpolation or extrapolation of the values obtained for these nominal frequency values should be used to obtain field strength values for any given required frequency using the method given in Annex 5, § 6.

The curves are based on measurement data mainly relating to mean climatic conditions in temperate regions containing cold and warm seas, e.g. the North Sea and the Mediterranean Sea. The land-path curves were prepared from data obtained mainly from temperate climates as encountered in Europe and North America. The sea-path curves were prepared from data obtained mainly from the Mediterranean and the North Sea regions. Extensive studies reveal that propagation conditions in certain areas of super-refractivity bounded by hot seas are substantially different.

However, the methods for interpolation and extrapolation between the families of field strength curves are general. Therefore, if families of curves exist for regions with different climates which experience substantially different prevailing radio propagation conditions, accurate characterization of radio propagation in these regions may be attained using the methods found in this Recommendation.

This Recommendation is not specific to a particular polarization.

Maximum field strengths

The curves have upper limits on the possible value of field strength which may be obtained under any conditions. These limits are defined in Annex 5, § 2 and appear as dashed lines on the graphs reproduced in Annexes 2, 3, and 4.

Computer-based tabulations

Although field strengths may be read directly from the curves presented as figures in Annexes 2, 3 and 4 of this Recommendation, it is intended that computer implementations (as ITU-R P.1546 Matlab programs listed in Appendix E) of the method will use tabulated field strengths available from the Radiocommunication Bureau.

Transmitting/base antenna height

The method takes account of the effective height of the transmitting/base antenna, which is the height of the antenna above terrain height averaged between distances of 3 to 15 km in the direction of the receiving/mobile antenna. For land paths shorter than 15 km where the information is available the method also takes account of the height of the transmitting/base antenna above the height of representative clutter (i.e. ground cover) at the location of the transmitting/base station. The transmitting/base antenna height, h_1, to be used for calculations is obtained using the method given in Annex 5, § 3.

Transmitting/base antenna heights used for curves

The field strength versus distance curves in Annexes 2, 3 and 4, and the associated tabulations, are given for values of h_1 of 10, 20, 37.5, 75, 150, 300, 600 and 1 200 m. For any values of h_1 in the range 10 m to 3 000 m an interpolation or extrapolation from the appropriate two curves should be used, as described in Annex 5, § 4.1. For h_1 below 10 m, the extrapolation to be applied is given in Annex 5, § 4.2. It is possible for the value of h_1 to be negative, in which case the method given in Annex 5, § 4.3 should be used.

Time variability

The propagation curves represent the field-strength values exceeded for 50%, 10% and 1% of time. A method for interpolating between these values is given in Annex 5, § 7. This Recommendation is not valid for field strengths exceeded for percentage times outside the range from 1% to 50%.

Mixed-path method

In cases where the radio path is over both land and sea the estimate of mixed-path field strength should be made using the method given in Annex 5, § 8. (This is an important concept that any of the other models takes into account and it should be further studied and quite recommended from my point of view for future Astrix versions).

Receiving/mobile antenna height

For land paths the curves give field-strength values for a receiving/mobile antenna height above ground, h_2 (m), equal to the representative height of ground cover around the receiving/mobile antenna location. The minimum value of the representative height of ground cover is 10 m. For sea paths the curves give field-strength values for h_2 = 10 m. To allow for values of h_2 different from the height represented by a curve a correction should be applied according to the environment of the receiving/mobile antenna. The method for calculating this correction is given in Annex 5, § 9.

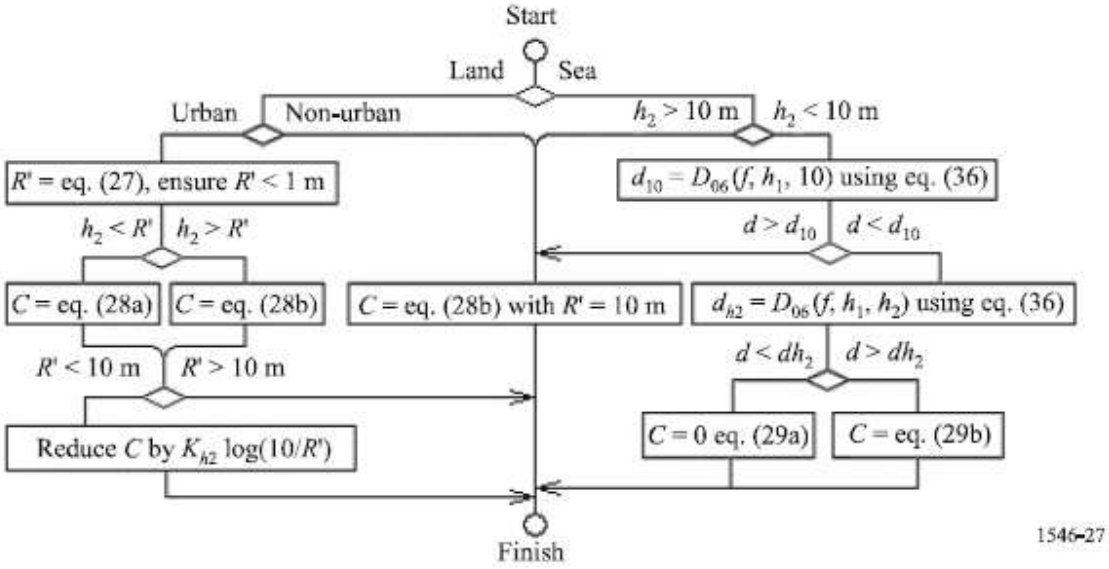

Figure 4.15: Flow chart for receiver/mobile antenna height correction [R2]

Terrain clearance angle correction

For land paths, improved accuracy of predicted field strengths can be obtained by taking into account terrain near the receiving/mobile antenna, if available, by means of a terrain clearance angle. When a calculation for a mixed path has been made, this correction should be included if the receiving/mobile antenna is adjacent to a land section of the path. More information on the terrain clearance angle correction is given in Annex 5, § 10.

Location variability

The propagation curves represent the field-strength values exceeded at 50% of locations within any area of typically 500 m by 500 m. For more information on location variability and the method for calculating the correction required for percentages of location other than 50%, see Annex 5, § 12.

Equivalent basic transmission loss

Annex 5, § 14 gives a method for converting from field strength for 1 kW ERP to the equivalent basic transmission loss.

Variability of atmospheric refractive index

It is known that median field strength and its variability over time varies in different climatic regions. The field strength curves given in Annexes 2, 3 and 4 apply to temperate climates. Annex 8 gives a method of adjusting the curves for different regions of the world based on the vertical atmospheric refractivity gradient data associated with Recommendation ITU-R P.453 [R6].

Compatibility with the Okumura-Hata method

Annex 7 gives the Hata equations for field strength prediction for mobile services in an urban environment, and describes the conditions under which this ITU Recommendation gives compatible results.

4.3.5 ITU-R P.452 Prediction procedure for the evaluation of microwave interference between stations on the surface of the Earth at frequencies above about 0.7 GHz

This Recommendation contains a prediction method for the evaluation of microwave interference between stations on the surface of the Earth at frequencies above about 0.7 GHz, accounting for both clear-air and hydrometeor scattering interference mechanisms.

Many types and combinations of interference path may exist between stations on the surface of the Earth, and between these stations and stations in space, and prediction methods are required for each situation. This Annex addresses one of the more important sets of interference problems, i.e. those situations where there is a potential for interference between microwave radio stations located on the surface of the Earth.

The prediction procedure is appropriate to radio stations operating in the frequency range of about 0.7 GHz to 50 GHz. For basic transmission losses, not exceeded for 1-50% time, the method is believed to be reliable at frequencies down to 50 MHz.

The method includes a complementary set of propagation models which ensure that the predictions embrace all the significant interference propagation mechanisms that can arise. Methods for analysing the radio-meteorological [R6,R7,R8] and topographical features [R9] of the path are provided so that predictions can be prepared for any practical interference path falling within the scope of the procedure up to a distance limit of 10 000 km.

Interference propagation mechanisms

Microwave interference may arise through a range of propagation mechanisms whose individual dominance depends on climate, radio frequency, time percentage of interest, distance and path topography. At any one time a single mechanism or more than one may be present. The principal interference propagation mechanisms are as follows:

– Line-of-sight (Figure 4.16): The most straightforward interference propagation situation is when a line-of-sight transmission path exists under normal (i.e. well-mixed) atmospheric conditions. However, an additional complexity can come into play when subpath diffraction causes a slight increase in signal level above that normally expected. Also, on all but the shortest paths (i.e. paths longer than about 5 km) signal levels can often be significantly enhanced for short periods of time by multipath and focusing effects resulting from atmospheric stratification (see Figure 4.17).

– Diffraction (Figure 4.16): Beyond line-of-sight (LoS) and under normal conditions, diffraction effects generally dominate wherever significant signal levels are to be found. For services where anomalous short-term problems are not important, the accuracy to which diffraction can be modelled generally determines the density of systems that can be achieved. The diffraction prediction capability must have sufficient utility to cover smooth-earth, discrete obstacle and irregular (unstructured) terrain situations.

– Tropospheric scatter (Figure 4.16): This mechanism defines the “background” interference level for longer paths (e.g. more than 100-150 km) where the diffraction field becomes very weak. However, except for a few special cases involving sensitive earth stations or very high power interferers (e.g. radar systems), interference via troposcatter will be at too low a level to be significant.

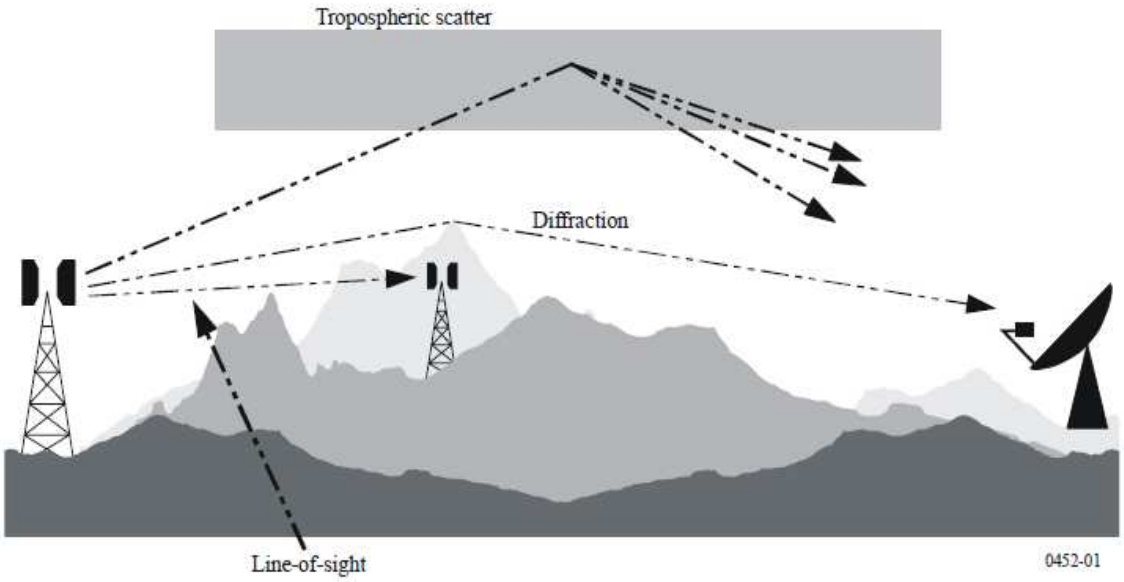

Figure 4.16: Long-term interference propagation mechanisms

– Surface ducting (Figure 4.17): This is the most important short-term interference mechanism over water and in flat coastal land areas, and can give rise to high signal levels over long distances (more than 500 km over the sea). Such signals can exceed the equivalent “free-space” level under certain conditions.

– Elevated layer reflection and refraction (Figure 4.17): The treatment of reflection and/or refraction from layers at heights up to a few hundred meters is of major importance as these mechanisms enable signals to overcome the diffraction loss of the terrain very effectively under favourable path geometry situations. Again the impact can be significant over quite long distances (up to 250-300 km).

– Hydrometeor scatter (Figure 4.17): Hydrometeor scatter can be a potential source of interference between terrestrial link transmitters and earth stations because it may act virtually omnidirectionally, and can therefore have an impact off the great-circle interference path. However, the interfering signal levels are quite low and do not usually represent a significant problem for frequencies below about 5 GHz.

A basic problem in interference prediction (which is indeed common to all tropospheric prediction procedures) is the difficulty of providing a unified consistent set of practical methods covering a wide range of distances and time percentages; i.e. for the real atmosphere in which the statistics of dominance by one mechanism merge gradually into another as meteorological and/or path conditions change. Especially in these transitional regions, a given level of signal may occur for a total time percentage which is the sum of those in different mechanisms. The approach in this procedure has been to define completely separate methods for clear-air and hydrometeor-scatter interference prediction, as described in § 4 and 5 [R3] respectively.

The clear-air method consists of separate models for diffraction, ducting/layer-reflection, and troposcatter. All three are applied for every case, irrespective of whether a path is LoS or transhorizon. The results are then combined into an overall prediction using a blending technique that ensures for any given path distance and time percentage that the signal enhancement in the equivalent notional line-of-sight model is the highest attainable.

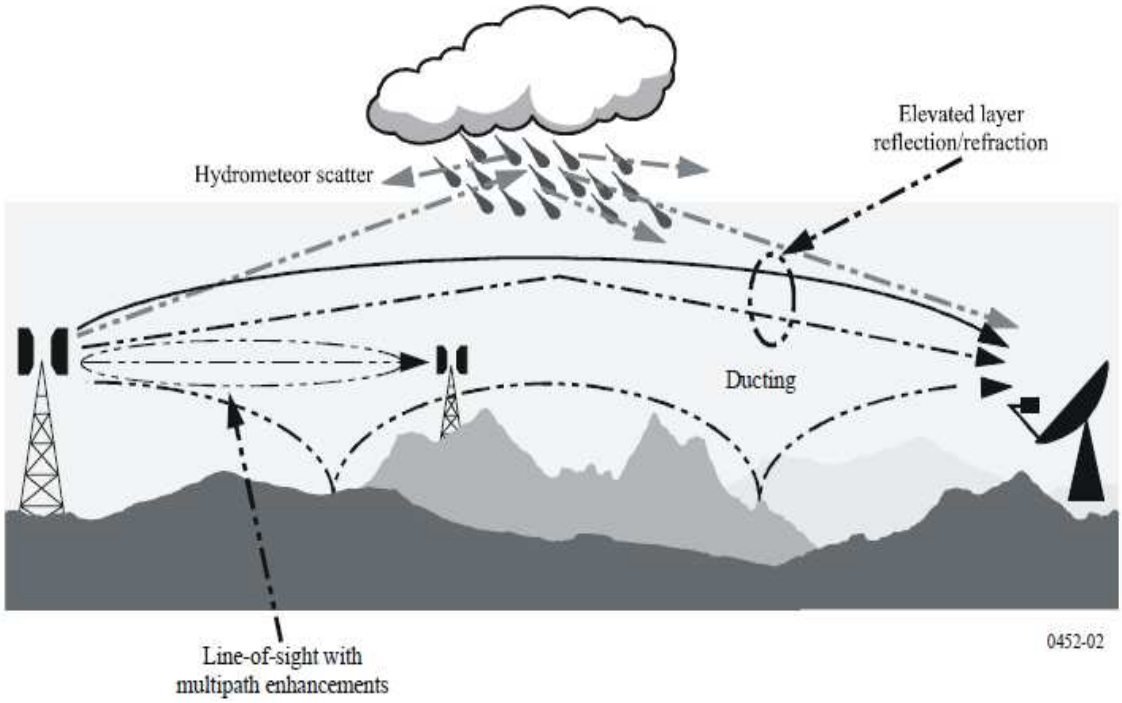

Figure 4.17: Anomalous (short-term) interference propagation mechanisms

Despite not being central within the scope of this thesis, there are some atmospheric conditions such as moisture and climate effects [R10] that must be considered for systems operating at frequencies above 1GHz and must be studied by Teleplan AS in order to know if they may implement an extension on the program taken into account the amount of new charge to the tool computationally speaking compared with the newly improvement obtained. It seems anyway that due to the difficulty of providing a unified consistent set of practical methods covering a wide range of distances and time percentages, it might not be an additional term on the recent future versions.

4.3.6 ITU-R P.1411 Propagation data and prediction methods for the planning of short-range outdoor radio communication systems and radio local area networks in the frequency range 300 MHz to 100 GHz.

This Recommendation provides guidance on outdoor short-range propagation over the frequency range 300 MHz to 100 GHz. Information is given on path loss models for line-of-sight (LoS) and non-line-of-sight (NLoS) environments, building entry loss, multipath models for both environments of street canyon and over roof-tops, number of signal components, polarization characteristics and fading characteristics.

Propagation over paths of length less than 1 km is affected primarily by buildings and trees, rather than by variations in ground elevation. The effect of buildings is predominant, since most short-path radio links are found in urban and suburban areas. The mobile terminal is most likely to be held by a pedestrian or located in a vehicle.

Although the models for urban and suburban areas are valid up to 5 km, this Recommendation is intended for distances only up to 1 km and based on Recommendation ITU-R P.526 for over roof-top propagation and another one is given for propagation between terminals located below roof-top height.

Influence of vegetation is the new effect found not covered from the previous models

The effects of propagation through vegetation (primarily trees) are important for outdoor short-path predictions. Two major propagation mechanisms can be identified:

– propagation through (not around or over) trees;

– propagation over trees.

The first mechanism predominates for geometries in which both antennas are below the tree tops and the distance through the trees is small, while the latter predominates for geometries in which one antenna is elevated above the tree tops. The attenuation is strongly affected by multipath scattering initiated by diffraction of the signal energy both over and through the tree structures. For propagation through trees, the specific attenuation in vegetation can be found in Recommendation ITU-R P.833 [R11]. In situations where the propagation is over trees, diffraction is the major propagation mode over the edges of the trees closest to the low antenna. This propagation mode can be modeled most simply by using an ideal knife-edge diffraction model (see Recommendation ITU-R P.526), although the knife-edge model may underestimate the field strength, because it neglects multiple scattering by tree-tops, a mechanism that may be modeled by radiative transfer theory.

4.3.7 COST231

This is the main point of the thesis since the most important propagation prediction models on Astrix are based on COST231.

The predictions are based on the knowledge of topography, land usage and building height information. This section deals with five different topics, modeling in urban areas, influence of vegetation, large-scale terrain effects, multipath prediction and the combination of the different aspects yielding more general models.

One important output of COST 231 is the development of outdoor propagation models for applications in urban areas at 900 and 1800 MHz bands. Based on extensive measurement campaigns in European cities, COST 231 has investigated different existing models and has created new propagation models. These models, valid for flat terrain, are based on the approaches of Walfisch-Bertoni [M8], Ikegami [M20] and Hata [M21].

4.3.7.1 COST 231 - Hata-Model

Path loss estimation is performed by empirical models if land cover is known only roughly, and the parameters required for semi-deterministic models cannot be determined. Four parameters are used for estimation of the propagation loss by Hata's well-known model: frequency f, distance d, base station antenna height hBase and the height of the mobile antenna hMobile. In Hata´s model, which is based on Okumura´s various correction functions [M22], the basic transmission loss, Lb, in urban areas is:

$$L_b = 69.55 + 26.16 \cdot \log\frac{f}{MHz} - 13.82 \cdot \log\frac{h_{Base}}{m} - a(h_{Mobile}) + (44.9 - 6.55 \cdot \log\frac{h_{Base}}{m}) \cdot \log\frac{d}{km} \quad (4.32)$$

where:

$$a(h_{Mobile}) = (1.1 \cdot \log\frac{f}{MHz} - 0.7)\frac{h_{Mobile}}{m} - (1.56 \cdot \log\frac{f}{MHz} - 0.8) \quad (4.33)$$

The model is restricted to:

f : 150 ... 1000 MHz

hBase : 30 ...200 m

hMobile: 1 ...10 m

d : 1 ...20 km

COST 231 has extended Hata´s model to the frequency band 1500 < f(MHz) < 2000 by analysing Okumura´s propagation curves in the upper frequency band. This combination is called "COST-Hata-Model" [M23]:

$$L_b = 46.3 + 33.9 \log \frac{f}{MHz} - 13.82 \log \frac{h_{Base}}{m} - a(h_{Mobile}) + (44.9 - 6.55 \log \frac{h_{Base}}{m}) \log \frac{d}{km} + C_m \quad (4.34)$$

where a(hMobile) is defined in equation (4.33) and

$$C_m = \begin{cases} 0 \text{ dB} & \text{for medium sized city and suburban} \\ & \text{centres with medium tree density} \\ 3 \text{ dB} & \text{for metropolitan centres} \end{cases} \quad (4.35)$$

The COST-Hata-Model is restricted to the following range of parameters:

f : 1500 ... 2000 MHz

hBase : 30 ... 200 m

hMobile : 1 ... 10 m

d : 1 ... 20 km

The application of the COST-Hata-Model is restricted to large and small macro-cells, i. e. base station antenna heights above roof-top levels adjacent to the base station. Hata´s formula and its modification must not be used for micro-cells.

4.3.7.2 COST 231 - Walfisch-Ikegami-Model

Furthermore COST 231 proposed a combination of the Walfisch [M8] and Ikegami [M20] models. This formulation is based on different contributions from members of the "COST 231 Subgroup on Propagation Models" [M23]. It is called the COST-Walfisch-Ikegami-Model (COST-WI). The model allows for improved path-loss estimation by consideration of more data to describe the character of the urban environment, namely

- heights of buildings hRoof,

- widths of roads w,

- building separation b and

- road orientation with respect to the direct radio path j.

The parameters are defined in Figs. 4.18 and 4.19. However this model is still statistical and not deterministic because only characteristic values can be inserted and no topographical data base of the buildings is considered.

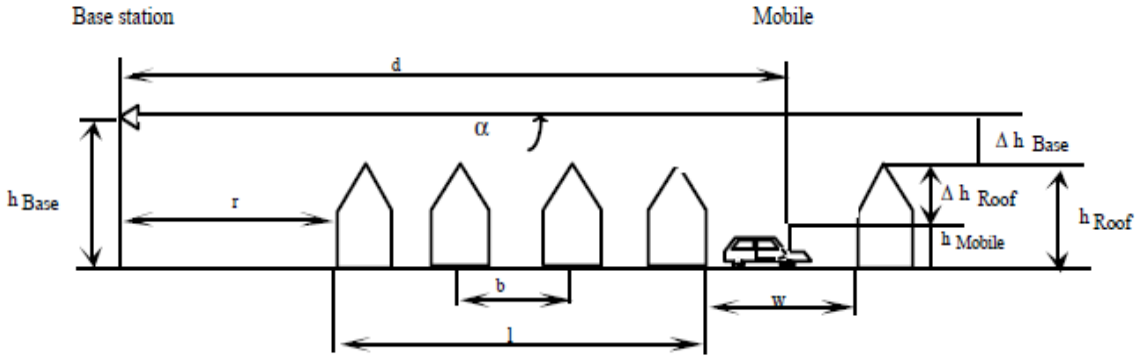

Figure 4.18: Typical propagation situation in urban areas and definition of the parameters used in the COST-WI model and other Walfisch-type models [M8], [M12], [M24].

The model distinguishes between line-of-sight (LOS) and non-line-of-sight (NLOS) situations. In the LOS case -between base and mobile antennas within a street canyon - a simple propagation loss formula different from free space loss is applied. The loss is based on measurements performed in the city of Stockholm:

$$L_b(\mathrm{dB}) = 42.6 + 26\log(d/\mathrm{km}) + 20\log(f/\mathrm{MHz}) \quad \text{for } d \geq 20 \text{ m} \tag{4.36}$$

where the first constant is determined in such a way that Lb is equal to freespace loss for d = 20 m. In the NLOS-case the basic transmission loss is composed of the terms free space loss L0, multiple screen diffraction loss Lmsd, and roof-top-to-street diffraction and scatter loss Lrts.

$$L_b = \begin{cases} L_0 + L_{rts} + L_{msd} & \text{for } L_{rts} + L_{msd} > 0 \\ L_0 & \text{for } L_{rts} + L_{msd} \leq 0 \end{cases} \tag{4.37}$$

The free-space loss is given by

$$L_0(\mathrm{dB}) = 32.4 + 20\log(d/\mathrm{km}) + 20\log(f/\mathrm{MHz})$$

The term Lrts describes the coupling of the wave propagating along the multiple-screen path into the street where the mobile station is located. The determination of Lrts is mainly based on Ikegami's model. It takes into account the width of the street and its orientation. COST 231, however, has applied another street-orientation function than Ikegami:

$$L_{rts} = -16.9 - 10\log\frac{w}{m} + 10\log\frac{f}{\mathrm{MHz}} + 20\log\frac{\Delta h_{Mobile}}{m} + L_{Ori}$$

$$L_{Ori} = \begin{cases} -10 + 0.354\frac{\varphi}{\mathrm{deg}} & \text{for } 0° \leq \varphi < 35° \\ 2.5 + 0.075(\frac{\varphi}{\mathrm{deg}} - 35) & \text{for } 35° \leq \varphi < 55° \\ 4.0 - 0.114(\frac{\varphi}{\mathrm{deg}} - 55) & \text{for } 55° \leq \varphi < 90° \end{cases}$$

$$\Delta h_{Mobile} = h_{Roof} - h_{Mobile}$$

$$\Delta h_{Base} = h_{Base} - h_{Roof}$$

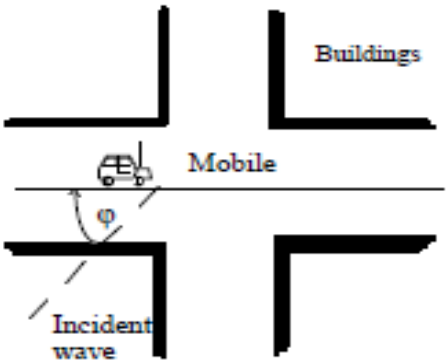

Figure 4.19: Definition of the street orientation angle φ

Scalar electromagnetic formulation of multi-screen diffraction results in an integral for which Walfisch and Bertoni published an approximate solution in the case of base station antenna located above the roof-tops. This model is extended by COST 231 for base station antenna heights below the roof-top levels using an empirical function based on measurements. The heights of buildings and their spatial separations along the direct radio path are modelled by absorbing screens for the determination of Lmsd:

$$L_{msd} = L_{bsh} + k_a + k_d \log\frac{d}{km} + k_f \log\frac{f}{MHz} - 9\log\frac{b}{m} \tag{4.38}$$

where

$$L_{bsh} = \begin{cases} -18\log(1+\frac{\Delta h_{Base}}{m}) & \text{for } h_{Base} > h_{Roof} \\ 0 & \text{for } h_{Base} \le h_{Roof} \end{cases} \tag{4.39}$$

$$k_a = \begin{cases} 54 & \text{for } h_{Base} > h_{Roof} \\ 54 - 0.8\frac{\Delta h_{Base}}{m} & \text{for } d \ge 0.5 \text{ km and } h_{Base} \le h_{Roof} \\ 54 - 0.8\frac{\Delta h_{Base}}{m}\ \frac{d/km}{0.5} & \text{for } d < 0.5 \text{ km and } h_{Base} \le h_{Roof} \end{cases} \tag{4.40}$$

$$k_d = \begin{cases} 18 & \text{for } h_{Base} > h_{Roof} \\ 18 - 15\frac{\Delta h_{base}}{h_{roof}} & \text{for } h_{Base} \le h_{Roof} \end{cases} \tag{4.41}$$

$$k_f = -4 + \begin{cases} 0.7\left(\frac{f/MHz}{925} - 1\right) & \text{for medium sized city and suburban} \\ & \text{centres with medium tree density} \\ 1.5\left(\frac{f/MHz}{925} - 1\right) & \text{for metropolitan centres} \end{cases} \quad (4.42)$$

The term ka represents the increase of the path loss for base station antennas below the roof tops of the adjacent buildings. The terms kd and kf control the dependence of the multi-screen diffraction loss versus distance and radio frequency, respectively. If the data on the structure of buildings and roads are unknown the following default values are recommended:

hRoof = 3 m x { number of floors } + roof-height

$$\text{roof - height} = \begin{cases} 3 \text{ m pitched} \\ 0 \text{ m flat} \end{cases}$$

b = 20 ... 50 m

w = b / 2

φ = 90°

The COST-WI model is restricted to:

f : 800 ... 2000 MHz

hBase : 4 ... 50 m

hMobile : 1 ... 3 m

d : 0.02 ... 5 km

The model has also been accepted by the ITU-R and is included into Report 567-4. The estimation of path loss agrees rather well with measurements for base station antenna heights above roof-top level. The mean error is in the range of +3 dB and the standard deviation 4-8 dB. However the prediction error becomes large for hBase>> hRoof compared to situations where hBase >> hRoof. Furthermore the performance of the model is poor for hBase << hRoof. The parameters b, w and φ are not considered in a physically meaningful way for micro-cells. Therefore the prediction error for micro-cells may be quite large. The model does not consider multipath propagation and the reliability of pathloss estimation decreases also if terrain is not flat or the land cover is inhomogeneous.

4.3.7.3 Comparison with other models

Saunders and Bonar [M12] as well as Bertoni and Xia [M24], [M25], [M26] published different closed-form solutions for Lmsd which are applicable for all values of base station antenna heights. Several papers compare the different approaches with measurements [M27], [M28].

The results, however, differ markedly depending on the situation, where the models are applied. This effect can be explained by the different validity limits of the different approaches. The Walfisch-Bertoni-Model supposes a high base station antenna (hBase > hRoof). The COST-Walfisch-Ikegami- Model is valid for base station antenna heights below 50 m and gives reasonable agreement with measured values for l > ds (see Fig. 4.18), where ds is called the "settled-field"- distance [M29]:

$$d_s = \frac{\lambda d^2}{\Delta h_{Base}^2} \tag{4.43}$$

where l is the wave length in m. The case l < ds covers grazing incidence, where the COST-Walfisch-Ikegami-Model is poor. On the other hand Saunder's Flat-Edge-Model covers grazing incidence as long as the condition r >> l is fulfilled. Furthermore the COST-Walfisch-Ikegami-Model and an approach of Maciel et. al [M26] include corrections for taking into account the street orientation at the mobile.

4.3.7.4 Influence of vegetation

A few papers within COST 231 investigated propagation models for wooded environments in the 900 and 1800 MHz bands. A comparative study [M30] has been done in Finland applying the Okumura-Hata-Model (945 MHz), the COST-Hata-Model (1807 MHz) and the Blomquist-Ladell-Model [M31] (both frequencies) to forested terrain. The Finnish experiments revealed that Hata's model can be used for path loss estimation, except for wet forests at 1800 MHz where an additional path loss of about 5 dB has to be taken into account. Middle European forests containing denser and higher trees than typical nordic woods result in larger additional attenuation.

This last section of COST231 presents Blomquist-Ladell model, which is the latest model included in Astrix 5.2 for better accurate radio planning over forested areas.

4.3.8 The Walther Åsen Model

This model has been one of the latest improvements of the new updated Astrix 5.2 versions so it is worth of mentioning since it is an improved model of the ITU-R P.526 model for propagation by diffraction.

A comparison between three methods for predicting attenuation due to diffraction were tested against a large database of measurement points, representing different path profiles of 100-m horizontal resolution, and vertical root mean square error of about 6 m. The signal level at each geographic measurement point was calculated as the median of about 40 basic measurements, and the measurement database is thus reduced from about four million basic measurements. The mobile measurements were taken from main FM (88–108 MHz) broadcasting emitters located in southern Norway, and the corresponding broadcasting antenna diagrams were measured by helicopter. Path profiles were categorized by number of terrain obstructions between emitter and receiver, in order to study their effect on each propagation loss method.

One of the methods is widely used and recommended by ITU as a general method for diffraction [R1]. The second method that was tested is Picquenard's construction [M17]. It was chosen because it is easy to understand and uses no empirical corrections. It is also straight forward to extend the Picquenard model and fit it empirically to take a selected number of terrain obstacles into account. Therefore, a third and new, fitted, method was tested, based on Picquenard, which includes a limited number of terrain obstacles.

He chose to use the root mean square error (rms) as an absolute measure of how well the different propagation models fit the measurements. A systematic deviation from zero of the mean of the difference between modeled and measured propagation loss increases the rms. In order to investigate the symmetry of the errors, he also calculated the 0.1, 1, 10, 50 (median), 90 and 99.9% occurrences of the differences.

Complete measurement series that clearly and consistently contain errors, either due to incorrect broadcasting antenna diagram, or due to interference or other systematic errors, were excluded from the comparison analysis.

For the purpose of comparing models and measurements he categorized the propagation paths according to the number of obstacles found using the Picquenard construction. He thus, obtained statistical parameters for the rms and for deviations of the propagation loss calculations for each of paths having 0 obstructions, 1 obstruction, 2 obstructions, etc., up to and including 9 obstructions.

He studied two different versions of the Picquenard model. One of them takes all terrain obstacles into account. This is the general Picquenard model. The other takes the biggest diffraction term into account, and adds 0.67 multiplied with the next biggest diffraction term. He refers to this method, which only takes two terms into account, as Picquenard 1,67. There is a slight difference between Picquenard's way of defining obstructions and the ITU method. In order to compare the different propagation methods for similar paths (categorization), he is always referring to the number of obstacles found using the Picquenard algorithm.

As mentioned before, Deygout's method considers the whole path, determines the "main edge," and divides the path at both sides of the "main edge" into subpaths, where subsidiary "main edges" are found, etc., in a hierarchical way. Picquenard's method calculates all diffraction terms from all edges from emitter to receiver, and considers all contributions. The main difference between the methods is that all diffraction terms are considered by the Picquenard method, while some important terms can actually be missed out due to the hierarchical structure of the Deygout method.

RMS Comparison

The rms's for the ITU model, the general Picquenard model and the Picquenard 1,67 model are summarized over all measurement series in Table 4.3. We note that the Picquenard 1,67 construction is better than the ITU construction for any number of obstacles in the path between emitter and receiver. The rms of the ITU model is generally increasing with the number of obstacles in the propagation path. This results in an overall better rms performance of Picquenard 1,67 of about 2.7 dB compared to the ITU model.

RMS (IN DECIBELS) FOR THE ITU MODEL, THE GENERAL PICQUENARD MODEL AND THE PICQUENARD 1,67 MODEL

RMSE (dB)	ITU model	Picquenard (all diffraction terms included)	Picquenard (1,67 diffractions included)	-	**Number of observations**
line-of-sight	9.1	8.5	8.5	-	10920
1 obstacle	11.5	8.2	8.3	-	27742
2 obstacles	11.6	12.5	9.1	-	35345
3 obstacles	12.2	23.9	9.5	-	23696
4 obstacles	12.5	37.5	9.6	-	11333
5 obstacles	13.1	51.8	9.4	-	4501
6 obstacles	13.3	65.9	9.5	-	1506
7 obstacles	13.4	82.0	8.7	-	411
8 obstacles	12.7	95.7	7.8	-	118
9 obstacles	14.7	112.7	6.8	-	37
----------	-------	----------	----------	-	----------
Overall	**11.7**	**22.9**	**9.0**	-	**115614**

Table 4.3: RMS (in dBs) for the ITU Model, the general Picquenard model and the Picquenard 1,67 Model

From the 50% (median) value, he showed that the general Picquenard method with all obstructions included is very pessimistic, especially for paths of many obstructions. All knife-edge diffraction methods, like Deygout and Picquenard, are based on very simplified assumptions about possible radio wave paths from emitter to receiver. However, the emitted radio waves are distributed across space and will follow paths of least resistance, so that in practice it is found that only a few (three or less) important diffractions should be taken into account. The particular inclusion of terms in the Picquenard 1,67 method was chosen because

it gave an optimum fit to the measured data (smallest rms) in the presence of an arbitrary number of obstacles in the path.

The median value of the Picquenard 1,67 method is slightly optimistic independently of the number of path obstructions. He showed that the ITU model is optimistic for up to, and including, four terrain obstacles. For more complicated paths also the ITU model becomes pessimistic, while its overall performance remains optimistic. It is also possible to compare the overall performance of the models without doing paired comparisons between model and measurement. In Figure 4.20 he plotted the cumulative distribution of predicted propagation loss relative to an arbitrary threshold, minus the cumulative distribution of the measured loss relative to the same threshold, employing the different models discussed in this paper. In this way he averaged out some of the uncertainty associated with vehicle positioning and the uncertainty associated with the digital terrain elevation database. The low percentages in Figure 4.20 are thus representing high attenuation. Figure 4.20 confirms his previous conclusions that the ITU on average is optimistic except for high attenuation values. His Picquenard 1,67 method is neither overly optimistic nor pessimistic for any percentage of the measurements. The mean value of difference to measurements of Picquenard 1,67 in Figure 4.20 is dB, while it is dB for the ITU model.

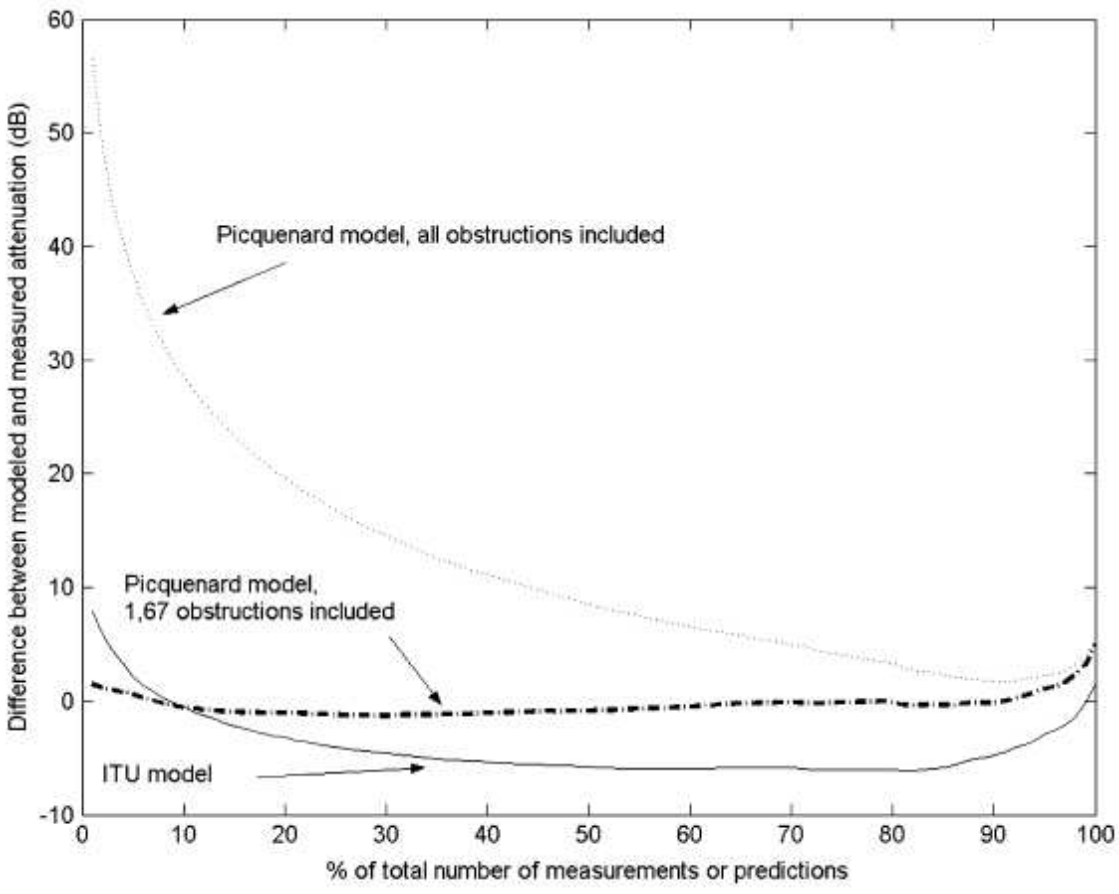

Figure 4.20: Cumulative distribution of predicted propagation loss relative to an arbitrary threshold, minus the cumulative distribution of measured loss relative to the same threshold.

The conclusion he found were:

By comparing propagation models with a large set of measurements, he found the current ITU model to be optimistic, and to have a bigger rms than the simpler Picquenard 1,67 model. The successful simpler model employs only the two largest diffraction contributions, and does not rely on additional empirical fitting of parameters. It is found to be within the expected error contributed by the rms of the Norwegian digital terrain elevation data. (This is the main reason for implementing it)

The ITU method, which is based on the Deygout method, has been used as a baseline for comparison for the Norwegian measurements. The improvement of the new Picquenard 1,67 method over the Deygout/ITU implementation for paths of many obstructions is about 4–5 dB better in rms, in Norwegian terrain.

A future work suggested by Aasen could be to test the new Picquenard 1,67 implementation at other frequencies than 88–108 MHz. It may well be that the optimal fitted inclusion of diffraction terms is different at other frequencies.

The slope-UTD method of [M33] is shown to be superior to the Deygout method in UK terrain, showing about 2.5–3 dB better standard deviation of error. The frequencies used for the experiments in UK and Norway are different, and another future work it would therefore, be interesting to compare directly the performance of the Picquenard 1,67 model to the more physical slope-UTD solution.

Categorization of propagation paths by the number of obstructions was proved to be a good way of studying the success of different propagation models. When conducting automated propagation measurements, it is important to include extra measurements for quality assurance.

4.3.9 Tzaras and Saunders recommendation

This paper investigates and compares the efficiency and accuracy of existing multiple diffraction prediction techniques in real outdoor environments. Extensive comparisons are presented, including more than 20.000 path profiles. It is believed that this study will enable broadcasters to design and maintain broadcast networks with an accuracy commensurate with the highly demanding requirements for new and more efficient digital services. The comparisons involve the most well-known deterministic approaches (Deygout, Causebrook, Giovaneli, Vogler) whose key feature is either the high accuracy of their predictions or their low computation times.

In Section 4.3.9.1 he introduces the existing models. In Sections 4.3.9.2 and 4.3.9.3 these models are compared against the measurements for accuracy. The trade-off between accuracy and computation time is then shown in Section 4.3.9.4. A conclusion is then given in Section 4.3.9.5.

4.3.9.1 Multiple knife-edge diffraction methods

A. Deygout Method

The Deygout method [M10] has already been presented above in a previous point so it is not worth mentioning again.

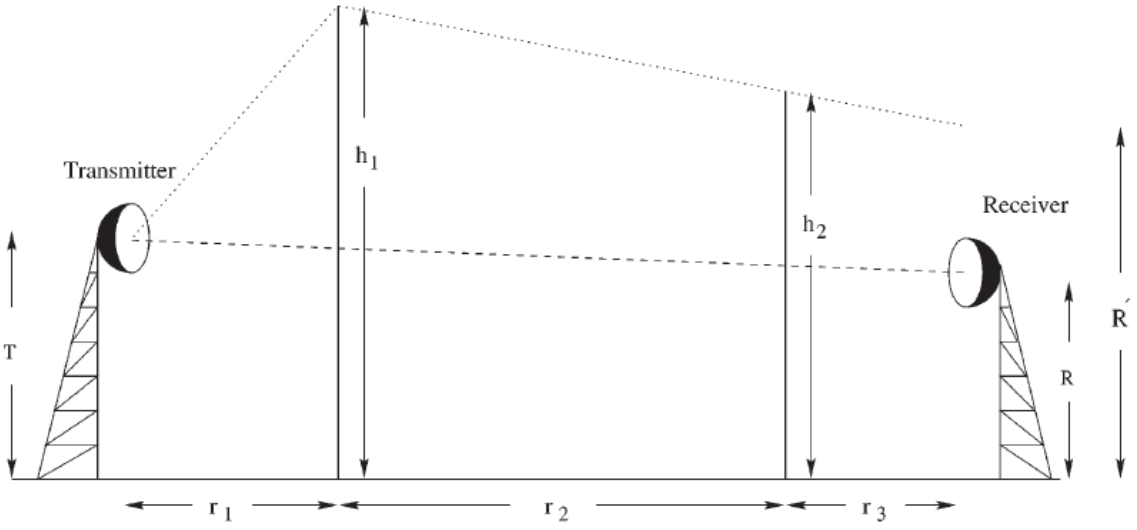

Figure 4.21: Geometrical arrangement for the Deygout and Causebrook methods

B. Causebrook Method

The Causebrook solution [M23] may be classified as a modified version of Deygout's model [M10], since it follows the same process for estimating the diffraction loss. The only difference is that different correction formulas are applied to compensate for the overestimated path loss. Hence, following Figure 4.21, the total attenuation coefficient is given by

$$L = L_1 + L_2 - (6 - L_1 + L_2)\cos\alpha_2 + L_3 - (6 - L_1 + L_3)\cos\alpha_3 \quad \text{in dB} \tag{4.44}$$

where

$$\cos\alpha_2 = \sqrt{\frac{r_1(r_3 + r_4)}{(r_1 + r_2)(r_2 + r_3 + r_4)}} \tag{4.45}$$

$$\cos\alpha_3 = \sqrt{\frac{(r_1 + r_2)r_4}{(r_1 + r_2 + r_3)(r_3 + r_4)}} \tag{4.46}$$

C. Giovaneli Method

This method also follows the Deygout concept, involving many single diffraction integrals [M9].

D. Vogler Method

Fundamental formulas for field strength over irregular terrain were obtained by Furutsu [M35]. In his study, mixed paths over a smooth ground are considered, hence, the waves propagate over several sections with different electrical properties.

The Vogler technique may be regarded as a reference in terms of accuracy against which to judge all other techniques. It has usually been discarded for practical system prediction, however, due to the computation time required and the complexity of implementation.

E. Slope—UTD Method

This UTD method developed by Tzaras and Saunders [M36] is characterized by accurate and reliable output which, in most cases, has almost the same accuracy as the Vogler solution.

4.3.9.2 Comparison of results

A key factor when investigating theoretical multiple diffraction prediction tools is to determine the explicit trade-off between data resolution, computation time and prediction accuracy, leading to optimal approaches for practical broadcast network design. Given that data resolution affects all of the prediction methods in the same way, computational needs and prediction accuracy are the two parameters that will be examined.

According to the simulations, the curves of the Deygout and the Giovaneli solution were very sensitive to the number of edges selected for prediction, hence, these methods cannot be regarded as reliable since it is difficult to know how many edges should be considered for accurate estimation in each case. Such behavior was not found in the Causebrook solution, although it calculates the diffraction loss in a similar fashion to Deygout and Giovaneli. Therefore, the slope-UTD and the Vogler solution predict the measured values best, with the Causebrook solution performing better than the Deygout and the Giovaneli solution. The same result was noticed in all path profiles which verifies the consistency and reliability of the Causebrook, slope-UTD and Vogler solutions in contrast with the Deygout and Giovaneli solutions. For the total number of sites, the Causebrook solution had a standard deviation of error of approximately 8 dB with a mean error of 3 dB, whereas the Vogler and slope-UTD solutions had a standard deviation of prediction error of 7.5 dB with a mean error of 1.8 dB and 2 dB respectively.

4.3.9.3 Model performance versus the number of edges

It is important to know how the number of edges per path profile affects the standard deviation of the prediction error since such a procedure can determine the reliability of each method and also the potential to exhibit how the mechanism of diffraction affects the performance of a broadcasting system, particularly when applying the models to real outdoor environments. The slope-UTD and the Vogler method are the only methods which produce a decrease of the standard deviation of the prediction error while for the other methods the prediction error increases, particularly for the Deygout method. It is thus clear that only these methods correctly model the basic physical mechanism of multiple diffraction.

4.3.9.4 Computation time

Computation time is an important parameter when processing large number of path profiles. Unlike the other methods, the Vogler model needs an excessive amount of time,especially when considering many knife-edges between the transmitter and the receiver. However, for 5 edges, it cannot be regarded as a constraint since it follows a linear behavior with an average of 0.1 seconds per path profile (Figure 4.22) in aSUNUltra Enterprise 3000 server machine with 250 MHz RISC processors.

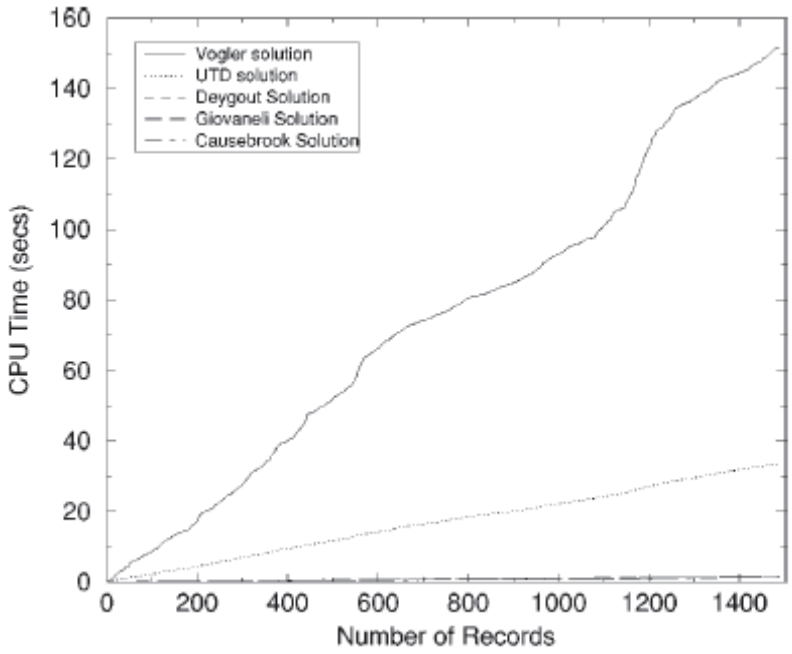

Figure 4.22: CPU time for the different Tzaras and Saunders solutions

As regards the slope-UTD solution, although it offers the same accuracy with the Vogler solution, it has a much lower computation time than Vogler, with an average CPU time of 0.018 seconds per path profile. In addition, as the number of edges increases, the CPU time increases exponentially but with a lower value for the exponential factor if compared with Vogler CPU time. As given in Table 4.4, for 5 edges the slope-UTD solution is approximately 6 times faster that Vogler, whereas for 7 edges it is approximately 12 times faster for the same path configurations. As regards the other methods, their computation time is almost negligible, less than one second in Figure 4.22.

COMPUTATION TIMES FOR UTD AND VOGLER SOLUTION

Number of edges	Average CPU Time (secs)	
	Vogler	UTD
5	0.1	0.018
6	0.55	0.035
7	1.2	0.102

Table 4.4 Computation times for UTD and Vogler solution

4.3.9.5 Conclusion

The conclusion they arrived to was:

Extensive comparison tests were conducted by employing some of the most commonly used multiple diffraction models. Following the results, the models were classified into two categories, being those with high accuracy and high computation time and those with negligible computation time but poor reliability.

The slope-UTD and the Vogler solution were found to fit in the first category whereas the Causebrook, Deygout and Giovaneli fit in the second category. As regards the second category of models, the Causebrook solution showed reasonable accuracy and low complexity and computation time which is also an important factor when applying deterministic propagation models (that is the main reason I suggested Teleplan AS an in-depth study of the Causebrook solution as a improvement from Deygout since computationally are similar but it gives a better performance of 2-3 dB in comparison with Deygout).

The Deygout and Giovaneli solutions performed much worse, especially as the number of edges was increased which revealed that these models were not able to accurately model the physical mechanism of diffraction. However, the slope-UTD solution is regarded by the authors as the method that performed best on balance, since it combined the accuracy of the Vogler solution with low computation times within acceptable limits even when dealing with coverage over large areas. Work continues on characterizing its performance in built-up areas, where Deygout, Causebrook and Giovaneli are known to perform poorly due to the large number of building edges occurring close to grazing incidence.

Part II

Radio Planning and Measurements

5

Radio Planning (Astrix 5.2)

Providing ubiquitous coverage in a predefined area is the main purpose of setting up a wireless communication network. Knowledge about wireless communication theory, technology standard, equipment together with topology and demographics are important prerequisites. Furthermore, knowledge and experience with the radio planning tool is also important. A description of wireless communication theory linked with LTE was mentioned in previous chapters. Whereas, topology and demographics has been mentioned in appendix A. The reason for studying topology and demographics is to define the desired area to cover with LTE.

From an operators point of view, ubiquitous coverage provided by minimum number of base stations is desirable, making the system more cost efficient. Furthermore, a data rate threshold has to be taken in consideration in order to provide the desired QoS. Quality of Service requires a given throughput. In urban areas, wireless communication systems are often capacity limited rather than range limited. Increasing the number of base station in an area where it is expected to be capacity limited is thus a countermeasure which has to be taken in consideration.

5.1 The radio planning process

Building an LTE network demands a thorough radio planning process in order to deliver great services while keeping the business aspect intact, minimum input - maximum output.

Important features on the way of planning a broadband wireless network are to create a good business case, and a reliable budget. The network planning alone serves one purpose, to satisfy the coverage and capacity requirements in order to deliver the promised services.

Preliminary planning may be viewed as a "get to know the equipment" phase. A thorough market analysis sets up the customer requirements, and implements the results in the business case. The next phase is thus to make the system deliver such services, and to know its features and limitations. A thorough analysis of coverage, capacity, and antenna configurations on a preliminary network increases the quality of the following radio planning process.

Moreover, by knowing the system performance, radio propagation models may be tuned and tailored to fit the deployed scenario. Along with detailed topographical data and propagation models, radio planning tools can estimate and predict the desired coverage to optimize the network in terms of resource allocation.

Unfortunately, base stations can not be deployed wherever the radio planner desires. Sites have to be analyzed and viewed to see if they fit the requirements of being a base station sites. The site survey phase requires information regarding obstructions in the surroundings, the physical environment, and installation requirements. Hence multiple site candidates have to be considered before one is chosen. (In my case I did not have to do it because I got the exact positions from of the Oslo Networking sites.)

Furthermore, with a set of site candidates, tailored propagation models, topographical data, and a radio planning software, coverage prediction can be performed according to the requirements in the business model. When radio planning, considerations have to be taken regarding signal strength, data rate, interference, frequency reuse, estimated customer traffic, capacity, and handover but for the scope of this thesis I would just present radio planning regardind with path loss and signal strength.

5.2 Radio Planning Tool

A radio planning tool implements statistical propagation models to facilitate estimation of coverage. There exists several tools to predict radio propagation and coverage. Astrix, ICS telecom nG, and Radio Mobile are some of many. The latter is a freeware suitable in open areas.

Effectively using the available software is a demanding task. Concentration and experience are key features for making the predictions as accurate and efficient as possible. Continuously comparing the prediction with real time measurement increases the accuracy of the software. Astrix has, for instance, a measurement logging tool. The measurements are thus implemented in the software, where a correction layer adjusts the predicted coverage data, resulting in an improved and more accurate coverage prediction.

Apart from having the software, high resolution terrain data which is up to date is imminent. Additional layers like clutters with building heights make the tool more accurate than a clutter only describing the ground occupancy. A building height layer provides reflection, scattering and absorption from actual buildings, and not from statistical buildings which would be the case in a ground occupancy layer.

5.2.1 Astrix 5.2

Astrix 5.2 is a radio planning tool by Teleplan Globe [A2] designed for planning and implementation of radio networks. Figure 5.1 is a print screen of Astrix 5.2.

Propagation models and antenna patterns are adjustable for the operator to adapt the software to the particular network. Previous versions of the software were specially tailored for planning GSM 900/GSM 1800, TETRA and UMTS. The latest release, 5.2 has implemented LTE, whereas Teleplan Globe is continuously improving the software and preparing for future 4G-systems. An Astrix User Case has been created in appendix D to provide a basic user guide for future radio planners.

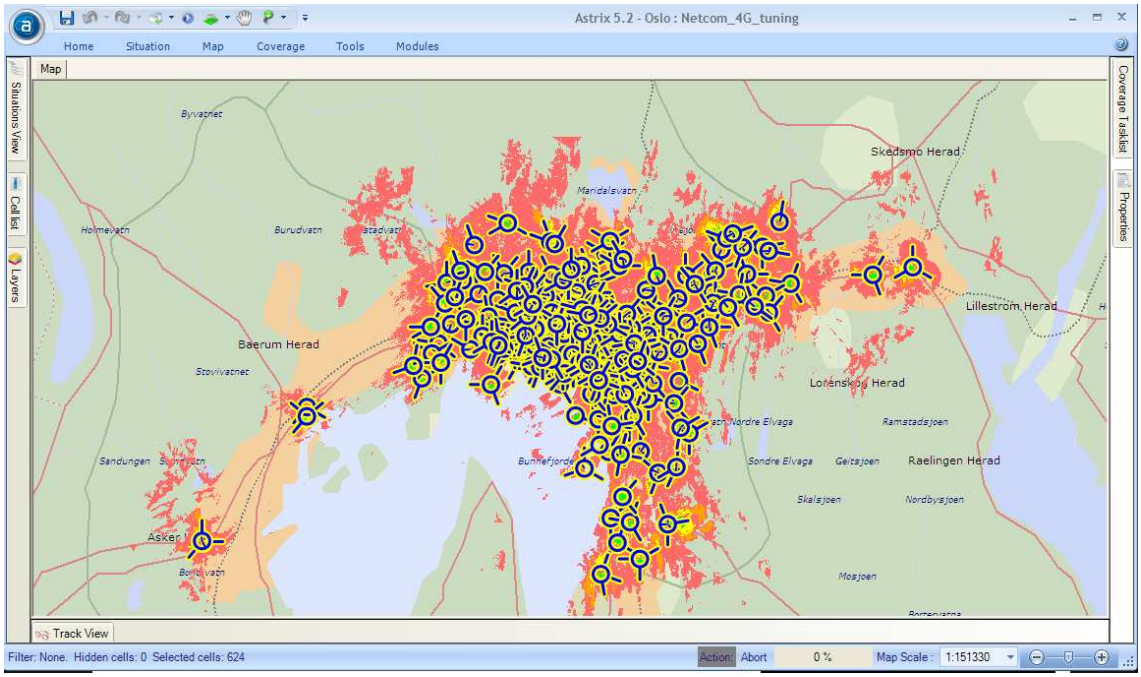

Figure 5.1: Print screen of Astrix 5.2

Base Station parameters

In the case of radio planning LTE for Networking Oslo, the base station parameters are set as a default according to Table 5.1. The antenna pattern have been plotted according to the data provided from the supplier, see appendix C. Figure 5.2 shows the antenna pattern of the vertical polarized antenna, plotted in Astrix. Appendix C contains the antenna specifications of the available antennas. Each base station has been set default with six (6) sectors, separated by 60 degrees. Experience shows that three (3) sectors are sufficient for covering a 360 degree angle. Tuning of each sector is possible to adapt to the base station location.

Single and combined coverage prediction is performed with a resolution of 10 meters. A higher resolution will only slow the system down, and not improve the prediction, because of the available resolution of the terrain.

Parameter	Value
Tx Power	40 dBm
Loss	2 dB
Antenna Gain	17.5 dB
Rx Sensitivity	-94 dBm
Frequency	2.6 GHz

Table 5.1: Base Station Parameters

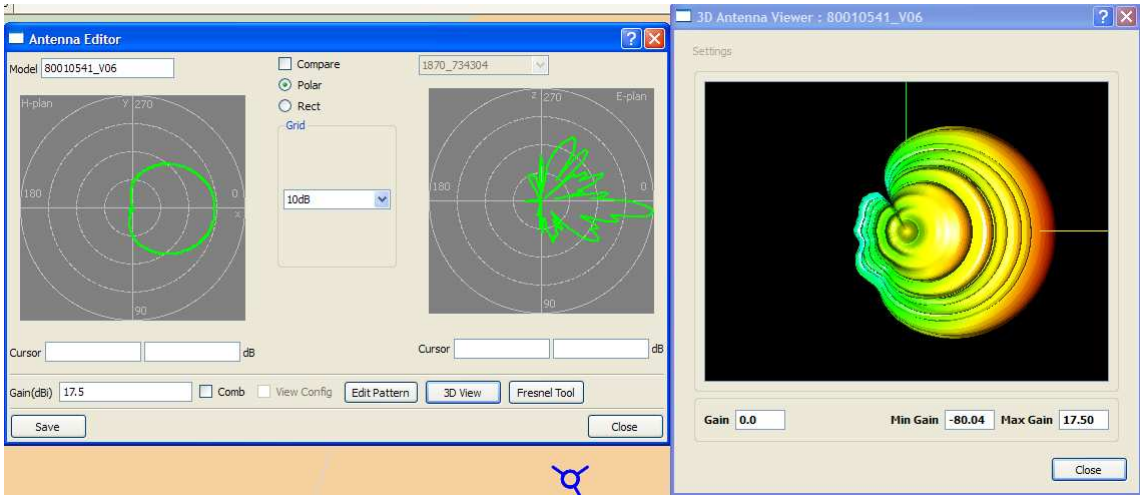

Figure 5.2: Example of an antenna pattern

Coverage prediction

Choosing the base station sites have been performed according to the site criterias mentioned in section 5.1. However as mentioned before I just got the location values from Teleplan AS, that is why I did not have to study what positions could have been optimal for a better area coverage.

I only had three (3) features to tune somehow for testing better area coverages:

- Tx Power

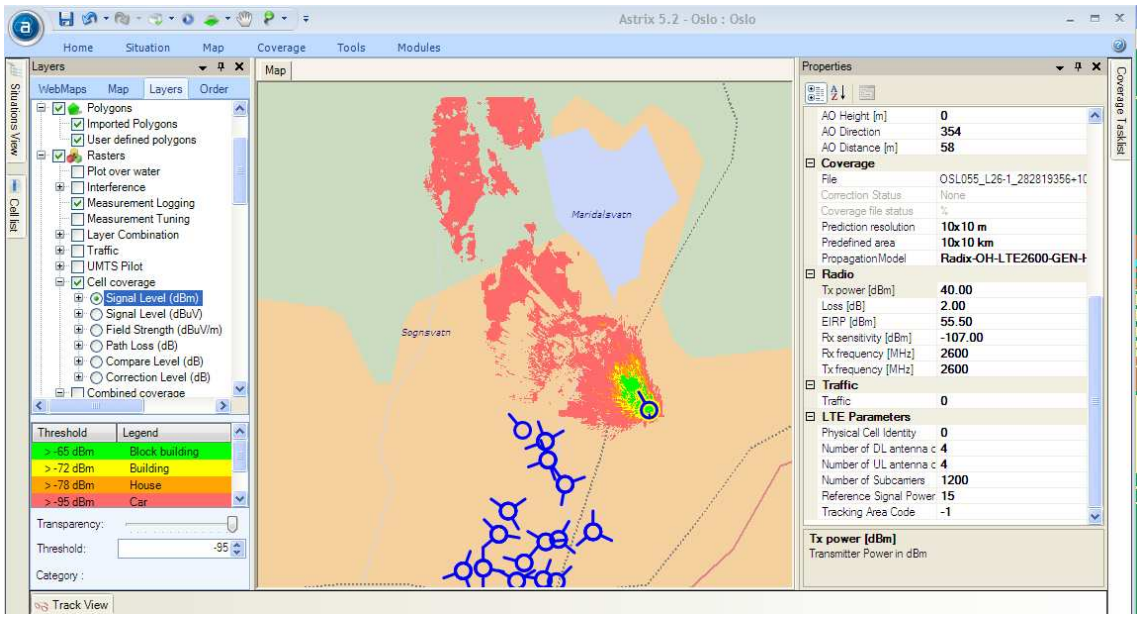

Figure 5.3: Example of coverage with 40dBm of Tx power

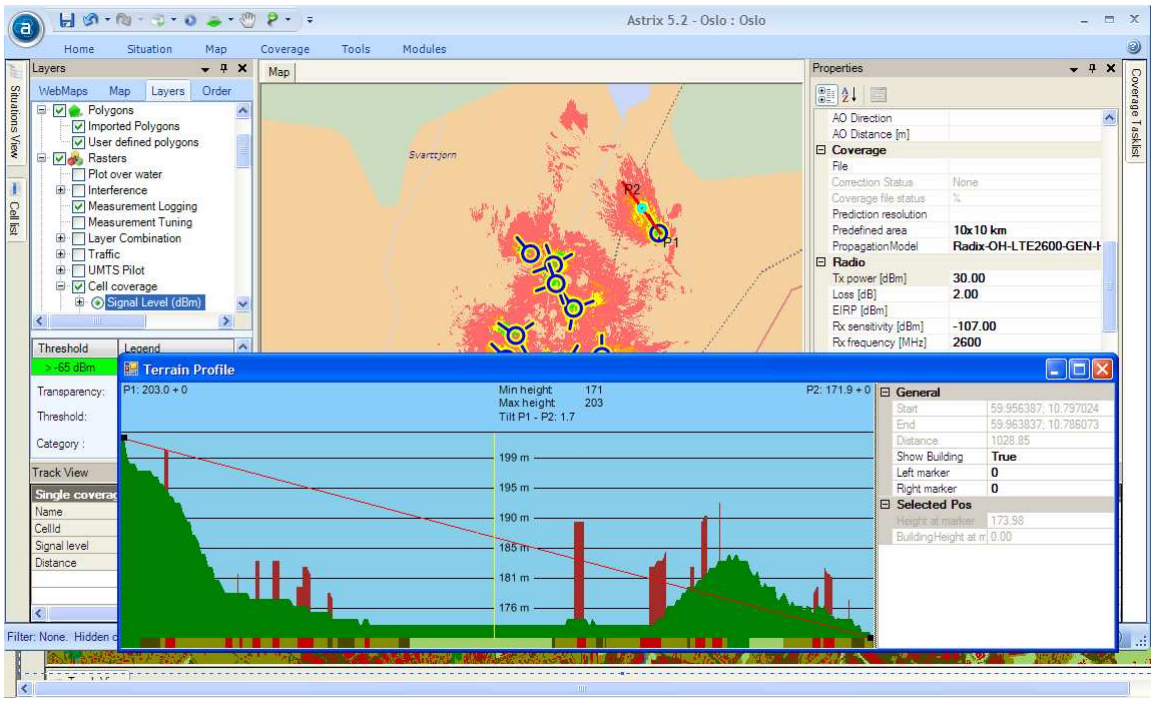

Figure 5.4: Example of coverage with 30dBm of Tx power

- Antenna Tilt

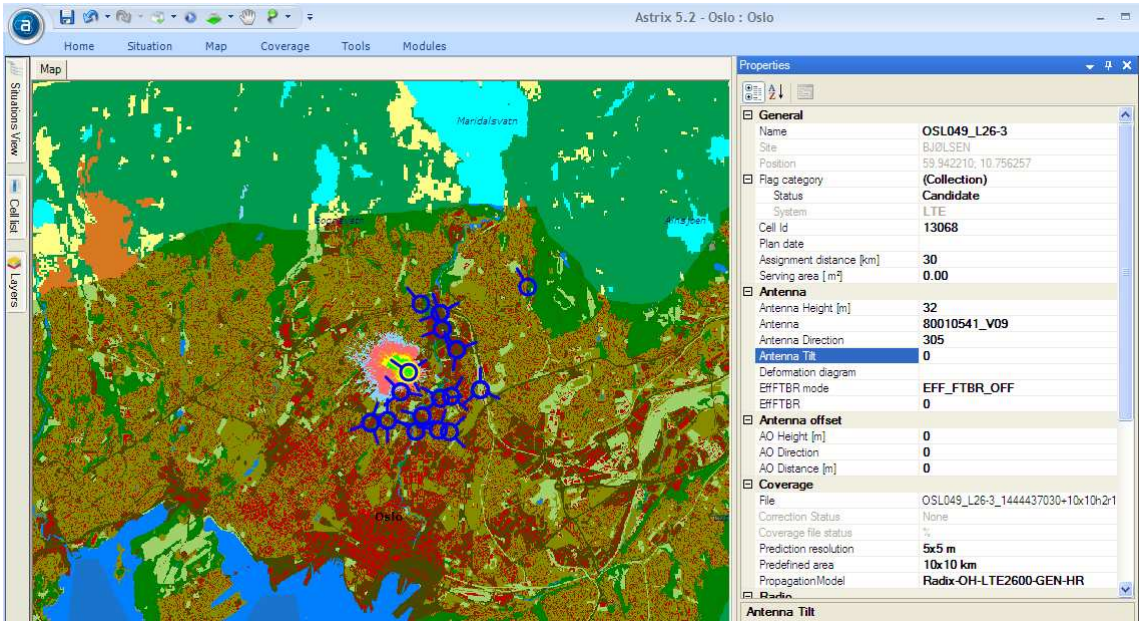

Figure 5.5: Example of coverage with Antenna Tilt 0 degrees

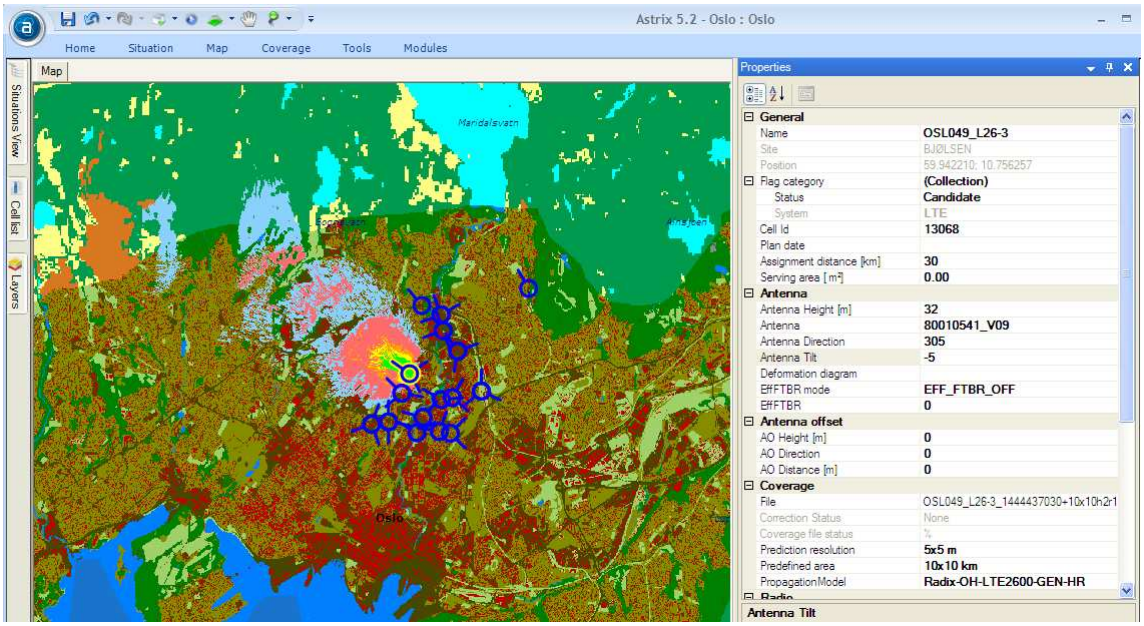

Figure 5.6: Example of coverage with Antenna Tilt -5 degrees

- Antenna Height

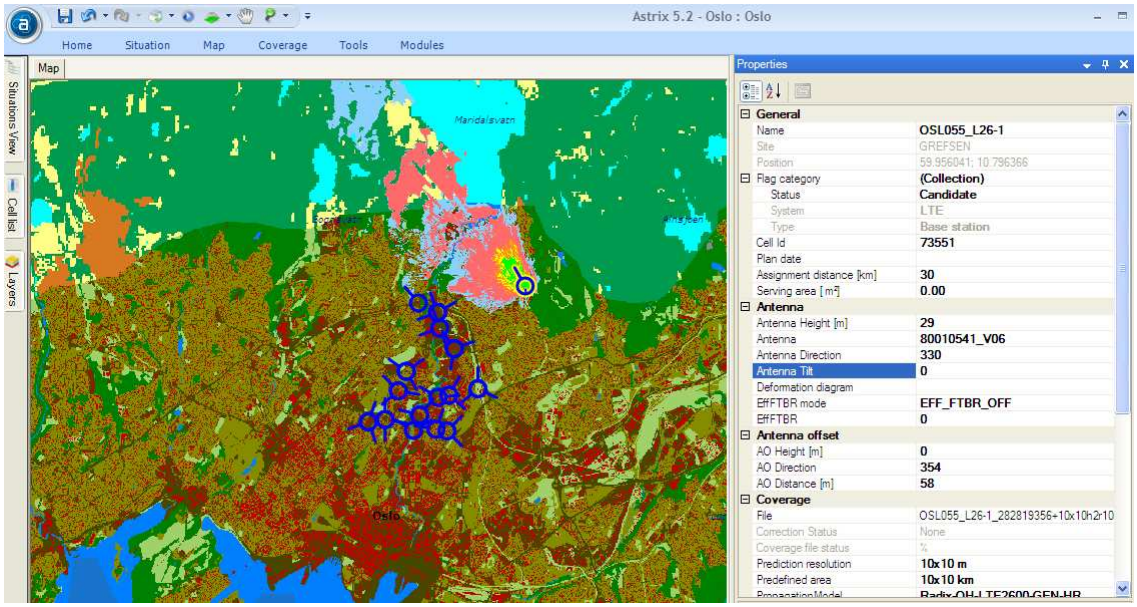

Figure 5.7: Example of coverage with Antenna Height of 29 meters

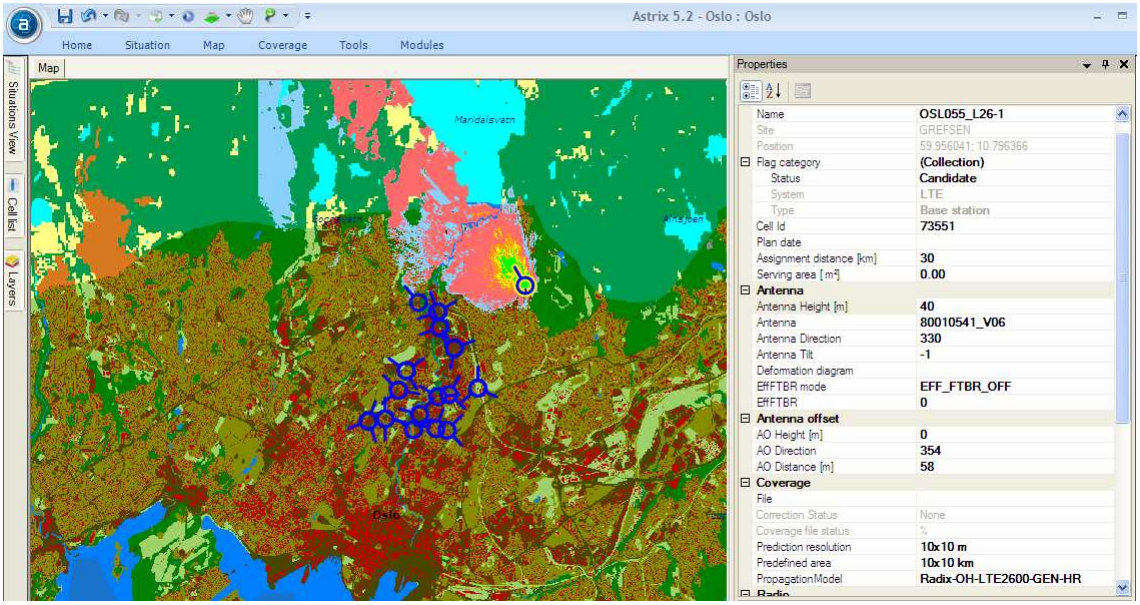

Figure 5.8: Example of coverage with Antenna Height of 40 meters

a) Path loss

As shown in Figure 5.3 path losses normally exceed 140 dB for distances higher than 500-600m at 2.6 GHz for OH-

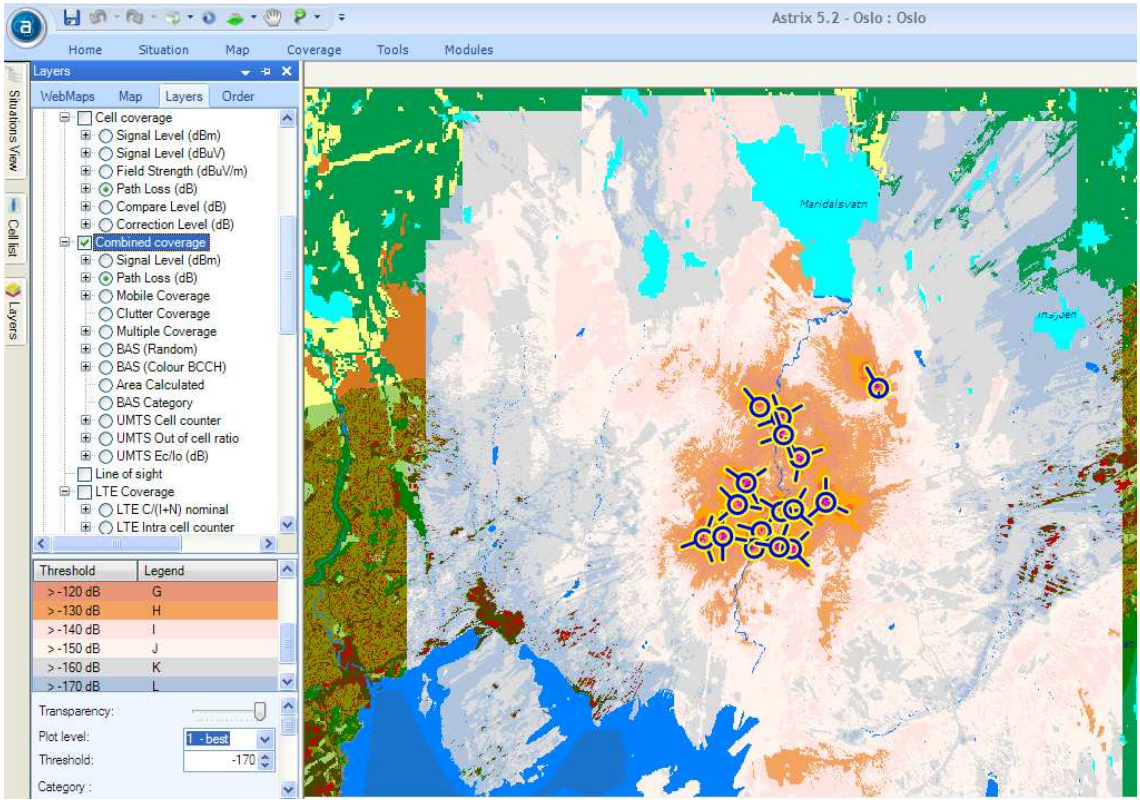

Figure 5.9: Path loss example

b) Signal strength

Teleplan AS has experienced that -110 dBm signal level for Reference Signal Received Reference (RSRP) is ok for planning threshold.

The model they originally calibrated with umts frequency, but is probably good enough for 2.6 GHz also.

The models in Astrix are tuned to have same mean value as measurement, that is 50%. Other word: Mean deviation (prediction minus measurement) is 0.

To get another confidence level e.g. 90% or 95 %, it must be added the corresponding dB offset to the planning signal.

They use RSRP as measure. This is then dependent of RS signal defined for cell, (typical 15dBm). RSRP is found by adding path loss, antenna and additional loss.

When they did measurement for Nteworking Oslo, they experienced connection down to appr. -120dBm (RSRP) but they needed appr.-110dBm to reconnect after lost connection. (Huawei equipment)

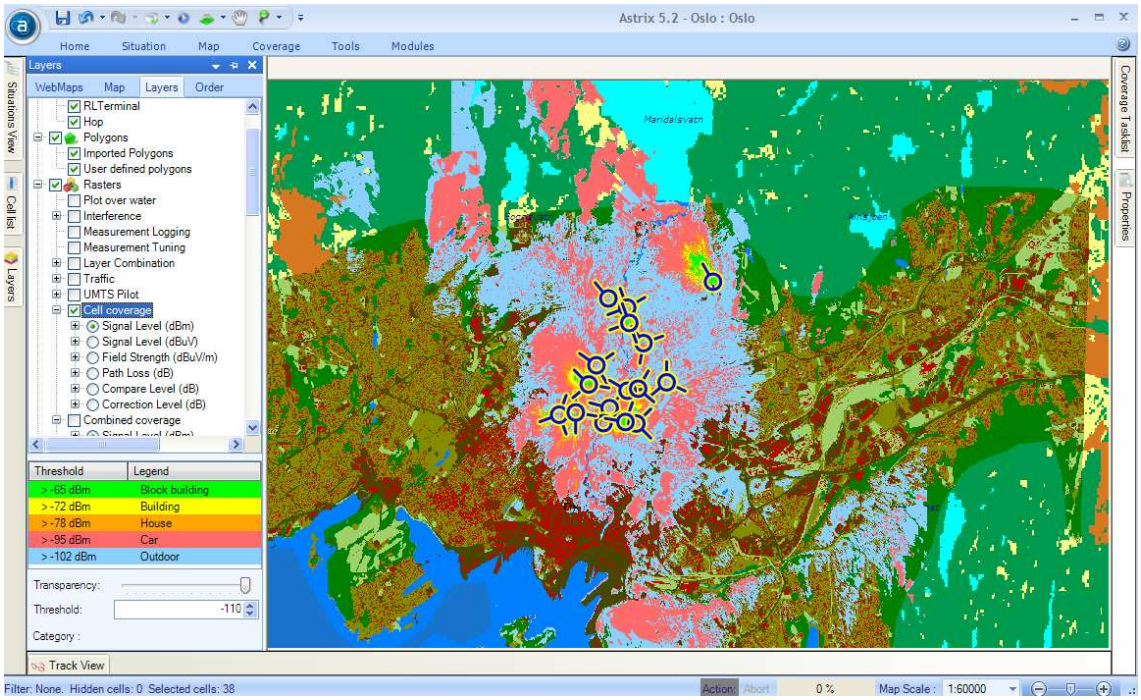

Figure 5.10: Signal strength example

Measurement logging

Astrix 5.2 has a measurement logging tool and a measurement tuning tool to implement the real-life measurements into the radio planning software. The logging tool is used to analyse drive test measurements from the network. The tool can present network measurements as coloured tracks in the map, as 2D graphs or as numeric displays.

The input data consists of data like time, link direction, latitude and longitude, and signal strength. The input data uses the tab (white space) as delimiter between each column for .csv files.

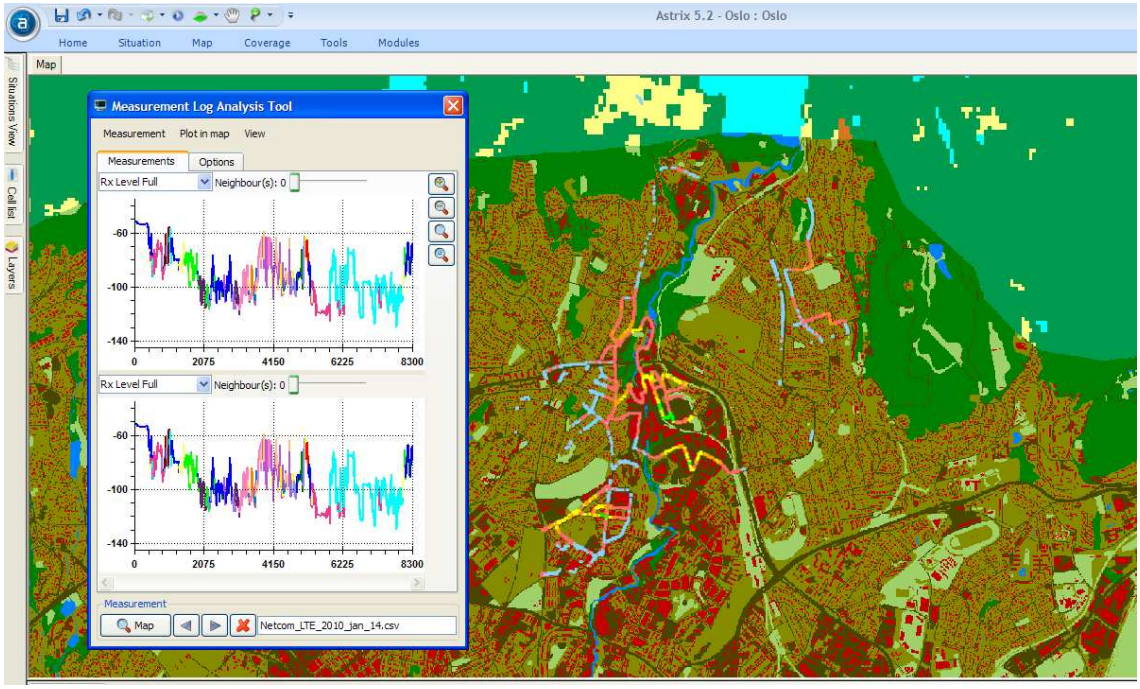

Figure 5.11: Measurement logging tool example

Tuning tool

This tool can be used to analyze the agreement between predicted and measured signal levels. The tool also includes algorithms and features for automatic tuning of propagation model coefficients.

To exclude spurious data, measurements can be filtered based on signal level, distance, angle, samples, and morphology type. The profile with morphology information from transmitter to each measurement point is found directly. The histogram of the error, the mean error, the median error, the RMS and the 10 % and 90 % values are presented for all loaded measurements or for the current measurement.

For the automatic tuning, the user can select which model coefficients to tune and set limits or constraints to resulting allowable model coefficient values.

The optimisation algorithm will then calculate new estimates of the selected coefficients within the defined constraints.

Figure 5.12: Measurement tuning tool example

Part III

Conclusion

6

Conclusion and Future Work

The following chapter will conclude upon the work performed in this thesis, and recommend some future work in the area of LTE deployment in Networking Oslo.

6.1 Conclusion

The report consists of three (3) parts, where the part one sums up some of the features of the LTE standard. Part two consists of a previous study over propagation prediction models for a possible implementation on future versions of Astrix. The third part of this report sums up the execution of an Astrix case within the Networking Oslo live measurements campaign.

The main point covered by this thesis is about the study and validation of some propagation prediction models for later use on the radio planning of an LTE network.

As I mentioned before in chapter 4 Astrix main models are based on Okumura-Hata and COST231 models but it must be studied the addition of new models such as Causebrook model instead of Deygout model for propagation by diffraction and the use of ITU-R. P.526 and ITU-R P.1546 for the addition of features like propagation over rounded obstacles and propagation over water.

Another recommendation would be to use ITU-R P.833 for propagation over forested areas as an optional model to Blomquist-Ladell.

6.2 Future Work

As a future work, I would recommend Teleplan AS to test all of these improvements found in the literature and strongly encourage them to calibrate their model for LTE frequencies since they tuned the models with UMTS frequencies (1800 MHz) which could be probably good enough as they experienced but I think that the models could like this be better accurate to reality.

Part IV

Appendix

A

Topology and Demography of Oslo

Oslo is the capital and largest city in Norway. The municipality is the first (1st) most populated municipality and is also the first (1st) largest urban area in Norway, [A1]. The city is situated at 59.9 degrees north at the end of the Oslofjord where the city sprawls out in three distinct corridors from its centre; inland north-eastwards and southwards lining both sides of the fjord giving the city area more or less the shape of a large, reclining ‘’Y’’ when seen from the north. It has humid continental climate since there is on a zone of conflict between polar and tropical air masses.

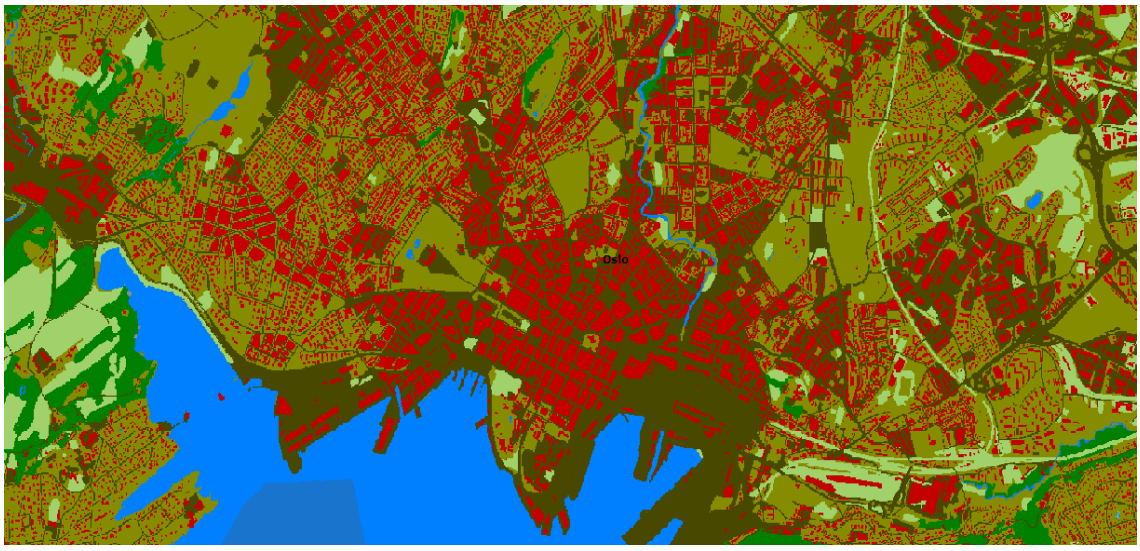

Figure A.1: Clutter raster of Oslo city. [A2]

Oslo is the seat of Norway's national government, most government offices are located there, and is also an important centre of maritime knowledge in Europe and is home to approximately 980 companies and 8,500 employees within the maritime sector, some of which are the world's largest shipping companies, shipbrokers, and insurance brokers.. As a result, Oslo consists of many high-end users, making the city well suited for employing and testing new wireless technologies such as LTE or 4G.

As most metropolitan areas, Oslo has a densely populated city center with decreasing population density further away from the city core. Characterizations of the metropolitan areas are divided into the common five (5) categories. Figure A.1 shows how the different areas are characterized in the radio planning tool Astrix 5.2, [A2]. Underneath follows a description of the five area classifications. Table A.1 provides the color-mapping of the clutter layer in Figures A.1 and A.2.

Building areas are found in the city center. Commercial buildings and multi-dwelling homes provides a hostile propagation environment with many reflections and multipaths. Building areas are marked in red (commercial buildings), see Figure A.1.

Urban areas consist of more sparsely separated multi-dwelling buildings with lower building heights. The radio propagation is approximately equal with a dense urban area. Figure A.2 marks the urban areas in purple, which symbolizes multi dwelling buildings.

Suburban areas have lower building density, where buildings are single dwelling homes. The propagation environment is better due to the more open areas. Single dwelling homes are marked with brown in Figure A.2.

Other areas are in the outskirt of a city. The areas consist of widely separated single dwelling homes. They are presented in light brown in Figure A.2.

Open space consists of open areas as parks, forests, river, lakes and sea. Parks and forests are colored green, river and lakes colored light blue and sea colored in dark blue in Figure A.2.

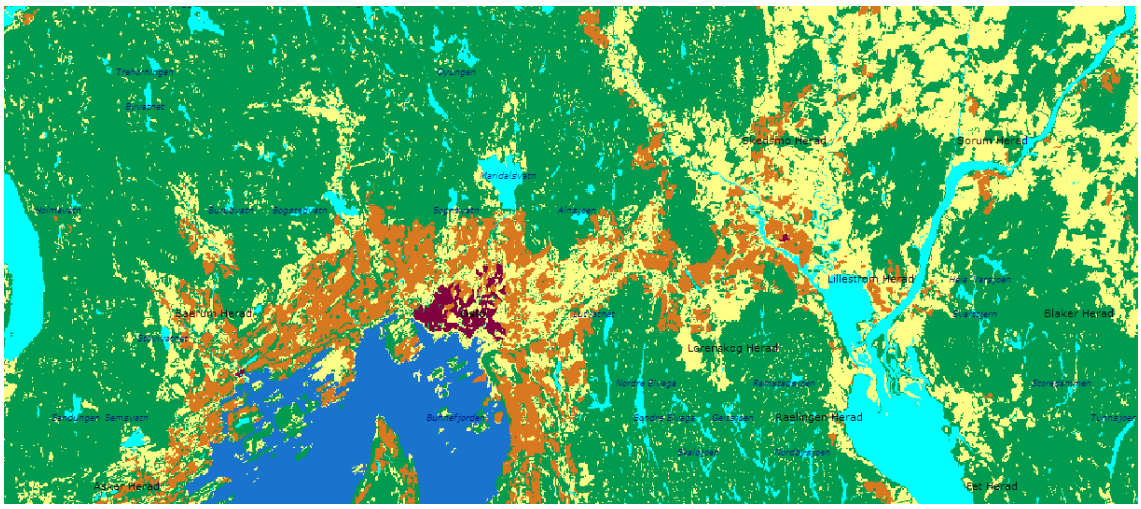

Figure A.2: Clutter ruster of Oslo municipality [A2]

It can be seen that propagation statistics changes within the city limits. Furthermore, another interesting feature to map is the demographics. Demographics tells us, among other factors, something about population density. Population density is important for a radio planner in order to decide where the radio planning is to be performed, and if the system is expected to be capacity limited or range limited within certain areas.

Table A.2 provide statistics gathered from [A1]. As mentioned, Oslo is the first (1st) most populated area in Norway with its 586 860 inhabitants, as of 1st of January 2010. The effective population of Oslo/Akershus is about 1 123 359, almost 25 % of the whole country.

It can be seen from table A.2 that the average population density is 1297.9 inhabitants per km2. Table A.2 and Figure A.3 shows that the main population, 99% live in the built up areas. Moreover, Table B.1 shows settlement divided per the seventeen (17) regions in Oslo, see Figure B.1, whereas Figure A.3 shows the distribution of the inhabitants.

Figure A.3 shows that the main population is settled in the city center and the immediate proximity. The implementation of LTE and 4G will thus be restricted to the high populated areas, and with the possibility of expansion.

Color	Definition
	Undefined, unknown
	Coast, sea
	Lake
	River
	Forest
	Marsh
	Glacier
	Urban area
	Suburban area
	Industry
	Airport
	Others
	Water
	Asphalt
	Park
	Building
	Plain
	Bedrock

Table A.1: Clutter color-definition in Astrix 5.2

Area	**452.14 km²**
Population	**586 860**
0-15 years old	**106 762**
16 - 79 years old	**457 025**
80+ years old	**23 073**
Population per km²	**1297.9**
Population in built-up areas	**99.5 %**

Table A.2: Statistics of Oslo municipality [A1]

Coverage and Capacity

Mobility and wide range of services increases the requirements to coverage and capacity. Building heights, density, material, and terrain do all affect the link budget and has to be considered during radio planning.

Mobility increases the requirement of ubiquitous coverage where mobile users may traverse through areas with low or no population. Fixed systems do thus not have the same requirement when it comes to coverage of open areas since fixed and/or nomadic equipment often require access to power.

Moreover, coverage and capacity do, unfortunately, not come hand in hand, and dense areas tend to be capacity limited rather than range limited. Hence another consideration is that business hours often require more capacity in central areas due to the commuter traffic. A population increment of 15 % is a common value for many metropolitan areas because of the commuting traffic.

The service demand from users span from web-browsing to video conferences. Users are often divided into three (3) categories.

Professional Users requires services for both business and personal usage. The most common services are: e-mail, VoIP, voice conference, video conference, and download.

High-end Consumers uses the services for personal usage. Video streaming, Internet, gaming, and e-mail are the most common services demanded for this type of users. Oslo is, as before mentioned, referred to as an important centre of maritime knowledge in Europe and the seat of Norway's national government, and have many high-end consumers. Thus, it is suitable for testing market penetration with new technologies.

Casual Users are persons with periodic usage of mainly web-browsing.

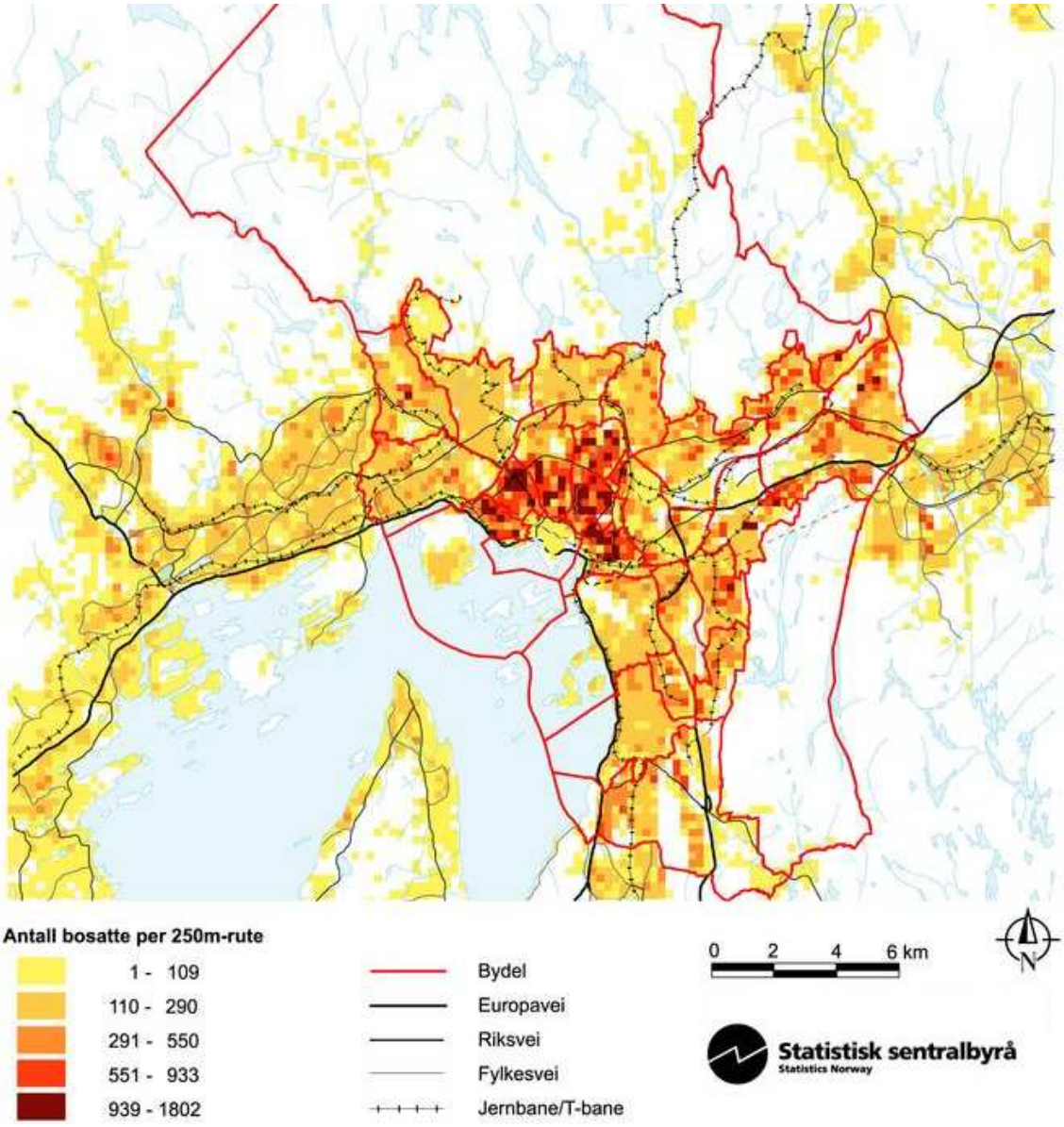

Figure A.3: Settlement in Oslo [A1]

B

Regions of Oslo municipality

Region *	Age			Total	Size	Density
	0-15	16-79	80+		km²	1/km²
1. Gamle Oslo	7 054	34 719	796	42 569	7.45	5 714
2. Grünerløkka	5 933	38 581	1 133	45 647	4.75	9 609.9
3. Sagene	4 363	28 949	974	34 286	3.1	11 060
4. St. Hanshaugen	3 547	27 820	887	32 254	3.59	8 984.4
5. Frogner	5 056	43 221	2 119	50 396	8.3	6 071.8
6. Ullern	5 849	22 735	1 666	30 250	9.4	3 218.1
7. Vestre Aker	9 210	32 109	2 138	43 457	16.59	2 619.5
8. Nordre Aker	9 568	34 641	2 078	46 287	13.57	3 411
9. Bjerke	6 059	20 284	1 289	27 632	7.72	3 579.3
10. Grorud	5 507	19 464	1 103	26 074	7.04	3 703.7
11. Stovner	6 634	22 263	849	29 746	8.25	3 605.6
12. Alna	9 574	35 284	1 745	46 603	13.75	3 389.3
13. Østensjø	9 227	33 492	2 858	45 577	12.24	3 723.6
14. Nordstrand	9 454	34 161	2 804	46 419	16.87	2 751.6
15. Søndre Nordstrand	9 097	26 111	560	35 768	18.42	1 941.8
16. Sentrum	26	886	6	918	-	-
17.Marka	340	1 255	43	1 638	301.1	5.44
Unknown	264	1 050	25	1 339	-	-
Oslo	106 672	457 025	23 073	586 860	452.14	1 297.9

Table B.1: Settlement per region.* See [A1]

Figure B.1: The seventeen (17) regions of Oslo municipality

C

Antenna Specifications

A. 800 10442 Omnidirectional Antenna [S1]

Specifications:

Frequency range	2500–2700 MHz
Gain	11 dBi
Impedance	50 ohms
VSWR	< 1.5:1
Intermodulation (2x20w)	IM3: <-150 dBc
Polarization	Vertical
Maximum input power	200 watts (at 50°C)
H-plane beamwidth	Omni
E-plane beamwidth	7 degrees (half-power)
Connector	7-16 DIN female
Weight	9.9 lb (4.5 kg)
Height approx.	44.6 inches (1132 mm)
Radome diameter	2 inches (51 mm)
Equivalent flat plate area	1.05 ft² (0.098 m²)
Wind survival rating*	120 mph (200 kph)
Shipping dimensions approx.	48.5 x 5.8 x 4.4 inches (1232 x 148 x 112 mm)
Mounting	For masts of 2 to 3.7 inch (50 to 94 mm) OD.

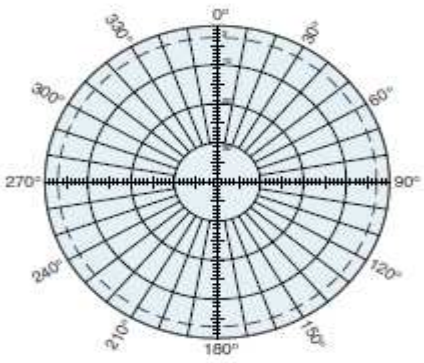

H-plane
Horizontal pattern
V-polarization

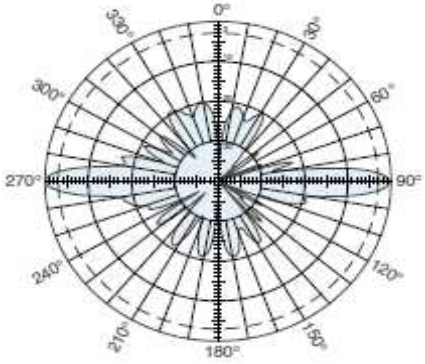

E-plane
Vertical pattern
V-polarization

Figure C.1: 800 10442 Omnidirectional Antenna [S1]

B. 800 10541 60° X-pol Panel Antenna 2300–2690 MHz [S1]

Specifications:	800 10541	800 10551
Frequency range	2300–2690 MHz	2300–2690 MHz
Gain	18 dBi	18 dBi
Impedance	50 ohms	50 ohms
VSWR	< 1.5:1	< 1.5:1
Intermodulation (2x20w)	IM3:< -150 dBc	N/A
Polarization	+45° and -45°	+45° and -45°
Front-to-back ratio (180°±30°)	>25 dB	>25 dB
Maximum input power	250 watts (at 50°C)	250 watts (at 50°C)
Horizontal beamwidth 2300–2500 MHz 2490–2690 MHz	 61 degrees (half power) 58 degrees (half power)	 61 degrees (half power) 58 degrees (half power)
Vertical beamwidth 2300–2500 MHz 2490–2690 MHz	 6.5 degrees (half power) 6.2 degrees (half power)	 6.5 degrees (half power) 6.2 degrees (half power)
Electrical downtilt continously adjustable	0–12 degrees	0–12 degrees
Connector	2 x 7-16 DIN female	2 x N female
Isolation	>30 dB	>30 dB
Sidelobe suppression for first sidelobe above main beam	0° 6° 12° ≥15 17 17	0° 6° 12° ≥15 17 17
Cross polar ratio Main direction 0° Sector ±60°	 20 dB (typical) ≥8 dB	 20 dB (typical) ≥8 dB
Weight	13.2 lb (6 kg)	13.2 lb (6 kg)
Dimensions	45.7 x 6.1 x 2.7 inches (1160 x 155 x 69 mm)	45.7 x 6.1 x 2.7 inches (1160 x 155 x 69 mm)
Equivalent flat plate area	2.69 ft² (0.25 m²)	2.69 ft² (0.25 m²)
Wind survival rating*	120 mph (200 kph)	120 mph (200 kph)
Shipping dimensions	56.4 x 6.8 x 3.6 inches (1432 x 172 x 92 mm)	56.4 x 6.8 x 3.6 inches (1432 x 172 x 92 mm)
Shipping weight	16.5 lb (7.5 kg)	16.5 lb (7.5 kg)
Mounting	Fixed and tilt-mount options are available for 2 to 5.7 inch (50 to 145 mm) OD masts.	

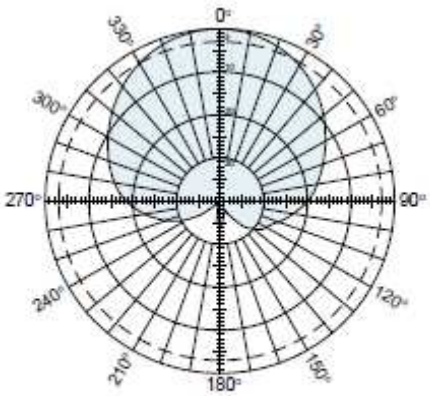

Horizontal pattern
±45°- polarization

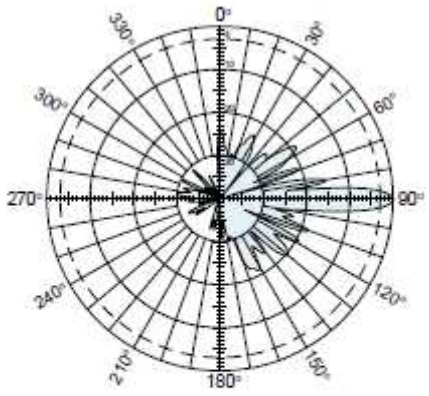

Vertical pattern
±45°- polarization
0°–12° electrical downtilt

Figure C.2: 800 10541 60° X-pol Panel Antenna 2300– 2690 MHz [S1]

C. 800 10544 65° Panel Antenna [S1]

Specifications:

	Column 1	Column 2
Frequency range	1710–2200 MHz	2300–2690 MHz
Gain	17.8 dBi	17.5 dBi
Impedance	50 ohms	50 ohms
VSWR	< 1.5:1	< 1.5:1
Intermodulation (2x20w)	IM3: <-150 dBc	IM3: <-150 dBc
Polarization	+45° and -45°	+45° and -45°
Front-to-back ratio (180°±30°)	≥25 dB	≥25 dB
Maximum input power	250 watts per input (at 50°C)	250 watts per input (at 50°C)
+45° and -45° polarization horizontal beamwidth	63° (half-power)	61° (half-power)
+45° and -45° polarization vertical beamwidth	7° (half-power)	6.5° (half-power)
Electrical downtilt continuously adjustable	0–15 degrees (manual or optional remote control)	0–12 degrees (manual or optional remote control)
Connector	2 x 7-16 DIN female	2 x 7-16 DIN female
Isolation between inputs	>30 dB	>30 dB
Cross polar ratio Main direction 0° Sector ±60°	 >20 dB >10 dB (typical)	 >20 dB >10 dB (typical)
Sidelobe suppression for first sidelobe above main beam	≥16 dB	≥15 dB

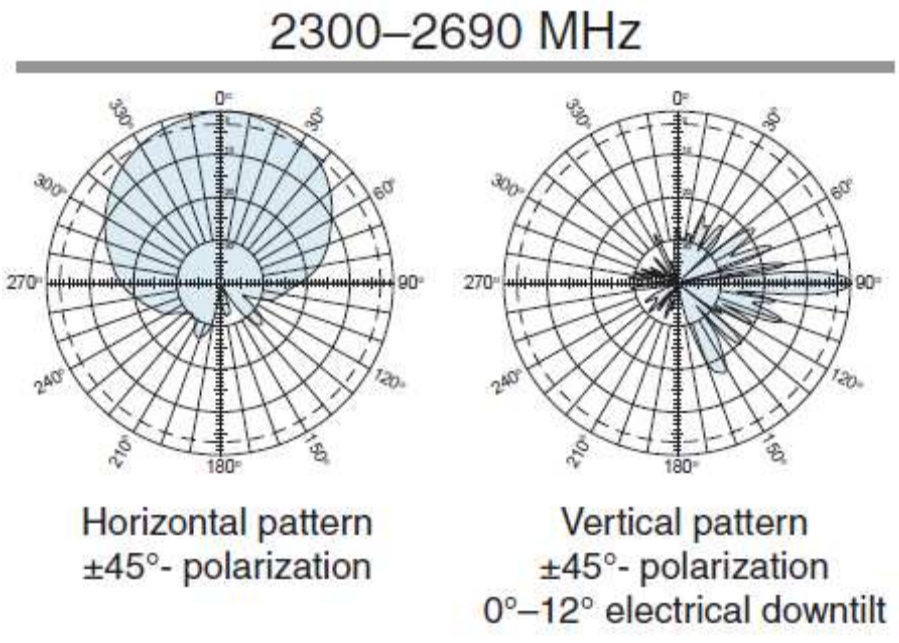

Figure C.3: 800 10544 65° Panel Antenna [S1]

D

Astrix User Case, a brief introduction

Astrix 5.2 is a radio planning tool designed by Teleplan Globe. The software is designed for frequency planning, coverage prediction, interference calculation, radio link planning and network design.

ASTRIX uses an integrated GIS as the basis for map handling. The GIS system provides advanced map features for best possible views and management of maps. The GIS system supports dynamic map resolution and various map formats.

There is no physical limitation in ASTRIX when it's up to the resolution that calculation of coverage can be done in. However, there is a practical limit, because of time and disk space. This limit lies normally between 1 and 5m in cities. For rural areas 100m resolution used to be normal just a few years ago but now most of Teleplan customers have settled for 20-30m resolution on the map (which gives the practical max resolution for coverage). Also when calculating combined coverage for the whole country 200m resolution is quite normal.

The following map layers are supported according to [A1]:

• Raster/grid ground heights

• Raster/grid morphology

• Vector/linear features

• Ortho photo

• Raster/grid building heights

• 3D vector of building foot-prints and heights

• Demographic data

The default propagation model in ASTRIX is based on industry standards:

• Okumura-Hata

• COST231-Hata

• COST231-Walfisch

• Walfisch-Bertoni

• Blomqvist-Ladell

Added to these models are a number of correction factors which have been developed to improve accuracy in hilly terrain. There are several diffraction methods as the one from Walther Aasen mentioned in chapter 4 recently implemented, effective antenna heights and LOS correction methods optimised for handling mountainous and water/sea areas.

In addition, ASTRIX includes multipath propagation models that identify areas with severe time dispersion problems for interference in GSM and multipath areas for LTE.

To address the need for ever denser urban networks, ASTRIX includes:

• Micro-cell models

• Advanced small cell models, based on an automatic combination of Okumura-Hata and Walfisch-Ikegami.

ASTRIX offers optional integration with WaveSight (http://www.wavecall.com/). WaveSight is a ray tracing module which employs vector data. The module is world leading for microcell predictions.

The following chapter is meant as an introductional guide for usage of Astrix 5.2. Teleplan has approved for the guide to be written and published in this thesis.

D.1 Getting started

In the initial stage, Astrix uses scenarios and situation. A scenario may be viewed as the main project, and include many situations. A scenario is created by executing Astrix 5.2, pressing the Astrix button -> New Scenario, see Figure D.1. Importion of terrain data is executed in Map -> Open Map. In a normal installation, the maps are found in C:\Documents and Settings\All Users\Maria Files\Map\Templates. The map provided by Teleplan is called "WorldDCW.m5map".

Default in the map, is the city of Oslo, zooming out is performed by using the "Map Scale" in the bottom right corner of the window, or by pushing the Ctrl button and scrolling with the mouse wheel. Panning the map is performed through right-click ->Map and Zoom -> Pan Map.

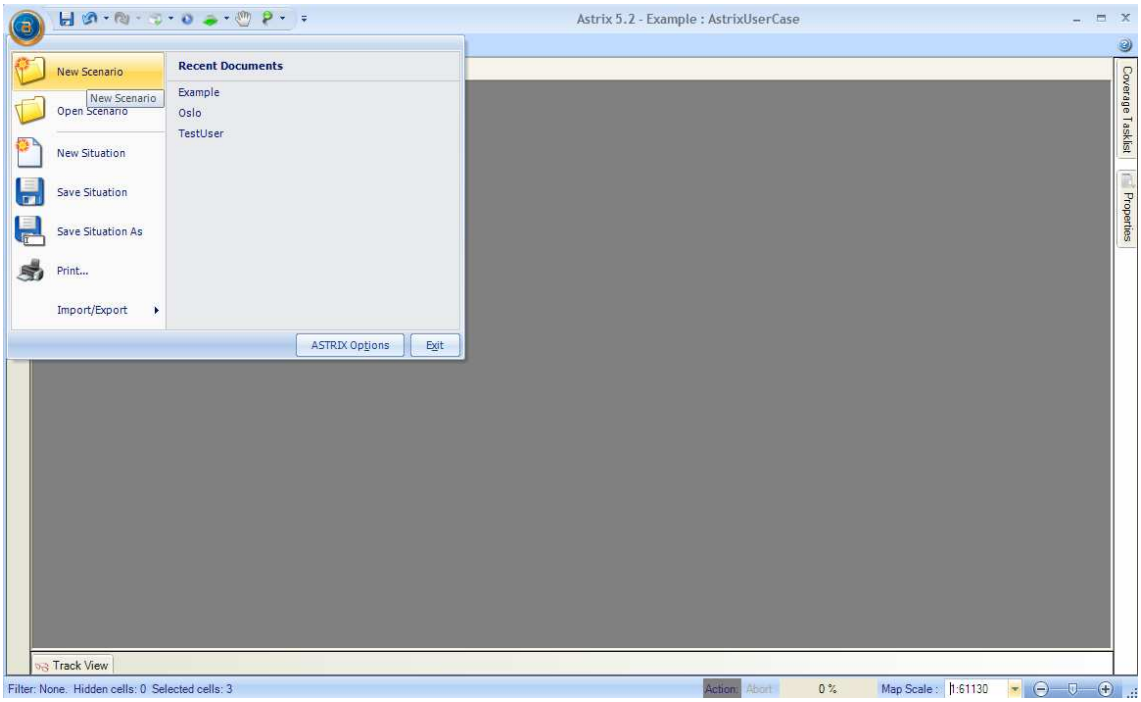

Figure D.1: ASRTRIX getting started example

Furthermore, a new situation is created through the Astrix button -> New Situation. The situation can be named by "Save Situation As". A PDF help file is available by clicking on the question mark in the upper right corner of the Astrix window, see Figure D.1.

D.1.1 Astrix Options

The Astrix Options sets default parameters for the deployed network. Flags, templates, and coordinate system are all set here. The option is found in Astrix button -> ASTRIX Options.

Flags

Base stations are often characterized as candidate, operative, rejected, and tested. Having all base stations plotted in the system, makes the tool look messy, and is quite inefficient. Flags is thus a feature to set on each site in order to filter base stations and cells, making the tool clearer and increasing the efficiency of the radio planning process. The number of flags the system planner wants to use is individual. Recommended is to add an area-flag, where all base stations and cells within the same area carries the same flag. If there exists several radio planners using the same scenario, a system planner flag may be an easy way for each system planner to find its own base stations and cells. Figure D.2 shows the ASTRIX Options menu, and the flag-window.

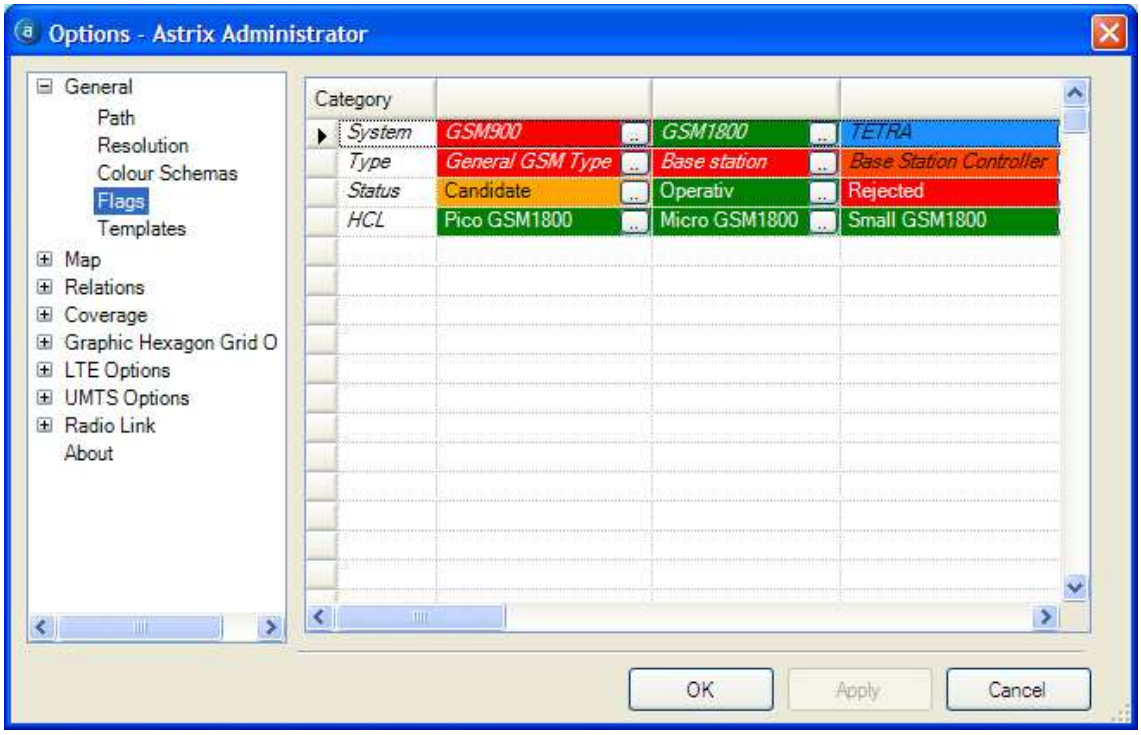

Figure D.2: ASTRIX Options for setting flags

Templates

Further in the process, while still having the ASTRIX Options window open, site and cell templates can be created. The site templates may be viewed as the base station parameter, and the cells as its sectors. The number of sectors and cells depends on the antenna patterns. For configuration of the antenna pattern, see section D.1.2. Creating sites are done by right-click -> New Site. The site template may then be named. Cells are created in the same manner. Antenna parameters such as pattern, height, direction, and tilt are all set for each cell. Moreover, the parameters are editable when deployed in the scenario. For prediction of coverage, resolution, predefined area and propagation models are all set here. The desired propagation model is chosen from a drop down list. Radio parameters such as transmitting power, loss, sensitivity and frequency are also set for each cell. Figure D.3 shows the Template menu for editing the mentioned parameters.

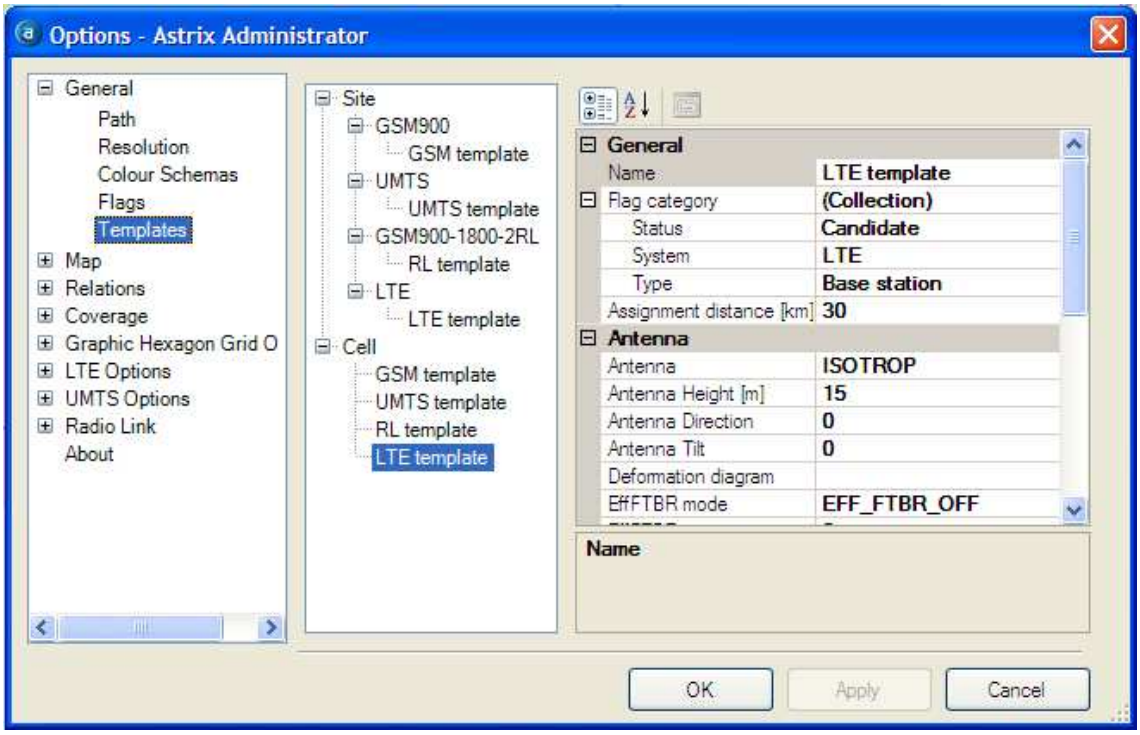

Figure D.3: Configuration of site and cell templates

Coordinate System

Coordinate systems are, as known, found in many different formats. Astrix 5.2 supports a total of six (6) different coordinate systems. The advantage of choosing between coordinate systems is for system adaption towards other systems such as a GPS or Google Earth. The coordinate systems are found in the Astrix Options under Map -> Coordinate systems.

D.1.2 Adding Antennas

In order to perform a realistic as possible radio planning, the antenna pattern has to be as close as possible to the employed antennas. Astrix 5.2 contains a list of 78 predefined antenna patterns. If the desired pattern is not found, a new antenna pattern is easily added if the system manufacturer has provided such information. Home -> Antenna List shows a list of the predefined antennas and the editor window, see Figure D.4.

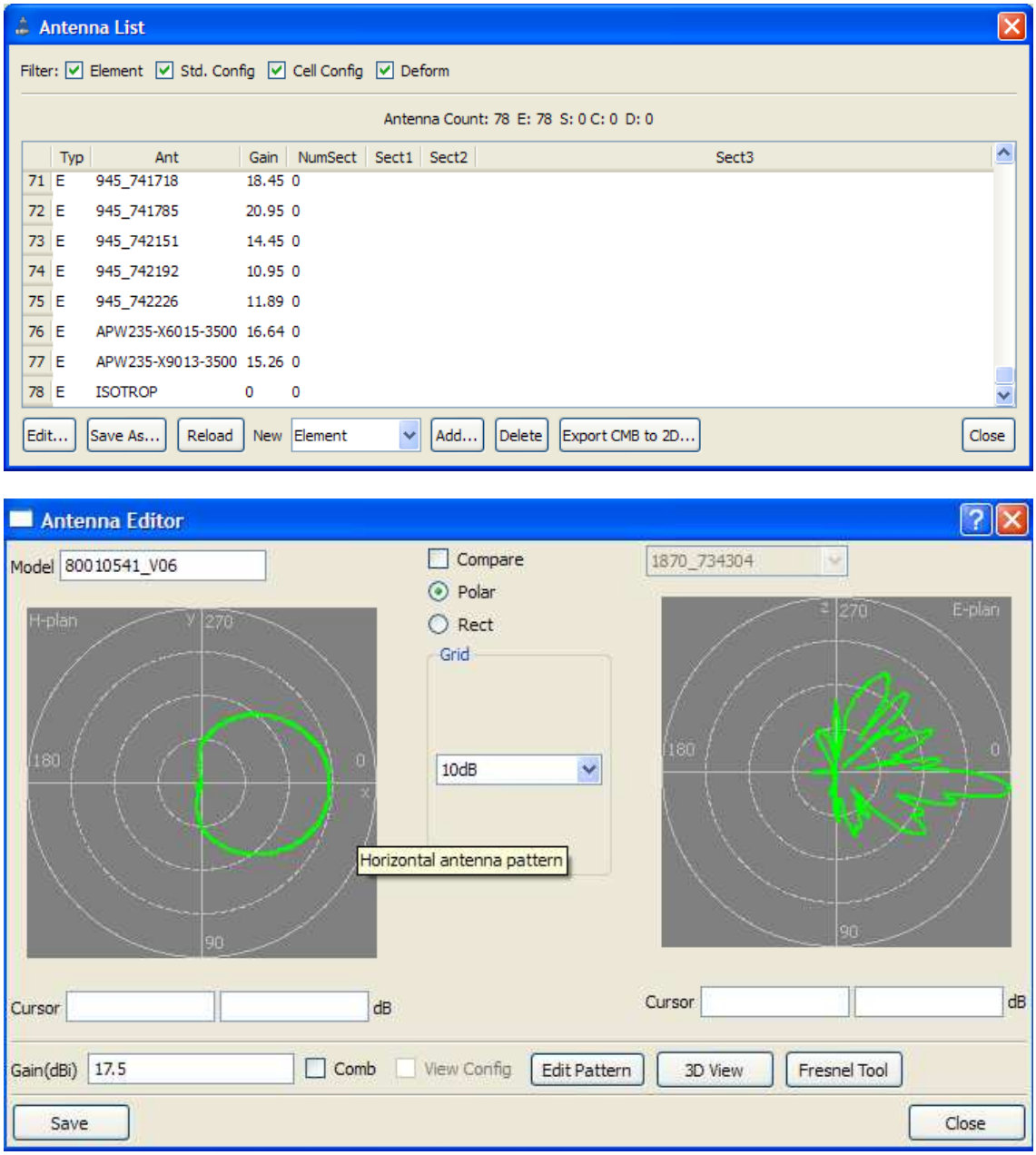

Figure D.4: List and configuration of predefined antennas

To create an antenna file, the setup has to be known. Figure D.5 shows an example file for importing an antenna element. It is worth noticing that the delimiter is tab. Furthermore, values are set for every degree increment from 0 up to 360 respectively for the horizontal and the vertical plane. When the file has been stored in the directory C:\AstrixFile\ant\element, Astrix has to be restarted before the antenna is found in the antenna list.

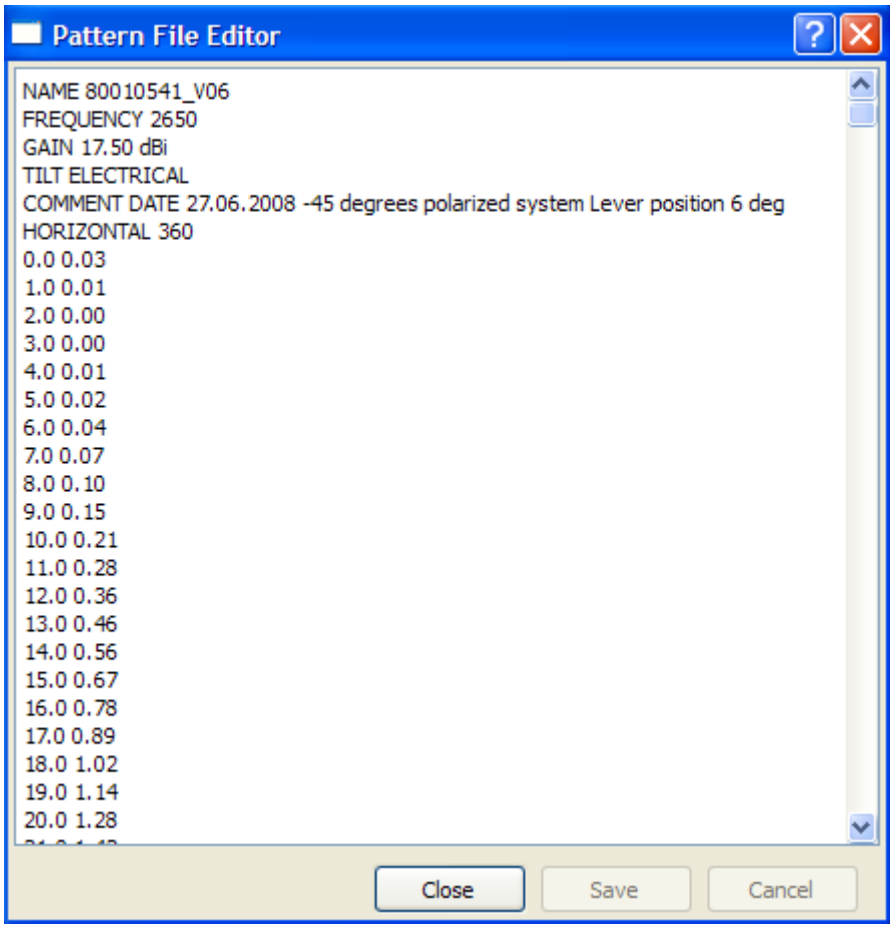

Figure D.5: Example file for importing antenna element

D.2 System Deployment

Setting up templates, system parameters, and antenna configurations is a great step towards the actual deployment of the system. The next step is thus to position and direct the base stations and cells. Before positioning the sites, windows should be placed for adjustments of the deployed sites. The subsequent section provides a brief description and suggestions of window-views in Astrix 5.2.

D.2.1 Window-views

The different windows views are found in Home -> Windows, see Figure D.6. As can be seen from the figure, a total of eleven (11) windows are available. The recommended windows when radio planning are:

- Track view

- Layers view

- Coverage Tasklist

- Situation Tree

- Properties

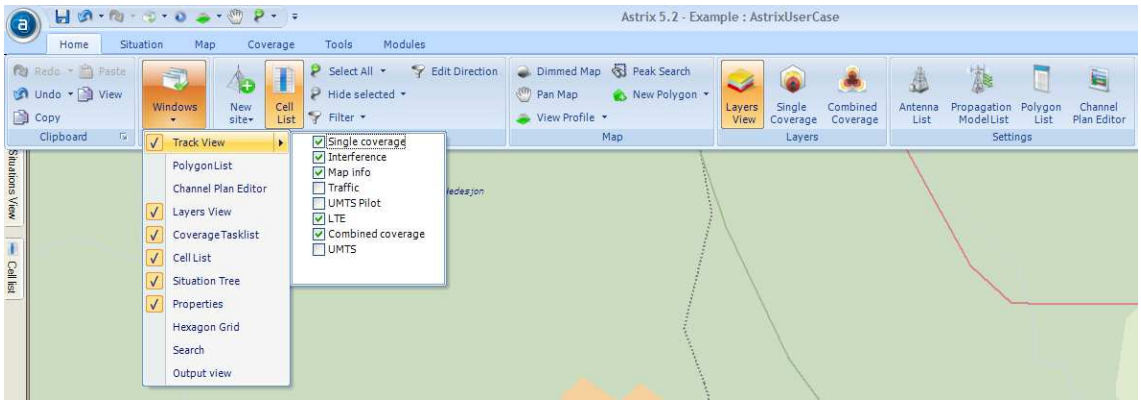

Figure D.6: Windows alternatives

D.2.2 Adding sites and cells

Site and cells are easily added as mentioned before, by right-click -> New Site, wherever it is desired to position the given site. The site and its cells are then available in the drop down menu, under the given situation, in the Situation View window. By marking the new site in the Situation View window, renaming, flagging, and entering the position is possible in the Properties Window. The same counts for each cell, where properties of each marked cell is viewed and editable. Common parameters are possible to edit by marking several cells and/or sites. Figure D.7 shows the recommended outline of the dockable windows, and how the properties of a marked cell are editable.

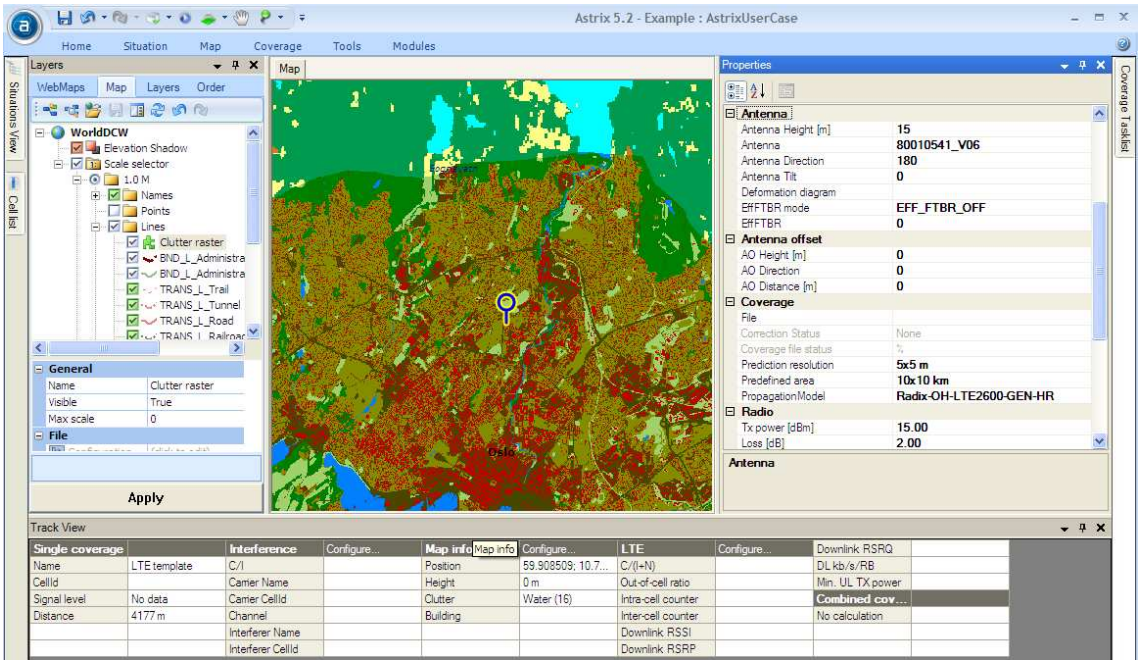

Figure D.7: View of the docked windows, and how a cell is editable

D.3 Coverage Prediction

Coverage prediction can be calculated in two ways, the single coverage, and combined coverage. Single coverage is for predicting coverage from one sector, where combined coverage predicts the total coverage from multiple cells and base stations. The coverage prediction is found by pressing the Coverage tab, see Figure D8. The options presented for coverage are propagation model, size of area to predict coverage, coverage resolution, and number of cells. If no adjustments are performed, then the software calculates with the default values set in the Astrix Options. By pressing the highlighted button, Coverage Prediction, in Figure D.8, an additional window appears. The window allows the user to set the height of the receiving client, and the other parameters just mentioned. It is recommended to use this window for coverage prediction.

Furthermore, when calculating, the process may be followed in the Coverage Tasklist window. Without this window, the user will not know if the software is calculating, or when the calculation has finished.

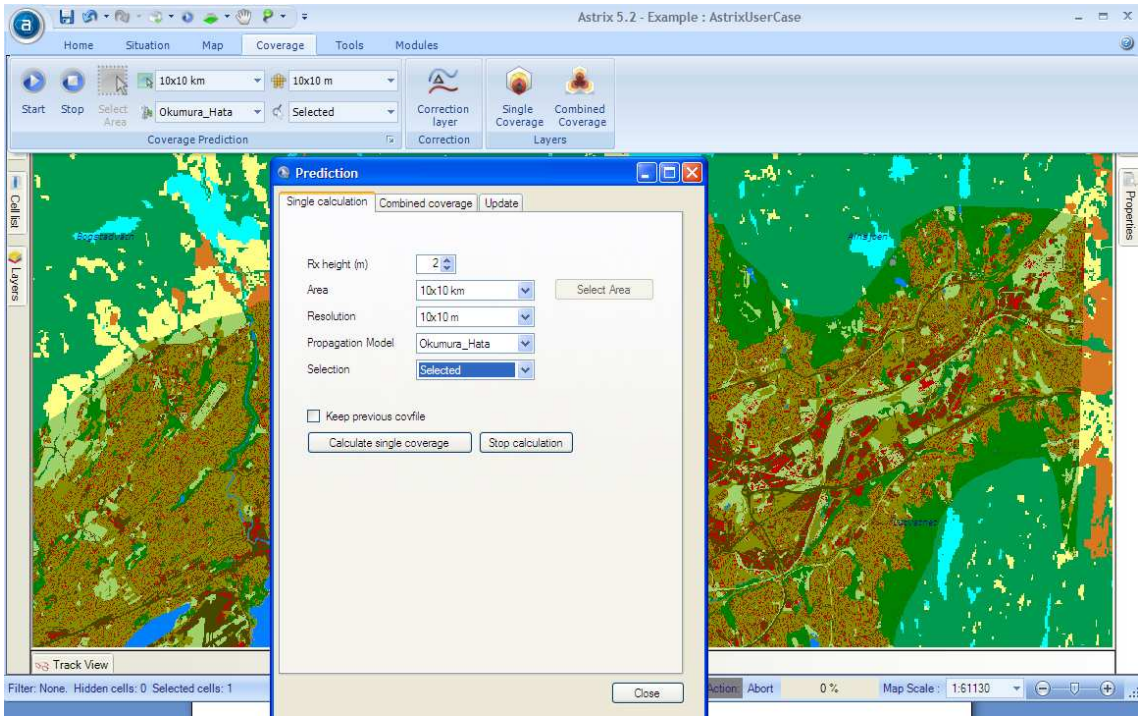

Figure D.8: Options in the Coverage menu

Combined coverage, however, is recommended to be calculated through the Coverage Prediction button, highlighted in Figure D.8, and the Combined coverage tab. The reason for recommending this way is that the combined coverage can be saved in several files, making it possible to have several combined coverages. When a single coverage calculation is performed, the combined coverage prediction is updated to the active combined coverage calculation, which is set in the Prediction window. Having only one combined coverage file makes it difficult to follow when many calculations are being performed. Figure D.9 shows the Prediction window for combined coverage.

The combined coverage taskbar is displayed on the bottom of the Astrix window, next to the Map Scale. Figure D.10 shows the predicted combined coverage from three sectors. A handy feature in Astrix, is the transparency mode. Highlighting the cell coverage or combined coverage in the Layers window -> Layers, gives the opportunity to make the coverage prediction transparent, see Figure D.10.

It has to be stressed that the Cell coverage or Combined coverage have to be checked in the Layers window -> Layers for single and combined coverage to be viewed respectively. Another way is to see if the Single Coverage or Combined Coverage are highlighted in the Coverage tab.

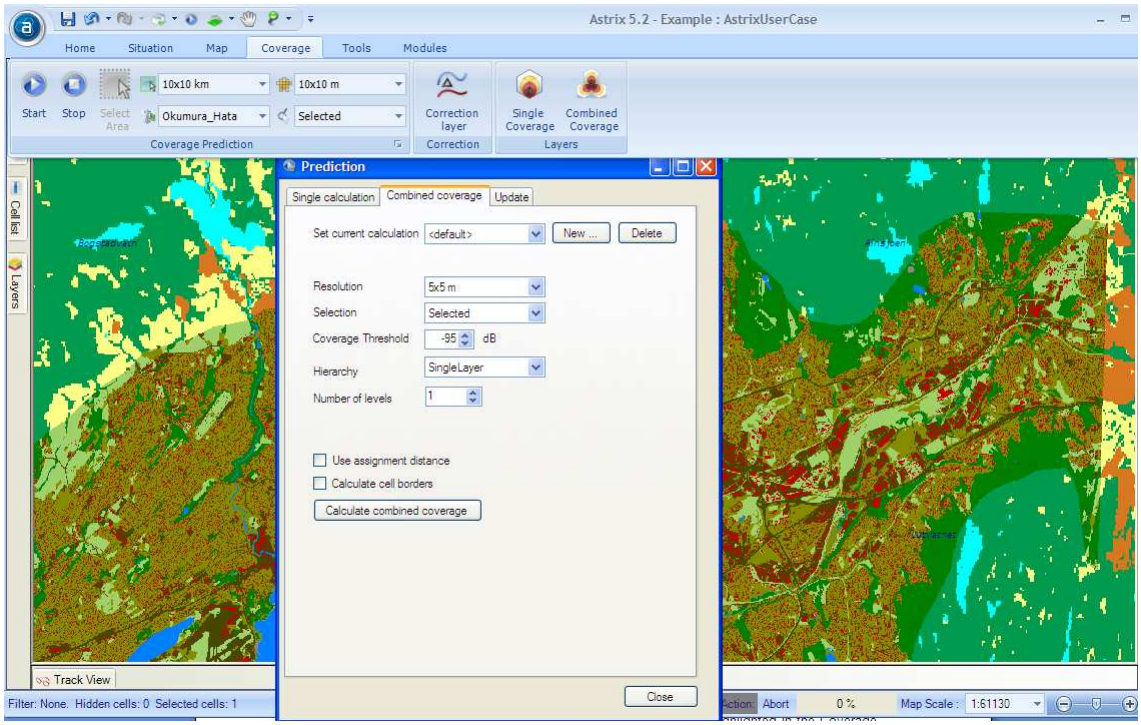

Figure D.9: Combined coverage calculation

D.3.1 Tracking

Tracking is a useful feature for checking the signal strength throughout the predicted area. Highlighting the desired antenna, and moving the cursor around on the map gives combined signal strength and signal strength from the selected cell along with other information such as distance from base station, clutter type, and position of the cursor. Figure D.10 shows predicted coverage at a point 665 meters away from the base station.

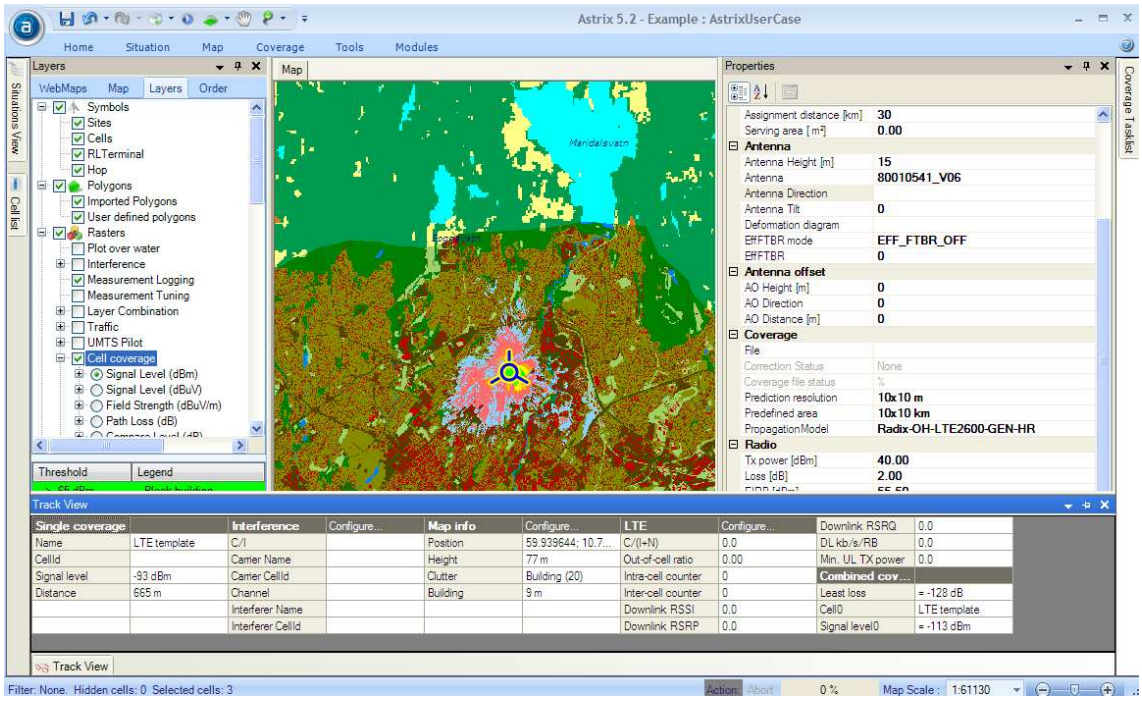

Figure D.10: Combined coverage, and track view

D.4 Logging and tuning tool

ASTRIX includes a sophisticated propagation model tuning tool. The tool can be used to analyse the agreement between predicted and measured signal levels. The tool also includes algorithms and features for automatic tuning of propagation model coefficients.

The idea behind the logging and tuning tool is to add a correction layer to improve the coverage prediction. The formats required to use the logging tool is .csv (comma separated values), which is normally obtained from an excel file, and for the tuning tool are .mtt or .mtc respectively.

ASTRIX offers a unique and advanced algorithm that combines calculated coverage predictions with drive test measurements to calculate significantly improved measurement based predictions. Using drive test measurements to produce a correction layer on top of normal coverage predictions the accuracy is improved to a standard deviation of 5 to 6 dB - close to the theoretical limit.

D.5 Backup

Backup is always a necessity. The files which are important to have backup on are the ones located in the Scenario folder. The default directory for this folder is C:\AstrixFiles\Scenarios. The folder contains the created situations, and all logs regarding coverage prediction.

E

Source code (Matlab)

The following appendix contains descriptions of the Matlab files suggested for testing the formulas of the ITU-R P.526, COST231 and ITU-R P.1546 recommendations. The files are enclosed in the subsequent sections for future radio planners to revise and edit. ITU-R P.1546 files were obtained from the PhD student Kun Yang co-supervisor of the thesis.

E.1 ITU-R P.526 files

The first two .m programs calculate the single knife-edge diffraction and the last two ones present the calculation of the additional parameter that must be taken into account due to over rounded obstacle diffraction.

a) Single knife-edge diffraction from ITU-R P.526

```
function [J,v] = single_knife_edge (h,freq,d_1,d_2)

%ITU-R p.526 page 12

% h [m]

% d_1, d_2 [km]

% freq [MHz]

% J [dB] works well
```

```
lambda = 3e2./freq;

v = h.*sqrt((2/lambda).*((1/d_1)+(1/d_2)));

for i=1:length(h)
   if v(i)<=-0.7
      J(i)=0;
   else
      J(i)=6.9+20.*log10(sqrt(((v(i)-0.1).^2)+1)+v(i)-0.1);
   end
end

plot(v,-J,'.'),set(gca,'Xlim',[-3,3]),grid
```

b) Single knife-edge diffraction from Rappaport approach

```
function [v,G] = diff_loss_Rappaport (h,freq,d_1,d_2)

% Theodore Rappaport 'Wireless Communications' Ed. Prentice Hall pages 126, 131
% h [m]
% d_1,d_2 [m] notice that is in meters!!!
% freq [MHz]
% G [dB] works well

lambda=3e2./freq;
v=h.*sqrt((2.*(d_1+d_2))./(lambda.*d_1.*d_2));

for i=1:length(v)

   if v(i)<=-1
      G(i)=0;
```

```
    elseif -1<=v(i)<0
        G(i)=20.*log10(0.5-(0.62.*v(i)));
    elseif 0<=v(i)<1
        G(i)=20.*log10(0.5*exp(-0.95.*v(i)));
    elseif 1<=v(i)<2.4
        G(i)=20.*log10(0.4-sqrt(0.1184-((0.38-0.1.*v(i)).^2)));
    else
        G(i)=20.*log10(0.225./v(i));
    end
end

plot(v,G),set(gca,'Xlim',[-3,5]),grid
```

c) Single rounded obstacle diffraction from ITU-R P.526

```
function [v,n,m,k,b,J,T] = single_rounded (R,h,h_p,freq,d_1,d_2)
% ITU-R P.526 pages 13,14

% R [m]
% h [m] for rounded obstacle is constant and positive (see Figure 4.4.c)
% h_p [m]
% freq [MHz]
% d_1, d_2 [m]

% A,J(v),T(m,n) [dB] works well
% e.g. >>h=linspace(a,b,length(h_p)); a & b positive values

% Single knife-edge obstacle losses

lambda=3e2./freq;
v = h_p.*sqrt((2./lambda).*((1./d_1)+(1./d_2)));
```

```
%alfa_1=asin(h/d_1);
%alfa_2=asin(h/d_2);

%d_a=acos(alfa_1)*d_1;
%d_b=acos(alfa_2)*d_2;
%d=d_a+d_b;

for i=1:length(h_p)
   if v(i)<=-0.7
      J(i)=0;
   else
      J(i)=6.9+20.*log10(sqrt(((v(i)-0.1).^2)+1)+v(i)-0.1);
   end
end

%subplot(2,1,1), plot(v,-J),xlabel('v'),ylabel('J(dB)'),set(gca,'Xlim',[-3,3]),grid

% Additional loss due to rounded obstacle T(m,n)

% Note that as R tends to zero, m and T(m,n) also tend to zero.
% R, d_1, d_2, h and lambda are in self-consistent units

%h=n*R.^(1/3)/((pi/lambda).^(2/3));

m=R.^(2/3).*((d_1+d_2)./(d_1.*d_2))./((pi./lambda).^(1/3));
n=h.*(((pi.*R)./lambda).^(2/3))./R;

b=0.73+0.27.*(1-exp(-1.43.*n));
k=8.2+12.*n;
```

```
T=k.*realpow(m,b);

% Adequate values to plot Figure 8 on page 14 (only for the plot)

N=[100 10 5 2 1 0.5 0.25 0];

M=0:.01:4;

for i=1:length(N)

for j=1:length(M)

t(i,j)=(8.2+12.*N(i)).*realpow(M(j),(0.73+0.27.*(1-exp(-1.43.*N(i)))));

end

end

%subplot(2,1,2),
plot(M,t),xlabel('m'),ylabel('T(m,n)(dB)'),set(gca,'Xlim',[0,4]),set(gca,'Ylim',[0,50]),grid
```

d) Additional parameter from Lee rounded hill diffraction approach

```
function[sigma_v,sigma_h,K,delta_v,delta_h]=additional_loss_Lee_matrix
(R,h_p,beta,freq,r_1,r_2)

%Lee pages 147,148

%Additional loss due to rounded hill

%R [m]

%h_p [m]

%r_1, r_2 [km]

%freq [MHz]

%sigma [dB]
```

```
lambda=3e2./freq;
%r(1,i)=1./((1./r_1)+(1./r_2(1,i)));
%theta=-h_p.*((1./r_1)+(1./r_2(1,i)));
%v=sqrt((2.*r)./lambda).*theta;

for j=1:length(R)
   for i=1:length(r_2)

      r(1,i)=1./((1./r_1)+(1./r_2(1,i)));
      theta(1,i)=-h_p(1,i).*((1./r_1)+(1./r_2(1,i)));

      delta_v(j,i)=0.316.*(1+(r_2(1,i)./r_1)).*lambda.*(nthroot((R(1,j)./lambda),3));
      delta_h(j,i)=-0.333.*(1+(r_2(1,i)./r_1)).*lambda.*(nthroot((R(1,j)./lambda),3));

   end
end

for j=1:length(R)
   for i=1:length(r_2)
         if r_1>r_2(1,i)
               K(1,i)=(1./2.*r_2(1,i)).*(1./2.*((r_1+r_2(1,i)).^2)).*sqrt((2.*beta.*r(1,i))/pi);
               sigma_v(j,i)=K(1,i).*delta_v(j,i);
               sigma_h(j,i)=K(1,i).*delta_h(j,i);
      end
   end
end

%subplot(2,1,1), plot(theta,sigma_v),grid
%subplot(2,1,2), plot(theta,sigma_h),grid
```

E.2 COST231 files

a) COST231 Walfisch_Ikegami Model

```
function [Lb,Lo,Lrts,Lmsd] = COST231_WI (f,d,w,b,phase,hb,hr,hm,urban_type)

% COST 231 Walfich-Ikegami model
% Loss based on measurements in Stockholm for d>=20m
% Lb equal to FSL for d=20m
% f [MHz], d[km], w[m]=b/2, b [m]
% w: width of roads, b: building separation
% recommendable: b[20-50] m, phase=90
% hb, hr, hm [m] : base station, roof, mobile
% hr= 3 * number of floors + roof-height {3m pitched, 0m flat}
% phase [degrees]
% Lb,Lo,Lrts,Lori,Lmsd [dB]

% This model is restricted to:
% f: [800-2000] MHz
% hb: [4- 50] m
% hm: [1-3] m
% d: [0.02-5] km

AHm=hr-hm;
AHb=hb-hr;

Lo=32.4+20.*log10(d)+20.*log10(f);

if (0<=phase<35)
    Lori=-10+0.354.*phase;
```

```
elseif (35<=phase<55)
    Lori=2.5+0.0075.*(phase-35);
else
    Lori=4-0.114.*(phase-55);
end

Lrts=-16.9-10.*log10(w)+10.*log10(f)+20.*log10(AHm)+20.*log10(f)+Lori;

if (hb>hr)
    Lbsh=-18.*log10(1+AHb);
else
    Lbsh=0;
end

if (hb>hr)
    ka=54;
elseif (d>=0.5 && hb<=hr)
    ka=54-0.8.*AHb;
else
    ka=54-0.8.*AHb.*(d./0.5);
end

if (hb>hr)
    kd=18;
else
    ka=18-15.*(AHb./hr);
end

if strcmp(urban_type,'Suburban area')==1
    kf=-4+0.7.*((f./925)-1); % Suburban area
```

```
else
   kf=-4+1.5.*((f./925)-1); % Metropolitan area
end

Lmsd=Lbsh+ka+kd.*log10(d)+kf.*log10(f)-9.*log10(b);

if (Lrts+Lmsd>0)
   Lb=Lo+Lrts+Lmsd;
else
   Lb=Lo;
end

plot(d,Lb)
```

b) COST231 Walfisch-Bertoni Model

```
function [Lp,Lo,Lex] = WB_model (fc,Rk,d,H,h,hm)

% Walfisch-Bertoni model
% 'A theoretical model of UHF propagation in urban environments'
% fc [MHz]
% Rk [km], d [km]
% H, h, hm [m]


Lo=32.4+20.*log10(fc)+20.*log10(Rk);
A=5.*log10(((d/2).^2)+((h-hm).^2))-9.*log10(d)+20.*log10(atan(2.*(h-hm)./d));
Lex=57.1+A+log10(fc)+18.*log10(Rk)-18.*log10(H)-18.*log10(1-((Rk.^2)./(17.*H)));
Lp=Lo+Lex;

plot(Rk,Lp)
```

E.3 ITU-R. P.1546 files

The ITU function is the main program. It is the one that calls the other subprograms for doing the different calculations within the model.

a) Antenna Condition function

```
function[Field_strength_data]=Antenna_condition(Propagation_type,Nominal_time_temp,Nominal_frequence_temp,Nominal_txantenna_height,Nominal_distance,Distance,TXAntenna_height )

   if [ TXAntenna_height >=10]

       if [ Nominal_txantenna_height(1,2)== 0 ]

[Field_strength_data]=Step_eight(Propagation_type,Nominal_time_temp,Nominal_frequence_temp,Nominal_txantenna_height(1,1),Nominal_distance,Distance) ;

       else

[Field_strength_data1]=Step_eight(Propagation_type,Nominal_time_temp,Nominal_frequence_temp,Nominal_txantenna_height(1,1),Nominal_distance,Distance) ;

[Field_strength_data2]=Step_eight(Propagation_type,Nominal_time_temp,Nominal_frequence_temp,Nominal_txantenna_height(1,2),Nominal_distance,Distance) ;

          Field_strength_data = Field_strength_data1 + ( Field_strength_data2 - Field_strength_data1 )...

             .*log10( TXAntenna_height./Nominal_txantenna_height(1,1) )./ log10( Nominal_txantenna_height(1,2)./Nominal_txantenna_height(1,1) ) ;

       end

    elseif [ TXAntenna_height >=1 && TXAntenna_height < 10 ]

       D_h1 = Fresnel_06(Nominal_frequence_temp,TXAntenna_height,10) ;

       E_fs1 = 106.9 - 20.*log10(D_h1) ;

       E_se1 = 2.38.*(1 - exp(-D_h1./8.94)).*log10(50./Nominal_time_temp) ;

       E_dh1 = E_fs1 + E_se1 ;
```

```
D_20 = Fresnel_06(Nominal_frequence_temp,20,10) ;

[Temp_distance]= distance_search(D_20);

  E_10D20=Field_strength(Propagation_type,Nominal_time_temp,Nominal_frequence_te
  mp,10,Temp_distance(:,3)) ;

  E_20D20=Field_strength(Propagation_type,Nominal_time_temp,Nominal_frequence_te
  mp,20,Temp_distance(:,3)) ;

E_D20=E_10D20 + ( E_20D20 - E_10D20 ).*log10(TXAntenna_height./10)./log10(20./10) ;

d_h = 4.1.*sqrt(TXAntenna_height) ;

d_h10 = 4.1.*sqrt(10) ;

[Temp_index1]= distance_search(d_h10);

[Temp_index2]= distance_search(d_h);

  E_10dh10=Field_strength(Propagation_type,Nominal_time_temp,Nominal_frequence_t
  emp,10,Temp_index1(:,3)) ;

  E_10dh=Field_strength(Propagation_type,Nominal_time_temp,Nominal_frequence_tem
  p,10,Temp_index2(:,3)) ;

for  k=1:length(Distance)

   if [ Distance(k) <= D_h1 ]

      E_fs = 106.9 - 20.*log10(Distance(k)) ;

      E_se = 2.38.*(1 - exp(-Distance(k)./8.94)).*log10(50./Nominal_time_temp) ;

      Field_strength_data(k) = E_fs + E_se ;

   elseif [ Distance(k) > D_h1 && Distance(k) < D_20 ]

       Field_strength_data(k)=E_dh1+

          (E_D20-E_dh1).*log10(Distance(k)./D_h1)./log10(D_20./D_h1) ;

   else

      [Temp_distance]= distance_search(Distance(k));

          E_10d=Field_strength(Propagation_type,Nominal_time_temp,Nominal_frequen
          ce_temp,10,Temp_distance(:,3)) ;
```

```
                E_20d=Field_strength(Propagation_type,Nominal_time_temp,Nominal_frequen
                ce_temp,20,Temp_distance(:,3)) ;

                 E_p = E_10d + ( E_20d - E_10d ).*log10(TXAntenna_height./10)./log10(20./10)

                 F_s = ( Distance(k) - D_20 ) ./  Distance(k)  ;

                 if [ Distance(k) < d_h ]

%                 [Temp_distance]= distance_search(Distance(k));


%
          E_10d=Field_strength(Propagation_type,Nominal_time_temp(1,1),Nominal_frequence_
temp(1,1),10,Temp_distance(:,3)) ;

                E_pp =  E_10dh10 + E_10d - E_10dh ;

              elseif [ Distance(k) >=d_h ]

                temp =   d_h10 + Distance(k)- d_h ;

                if [ temp  > 1000 ]


                  E_inf=Field_strength(Propagation_type,Nominal_time_temp,Nominal_frequenc
                  e_temp,10,length(Distance)-1 ) ;


                  E_sup=Field_strength(Propagation_type,Nominal_time_temp,Nominal_frequen
                  ce_temp,10,length(Distance) ) ;



                   E_pp  =  E_inf  +  (  E_sup  -  E_inf  ).*log10(Distance(k)./Distance(end-
1)).log10(Distance(end)./Distance(end-1)) ;

                else

                  [Temp_index]= distance_search(temp);


                  E_pp=Field_strength(Propagation_type,Nominal_time_temp,Nominal_frequenc
                  e_temp,10,Temp_index(:,3)) ;

                end

              end

               Field_strength_data(k) = E_p.*( 1 - F_s ) + E_pp.*F_s ;

            end

        end
```

```
    end

    clear Field_strength_data1 Field_strength_data2 ;
```

b) Correction Antenna Height calculation function

```
function [Correction_data]= Correction_antenna_height(Distance, Tx_antenna, Rx_antenna, Frequence)


K_h2 = 3.2 + 6.2.*log10(Frequence) ;


% R = 10 ; for sea paths the notional value of R is 10 m ;

% R_modified = ( 1000.*R.*Distance - 15.*Tx_antenna  )./( 1000.*d - 15 ) ;

% R_modified is ec. (27)


D_10 = Fresnel_06(Frequence,Tx_antenna,10) ;

D_h2 = Fresnel_06(Frequence,Tx_antenna,Rx_antenna) ;


C_10 =  K_h2.*log10(Rx_antenna./10) ;


if [ Rx_antenna == 10  ] % d<=dh2 ec. (29a)


    Correction_data = zeros(1,length(Distance)) ; % correction = 0dB;


elseif [ Rx_antenna > 10 ]


    Correction_data = K_h2.*log10(Rx_antenna./10).*ones(1,length(Distance)) ;


elseif [ Rx_antenna < 10 ]


    for  k=1:length(Distance)
```

```
        if [ Distance(k) >= D_10 ]

            Correction_data(k) = K_h2.*log10(Rx_antenna./10) ;

        elseif [ Distance(k) < D_10 ]

            if [ Distance(k) <= D_h2 ]

                Correction_data(k) = 0 ;

            elseif [ Distance(k) > D_h2 ]

                Correction_data(k) = C_10.*log10( Distance(k)./ D_h2  ).*log10( D_10./D_h2 ) ;
            end
        end
    end
end
```

c) Distance Search calculation function

```
function  [Nominal_distance]= distance_search(Distance)

Table = [[1:19],[20:5:95],[100:10:190],[200:25:1000] ];

Nominal_distance=zeros(length(Distance),2);

for k=1:length(Distance),

%     Temp=find(Table(1:length(Table)) < distance(k) & Table(2:length(Table)-1) > r(k)) ;
    Temp=find( Table(1:length(Table)) <= Distance(k), 1, 'last') ;
```

```
    if [Table(Temp) == Distance(k)]
        Nominal_distance(k,1)= Table(Temp);
        Nominal_distance(k,2)= 0;
        Nominal_distance(k,3)= Temp;
        Nominal_distance(k,4)= 0;
    else
        Nominal_distance(k,1)= Table(Temp);
        Nominal_distance(k,2)= Table(Temp+1);
        Nominal_distance(k,3)= Temp;
        Nominal_distance(k,4)= Temp+1;
    end
end


clear Temp Table Distance k;
```

d) Field Strength calculation function

```
function[Field_strength_data]=Field_strength(Propagation_type,Time_percentage,Frequence,T
XAntenna_height,Distance_index)


%map matix
Sheet_table(1,1,1)=4;
Sheet_table(1,1,2)=5;
Sheet_table(1,1,3)=6;
Sheet_table(1,2,1)=12;
Sheet_table(1,2,2)=13;
Sheet_table(1,2,3)=14;
Sheet_table(1,3,1)=20;
Sheet_table(1,3,2)=21;
Sheet_table(1,3,3)=22;
Sheet_table(2,1,1)=4;
```

```
Sheet_table(2,1,2)=7;

Sheet_table(2,1,3)=8;

Sheet_table(2,2,1)=12;

Sheet_table(2,2,2)=15;

Sheet_table(2,2,3)=16;

Sheet_table(2,3,1)=20;

Sheet_table(2,3,2)=23;

Sheet_table(2,3,3)=24;

if [ Propagation_type == 'Cold Sea' ]

    Level_1=1;

elseif [ Propagation_type == 'Warm Sea' ]

    Level_1=2;

end

Table_frequence = [ 100 600 2000 ];

Level_2=find(Table_frequence == Frequence);

Table_time = [0.50 0.10 0.01 ];

Level_3=find(Table_time == Time_percentage);

Sheet_index=Sheet_table(Level_1,Level_2,Level_3);
```

```
ITU_data = xlsread('C:\Documents and Settings\Antonio\Mis documentos\NTNU\Master Thesis\Matlab\ITU-R\tabulated field strength\Rec_P_1546_2_Tab_values',Sheet_index);


Original_data = ITU_data(7:end,2:end);


Table_txheight = [ 10 20 37.5 75  150  300  600  1200 0 ];


Column_index=find(Table_txheight == TXAntenna_height);


Field_strength_data = Original_data( Distance_index, Column_index);


clear Sheet_table Original_data Column_index ITU_data ;
```

e) Frequence Condition calculation function

```
function[Field_strength_data]= Frequence_condition(Propagation_type,Nominal_time_temp,Nominal_frequence,Nominal_txantenna_height,Nominal_distance,Distance,TXAntenna_height,Frequence);


if [ Nominal_frequence(1,2)==0 ]


[Field_strength_data]=Antenna_condition(Propagation_type,Nominal_time_temp,Nominal_frequence(1,1),Nominal_txantenna_height,Nominal_distance,Distance,TXAntenna_height);


   else


[Field_strength_data1]=Antenna_condition(Propagation_type,Nominal_time_temp,Nominal_frequence(1,1),Nominal_txantenna_height,Nominal_distance,Distance,TXAntenna_height);


[Field_strength_data2]=Antenna_condition(Propagation_type,Nominal_time_temp,Nominal_frequence(1,2),Nominal_txantenna_height,Nominal_distance,Distance,TXAntenna_height);


      Field_strength_data = Field_strength_data1 + (Field_strength_data2 - Field_strength_data1).*log10(Frequence./Nominal_frequence(1,1))...
```

```
        ./log10(Nominal_frequence(1,2)./Nominal_frequence(1,1)) ;

    end


    if [ Frequence > 2000 ]

        [Max_field_strength_data]= Max_field_strength(Nominal_time_temp, Distance) ;

        temp_index = find( Field_strength_data > Max_field_strength_data);

        for m = 1:length(temp_index)

            Field_strength_data(temp_index(m))= Max_field_strength_data(temp_index(m)) ;

        end

    end


clear Max_field_strength_data Field_strength_data1 Field_strength_data2 temp_index
```

f) Frequency Search calculation function

```
function  [Nominal_frequency]= Frequency_search(Frequency)

Nominal_frequency=zeros(length(Frequency),2);

for k=1:length(Frequency)

%     Temp=find(Table(1:length(Table)) < distance(k) & Table(2:length(Table)-1) > r(k)) ;
```

```
%     Temp=find( Table(1:length(Table)) <= Frequency(k), 1, 'last') ;

    if [Frequency(k) == 100]
        Nominal_frequency(k,1)= 100;
        Nominal_frequency(k,2)= 0;
    elseif [Frequency(k) == 600]
        Nominal_frequency(k,1)= 600;
        Nominal_frequency(k,2)= 0;
    elseif [Frequency(k) == 2000]
        Nominal_frequency(k,1)= 2000;
        Nominal_frequency(k,2)= 0;
    elseif [Frequency(k) < 600]
        Nominal_frequency(k,1)= 100;
        Nominal_frequency(k,2)= 600;
    elseif [Frequency(k) > 600]
        Nominal_frequency(k,1)= 600;
        Nominal_frequency(k,2)= 2000;
    end
end

clear Frequency k ;
```

g) Fresnel 06 function

```
function    [D_h1]= Fresnel_06(Frequence,Antenna_height1,Antenna_height2)

D_f = 0.0000389.*Frequence.*Antenna_height1.*Antenna_height2 ;

D_h = 4.1.*( sqrt(Antenna_height1) + sqrt(Antenna_height2) ) ;

D_h1 = D_f.*D_h./(D_f + D_h) ;
```

h) ITU Prediction

```
function[Distance,Field_strength_data]=ITU_prediction(Propagation_type,Time_percentage,Fre
quence, TXAntenna_height,RXAntenna_height)


% NUMERIC = xlsread('C:\Documents and Settings\Antonio\Mis documentos\NTNU\Master
Thesis\Matlab\ITU-R\tabulated field strength\Rec_P_1546_2_Tab_values','Figure 2')


Distance= [[1:19],[20:5:95],[100:10:190],[200:25:1000] ];

[Nominal_time]= Time_search(Time_percentage);              %two numbers

[Nominal_distance]= distance_search(Distance);             %maxtix

[Nominal_frequence]= Frequency_search(Frequence);          %two numbers


if [ TXAntenna_height >=10]

   [ Nominal_txantenna_height ] = TXAntenna_height_search(TXAntenna_height);

else

   Nominal_txantenna_height = [ 0 0 ] ;

end


% Correction  caused by Receiver antenna height

[Correction_data]=Correction_antenna_height(Distance,TXAntenna_height,  RXAntenna_height,
Frequence);


if [ Propagation_type == 'Cold Sea']


   if [ Nominal_time(1,2) == 0 ]



        [Field_strength_data]=Frequence_condition(Propagation_type,Nominal_time(1,1),Nomi
        nal_frequence,Nominal_txantenna_height,Nominal_distance,Distance,TXAntenna_heig
        ht,Frequence);
```

```
    else

        [Field_strength_data1]=Frequence_condition(Propagation_type,Nominal_time(1,1),Nom
        inal_frequence,Nominal_txantenna_height,Nominal_distance,Distance,TXAntenna_heig
        ht,Frequence);

        [Field_strength_data2]=Frequence_condition(Propagation_type,Nominal_time(1,2),Nom
        inal_frequence,Nominal_txantenna_height,Nominal_distance,Distance,TXAntenna_heig
        ht,Frequence);

      Field_strength_data=Field_strength_data2.*( Q_fun(Nominal_time(1,1)) -
Q_fun(Time_percentage) )./ ( Q_fun(Nominal_time(1,1)) - Q_fun(Nominal_time(1,2)) ) + ...

        Field_strength_data1.*( Q_fun(Time_percentage) - Q_fun(Nominal_time(1,2)) )./ (
Q_fun(Nominal_time(1,1)) - Q_fun(Nominal_time(1,2)) ) ;

    end

    Field_strength_data = Field_strength_data + Correction_data ;

elseif [ Propagation_type == 'Warm Sea']

    if [ Nominal_time(1,2) == 0 ]

        [Field_strength_data]=Frequence_condition(Propagation_type,Nominal_time(1,1),Nomi
        nal_frequence,Nominal_txantenna_height,Nominal_distance,Distance,TXAntenna_heig
        ht,Frequence);

    else

        [Field_strength_data1]=Frequence_condition(Propagation_type,Nominal_time(1,1),Nom
        inal_frequence,Nominal_txantenna_height,Nominal_distance,Distance,TXAntenna_heig
        ht,Frequence);
```

```
[Field_strength_data2]=Frequence_condition(Propagation_type,Nominal_time(1,2),Nom
inal_frequence,Nominal_txantenna_height,Nominal_distance,Distance,TXAntenna_heig
ht,Frequence);


Field_strength_data = Field_strength_data2.*( Q_fun(Nominal_time(1,1)) -
Q_fun(Time_percentage) )./ ( Q_fun(Nominal_time(1,1)) - Q_fun(Nominal_time(1,2)) ) + ...

Field_strength_data1.*( Q_fun(Time_percentage) - Q_fun(Nominal_time(1,2)) )./ (
Q_fun(Nominal_time(1,1)) - Q_fun(Nominal_time(1,2)) ) ;


end


Field_strength_data = Field_strength_data + Correction_data ;


end


clear Field_strength_data1 Field_strength_data2 Nominal_time Nominal_distance
Nominal_frequence Correction_data

%%plot


% figure

% semilogx( Distance, Field_strength_data )

% ylim( [-80  120 ] )

% grid


i) Maximum Field Strength calculation function

function  [Max_field_strength]= Max_field_strength(Time_percentage_temp, Distance)

%only for sea path

E_fs = 106.9 - 20.*log10(Distance) ;

E_se = 2.38.* ( 1 - exp(-Distance./8.94) ).* log10(50./Time_percentage_temp) ;

Max_field_strength = E_fs + E_se ;

%semilogx(Distance,Max_field_strength)
```

j) Plot function

```
clear all

clc

TXAntenna_height1 = 1200;

TXAntenna_height2 = 600;

TXAntenna_height3 = 300;

TXAntenna_height4 = 150;

TXAntenna_height5 = 75;

TXAntenna_height6 = 37.5;

TXAntenna_height7 = 20;

TXAntenna_height8 = 10;


Propagation_type = 'Cold Sea';

Time_percentage = 0.50 ;

Frequence = 3500 ;

RXAntenna_height = 10 ;


[Distance1,Field_strength_data1]=ITU_prediction(Propagation_type,Time_percentage,Frequenc
e, TXAntenna_height1,RXAntenna_height);

[Distance2,Field_strength_data2]=ITU_prediction(Propagation_type,Time_percentage,Frequenc
e, TXAntenna_height2,RXAntenna_height);

[Distance3,Field_strength_data3]=ITU_prediction(Propagation_type,Time_percentage,Frequenc
e, TXAntenna_height3,RXAntenna_height);

[Distance4,Field_strength_data4]=ITU_prediction(Propagation_type,Time_percentage,Frequenc
e, TXAntenna_height4,RXAntenna_height);

[Distance5,Field_strength_data5]=ITU_prediction(Propagation_type,Time_percentage,Frequenc
e, TXAntenna_height5,RXAntenna_height);

[Distance6,Field_strength_data6]=ITU_prediction(Propagation_type,Time_percentage,Frequenc
e, TXAntenna_height6,RXAntenna_height);

[Distance7,Field_strength_data7]=ITU_prediction(Propagation_type,Time_percentage,Frequenc
e, TXAntenna_height7,RXAntenna_height);

[Distance8,Field_strength_data8]=ITU_prediction(Propagation_type,Time_percentage,Frequenc
e, TXAntenna_height8,RXAntenna_height);
```

```
E_se = 2.38 * ( 1 - exp(-Distance1./8.94 ) ).* log10(50./Time_percentage) ;

E_fs = 106.9 - 20.*log10(Distance1) ;

E_max =  E_fs + E_se ;

% [Nominal_distance]= distance_search(Distance1);

%[E_max]=Field_strength(Propagation_type,Time_percentage,Frequence,0,(1:length(Distance
1)));

figure

semilogx( Distance1, E_max, 'b-','LineWidth',4 )

hold on

semilogx( Distance1, Field_strength_data1, 'r-','LineWidth',4  )

semilogx( Distance2, Field_strength_data2, 'y-','LineWidth',4  )

semilogx( Distance3, Field_strength_data3, 'g-','LineWidth',4  )

semilogx( Distance4, Field_strength_data4, 'b-','LineWidth',4  )

semilogx( Distance5, Field_strength_data5, 'k-','LineWidth',4  )

semilogx( Distance6, Field_strength_data6, 'm-','LineWidth',4  )

semilogx( Distance7, Field_strength_data7, 'c-','LineWidth',4  )

semilogx( Distance8, Field_strength_data8, 'b-','LineWidth',4 )

hold off

xlabel('Distance(km)','fontsize',30)

ylabel('Field Strength(dB({\mu}V/m) for 1kw e.r.p.','fontsize',30)

ylim( [-80  120 ] )

legend('Maximum (free space)','Height{\_}tx = 1200m','Height{\_}tx = 600m','Height{\_}tx =
300m','Height{\_}tx = 150m',...

   'Height{\_}tx = 75m', 'Height{\_}tx = 37.5m','Height{\_}tx = 20m','Height{\_}tx =
10m','Location','SouthWest')

grid
```

k) Q function

```
function  [Q_value]= Q_fun(Time_percentage_temp)


C_0=2.515517 ;

C_1=0.802853 ;

C_2=0.010328 ;

D_1=1.432788 ;

D_2=0.189269 ;

D_3=0.001308 ;


T_value = sqrt(-2.*log(Time_percentage_temp)) ;

Teta_value = ( (C_2.*T_value + C_1).*T_value + C_0 )./( ( (D_3.*T_value + D_2).*T_value + D_1).*T_value + 1 ) ;

T_value_inv = sqrt(-2.*log( 1 - Time_percentage_temp)) ;

Teta_value_inv = ( (C_2.*T_value_inv + C_1).*T_value_inv + C_0 )./( ( (D_3.*T_value_inv + D_2).*T_value_inv + D_1).*T_value_inv + 1 ) ;


if [ Time_percentage_temp <= 0.5 ]

   Q_value = T_value - Teta_value ;

else

   Q_value = -( T_value_inv - Teta_value_inv  ) ;

end
```

l) Step Eight function from Annex 6 of ITU-R P.526

```
function[Field_strength_data]=Step_eight(Propagation_type,Nominal_time1,Nominal_frequence
1,Nominal_txantenna_height1,Nominal_distance,Distance)


[Field_strength_dataL]=Field_strength(Propagation_type,Nominal_time1,Nominal_frequence1,N
ominal_txantenna_height1,Nominal_distance(:,3)) ;

        Non_zero_index = find( Nominal_distance(:,2) ~= 0 ) ;

        Temp_distance=nonzeros(Nominal_distance(:,4));


[Field_strength_dataH]=Field_strength(Propagation_type,Nominal_time1,Nominal_frequence1,
Nominal_txantenna_height1,Temp_distance) ;

        N=1;

        for  k=1:length(Distance)

           if [  find(Non_zero_index == k) ]

              Field_strength_data(1,k)=  Field_strength_dataL(k)+  (  Field_strength_dataH(N)-
Field_strength_dataL(k))...

                        .*log10(  Distance(k)./Nominal_distance(k,1)  )./log10(
Nominal_distance(k,2)./Nominal_distance(k,1) ) ;

              N = N + 1 ;

           else

              Field_strength_data(1,k)=Field_strength_dataL(k);

           end

        end


        clear Field_strength_dataL  Field_strength_dataH Temp_distance ;
```

m) Time Search function

```
function  [Nominal_time]= Time_search(Time_percentage)


Table = [ 0.01  0.10  0.50 ];


Nominal_time=zeros(length(Time_percentage),2);


for k=1:length(Time_percentage)


%     Temp=find(Table(1:length(Table)) < distance(k) & Table(2:length(Table)-1) > r(k)) ;
    Temp=find( Table(1:length(Table)) <= Time_percentage(k), 1, 'last') ;


    if [Table(Temp) == Time_percentage(k)]
        Nominal_time(k,1)= Table(Temp);
        Nominal_time(k,2)= 0;
    else
        Nominal_time(k,1)= Table(Temp);
        Nominal_time(k,2)= Table(Temp+1);
    end
end


clear Table k Temp Time_percentage ;
```

n) Transmitter Antenna Height Search function

```
function  [Nominal_txantenna_height]= TXAntenna_height_search(TXAntenna_height)

Table = [ 10 20 37.5 75  150  300  600  1200 ];

Nominal_txantenna_height=zeros(length(TXAntenna_height),2);

for k=1:length(TXAntenna_height)

   if [ TXAntenna_height(k) > 1200 ]
      Nominal_txantenna_height(k,1)= 600;
      Nominal_txantenna_height(k,2)= 1200;
   else
      Temp=find( Table(1:length(Table)) <= TXAntenna_height(k), 1, 'last') ;
%         size(Temp)
%         pause
      if [Table(Temp) == TXAntenna_height(k)]
         Nominal_txantenna_height(k,1)= Table(Temp);
         Nominal_txantenna_height(k,2)= 0;
      else
         Nominal_txantenna_height(k,1)= Table(Temp);
         Nominal_txantenna_height(k,2)= Table(Temp+1);
      end
   end
end

clear Table k Temp TXAntenna_height ;
```

F

References

LTE

[L1] 3GPP TR 25.913. Requirements for Evolved UTRA (E-UTRA) and Evolved UTRAN (E-UTRAN). Available at http://www.3gpp.org.

[L2] Rumney, Moray. "3GPP LTE: Introducing Single-Carrier FDMA". Agilent Technologies. http://cp.literature.agilent.com/litweb/pdf/5989-7898EN.pdf.

Path Loss and Shadowing

[P1] D. Parsons, The Mobile Radio Propagation Channel. New York: Halsted Press (Division of Wiley). 1992.

[P2] J.W. McKown and R.L. Hamilton, Jr., “Ray tracing as a design tool for radio networks,” IEEE Network , Vol. 5, No. 6, pp. 27–30, Nov. 1991.

[P3] H.-J. Li, C.-C. Chen, T.-Y. Liu, and H.-C. Lin, “Applicability of ray-tracing techniques for prediction of outdoor channel characteristics,” IEEE Trans. Vehic. Technol., pp. 2336–2349, Nov. 2000.

[P4] A. Domazetovic, L.J. Greenstein, N. Mandayan, and I. Seskar, “A new modeling approach for wireless channels with predictable path geometries,” Proc. IEEE Vehic. Technol. Conf, Sept. 2002.

[P5] J.H. Tarng, W.-S. Liu, Y.-F. Huang, and J.-M. Huang, “A novel and efficient hybrid model of radio multipathfading channels in indoor environments,” IEEE Trans. Ant. Prop., Vol. 51, pp. 585 - 594, March 2003.

[P6] Okumura-Hata Model. “Empirical Formula for Propagation Loss in Land Mobile Radio Services”. IEEE Transactions on vehicular technology, Vol. VT-29, no. 3, August 1980.

[P7] COST231 Final Report

[P8] J. Walfisch, H. L. Bertoni, "A theoretical model of UHF propagation in urban environments," IEEE Trans. on Antennas and Propagation, vol. 36, no. 12, pp. 1788-1796, Dec. 1988.

[P9] William C.Y.Lee. Mobile Communications Engineering. Theory and applications. 2nd ed. McGraw-Hill Telecommunications, 1998.

Propagation Prediction Models

[M1] Hecht, Eugene (2002). Optics (4th ed.). Addison Wesley. ISBN 0-321-18878-0.

[M2] P. Kreuzgruber, T. Bründl, W. Kuran, R. Gahleitner, "Prediction of indoor radio propagation with the ray splitting model including edge diffraction and rough surfaces," COST-231 TD(94) 50, Prague, Czech Republic, April 1994

[M3] J.-F. Wagen, M. Keer, "Comparison of diffraction coefficients for propagation prediction in microcells," COST-231 TD(93) 80, Grimstad, Norway, May 1993

[M4] J. B. Keller, " Geometrical Theory of Diffraction," J. Opt. Soc. Am., vol. 52, pp. 116-130, 1962

[M5] D. A. McNamara, C. W. I. Pistorius, J. A. G. Malherbe, Introduction to the Uniform Geometrical Theory of Diffraction, Artech House, Norwood, MA, USA, 1990, ISBN 0-89006-301-X

[M6] C. Bergljung, "Diffraction of Electromagnetic Waves by Dielectric Wedges," Ph.D. Thesis, Lund Institute of Technology, Sweden, 1994

[M7] S. R. Saunders, F. R. Bonar, "Explicit multiple building attenuation function for mobile radio wave propagation," Electronics Letters, vol. 27, no. 14, pp. 1276-1277, July 1991

[M8] J. Walfisch, H. L. Bertoni, "A theoretical model of UHF propagation in urban environments," IEEE Trans. on Antennas and Propagation, vol. 36, no. 12, pp. 1788-1796, Dec. 1988

[M9]] C. L. Giovaneli, “An analysis of simplified solutions for multiple knife-edge diffraction,” IEEE Trans. on Antenna. Propagat., vol. AP-32, pp. 297–301, 1984.

[M10] J. Deygout, “Multiple knife-edge diffraction of microwaves,” IEEE Trans. Antenna. Propagat., vol. AP-14, pp. 480–489, 1966.

[M11] J. H. Causebrook and B. Davies, “Tropospheric radio wave propagation over irregular terrain: The computation of field strength for UHF broadcasting,”, BBC Research Department Report RD 1971/43, 1971.

[M12] S. R. Saunders, F. R. Bonar, "Prediction of mobile radio wave propagation over buildings of irregular heights and spacings," IEEE Trans. on Antennas and Propagation, vol. 42, no. 2, pp. 137-144, 1994

[M13] Y. Okumura et al., “Field strength and its variability in UHF and VHF land-mobile radio service,” Rev. Elec. Commun. Lab.. vol. 16, 1968.

[M14] Okumura-Hata Model. “Empirical Formula for Propagation Loss in Land Mobile Radio Services”. IEEE Transactions on vehicular technology, Vol. VT-29, no. 3, August 1980.

[M15] Terje lectures. NTNU mobile komunikasjon kurs sider.

[M16] K. Bullington, “Radio Propagation at Frequencies above 30 Megacycles,” Proc. IRE, vol. 35, no. 10, 1947, pp. 1122–1136.

[M17] J. Epstein and D.W. Peterson, “An Experimental Study of Wave Propagation at 850 Mc/s,” Proc. IRE, vol. 41, 1953, pp. 595–611.

[M18] A. Picquenard, Radio Wave Propagation,Wiley, New York, 1974, p. 296.

[M19] K. Hacking, “U.H.F. Propagation over Rounded Hills,” Proc. IEE, March 1970, pp. 499–511.

[M20] F. Ikegami, S. Yoshida, M. Umehira, "Propagation factors controlling mean field strength on urban streets," IEEE Trans. on Antennas and Propagation, vol. 32, no. 8, August 1984, pp. 822-829

[M21] M. Hata, "Empirical formula for propagation loss in land mobile radio services," IEEE Trans. on Vehicular Technology, vol. 29, pp. 317-325, 1980

[M22] Y. Okumura, E. Ohmori, T. Kawano, K. Fukuda, "Field strength and its variability in VHF and UHF land-mobile service," Review of the Electrical Communication Laboratory, vol. 16, no. 9-10, 1968, pp. 825-873

[M23] COST 231, "Urban transmission loss models for mobile radio in the 900- and 1,800 MHz bands (Revision 2)," COST 231 TD(90)119 Rev. 2, The Hague, The Netherlands, September 1991

[M24] L. R. Maciel, H. L. Bertoni, H. H. Xia, "Unified approach to prediction of propagation over buildings for all ranges of base station antenna height," IEEE Trans. on Vehicular Technology , vol. 43, no. 1, 1993, pp. 35-41

[M25] H. H. Xia, H. L. Bertoni, "Diffraction of cylindrical and plane waves by an array of absorbing half-screens," IEEE Trans. on Antennas and Propagation, vol. 40, no. 2, 1992, pp. 170-177

[M26] L. R. Maciel, H. L. Bertoni, H. H. Xia, "Propagation over buildings for paths oblique to the street grid," Proc. PIMRC´92, Boston, USA, pp. 75-79

[M27] S. R. Saunders, F. R. Bonar, "Explicit multiple building attenuation function for mobile radio wave propagation," Electronics Letters, vol. 27, no. 14, pp. 1276-1277, July 1991

[M28] N. Cardona, P. Möller, F. Alonso, "Applicability of Walfisch-type urban propagation models," Electronics Letters, vol. 31, no. 23, November 1995

[M29] P. Eggers, "Note on the usage of Walfisch-type urban path loss prediction models," COST 231 TD(91)87, The Hague, September 1991

[M30] R. Leppänen, J. Lähteenmäki, S. Tallqvist, "Radiowave propagation at 900 and 1800 MHz bands in wooded environments," COST 231 TD(92)112, Helsinki, 1992

[M31] L. Ladell, "Transmission loss predictions in wooded terrain," Proc. Nordic Radio Symposium NRS´86, Sweden, 1986, pp. 41-50, ISBN 91-7056-072-2

[M32] Walther Åsen, “Comparison of Measurements With Prediction Methods for Propagation by Diffraction at 88–108 MHz” IEEE Transactions on antennas and propagation, vol. 52, no. 6, June 2004

[M33] C. Tzaras and S. R. Saunders, “Comparison of multiple-diffraction models for digital broadcasting coverage prediction,” IEEE Trans. Broadcasting, vol. 46, pp. 221–226, Sept. 2000.

[M34] J. H. Causebrook and B. Davies, “Tropospheric radio wave propagation over irregular terrain: The computation of field strength for UHF broadcasting,”, BBC Research Department Report RD 1971/43, 1971.

[M35] K. Furutsu, “On the theory of radio wave propagation over inhomogeneous Earth,” J. R. NBS, vol. 67D, no. 1, pp. 39–62, 1963.

[M36] C. Tzaras and S. R. Saunders, “An improved heuristic UTD solution for multiple-edge transition zone diffraction,” IEEE Trans. Antennas Propagation, to be published.

ITU-R recommendations:

[R1] ITU-R P.526 “Propagation by diffraction”

[R2] ITU-R P.1546 “Method for point-to-area predictions for terrestrial services in the frequency range 30 MHz to 3 000 MHz”

[R3] ITU-R P.452 “Prediction procedure for the evaluation of microwave interference between stations on the surface of the Earth at frequencies above about 0.7 GHz”

[R4] ITU-R P.530 “Propagation data and prediction methods required for the design of terrestrial line-of-sight systems”

[R5] ITU-R P.1411 “Propagation data and prediction methods for the planning of short-range outdoor radiocommunication systems and radio local area networks in the frequency range 300 MHz to 100 GHz ”

[R6] ITU-R P.453 “The radio refractive index: its formula and refractivity data”

[R7] ITU-R P.581 “The concept of worst month”

[R8] ITU-R P.676 “Attenuation by atmospheric gases”

[R9] ITU-R P.834 “Effects of tropospheric refraction on radiowave propagation”

[R10] ITU-R P.840 “Attenuation due to clouds and fog”

[R11] ITU-R P.833. “Attenuation in vegetation”

Appendices

[A1] Statistisk Sentralbyrå. Web page, 2010. http://www.ssb.no

[A2] Teleplan AS. Astrix 5.2. Web-page, 2010. http://www.teleplanglobe.com

[S1] LTE Kathrein antennas used at Oslo Networking. www.kathrein-scala.com